Corso di dottorato di ricerca in:

"Scienze e biotecnologie agrarie."

32° ciclo

Titolo della tesi

"New strategies to study and control plant diseases and their application to Kiwifruit Decline"

Dottorando
Francesco Savian

Supervisore
Prof. Marta Martini

Co-supervisore
Dr. Paolo Ermacora

Anno 2020

Table of content

I. Summary

In 2012, leaf scorches, wilting, sudden defoliation and dieback symptoms were observed for the first time on several kiwifruit plants in orchards located in Veneto (North-eastern of Italy). Diseased plants were also characterised by a heavily compromised root system with none or very few feeding roots, rotting tissues on smaller roots and lack of cohesion between the external cylinder of coarse roots and their core. In relation to these symptoms the new disease was named Kiwifruit Decline (KD). KD rapidly spread in all the most important Italian growing areas and probably up to date is the most concerning phyto-pathological issue for kiwifruit growers.

With the main aim to determine KD aetiology and to identify the epidemiological pattern of this disease outbreaks, canonical strategies and new technologies were integrated in an interdisciplinary approach.

The work started with the definition of a conceptual framework considering the symptoms observed in the field and the history of the disease evolution based on the farmers' experiences. These evidences were used as first-hand source of information and integrated with the experiences gathered by other Italian research groups to hypothesize the etiological causes most probably involved in the disease. From this analysis waterlogging and soil-borne pathogens emerged as the two most probable factors involved in the disease, although their role in the disease was still unknown.

Therefore, the following step was the setup of a canonical experimental trial, where the effect of the two most probable etiological causes were compared under controlled conditions. The trial gave unequivocal results clearly stating the necessary interaction between waterlogging and soil borne pathogens to incite the disease. Furthermore, axenic isolation starting from plants that became diseased during this trial, allowed to have a first insight on soil-borne microorganisms potentially involved in the disease, suggesting that one or more pathogens (most probably Oomycetes) might be involved in the disease.

Given these results a pathogenicity test was set up and confirmed that *Phytopythium vexans* was able to induce KD symptoms in both canopy and roots of kiwifruit plants.

Once the role of a biotic factor was demonstrated, the studies moved back to the field focusing mostly on remote sensing technologies able to infer the physiological traits of the plants. Thermal and multispectral imagery acquired over a diseased field and classified with unsupervised clustering algorithms allowed to efficiently distinguish asymptomatic from symptomatic plants and to predict, one year in advance, the disease outbreak.

Since the involvement of one or more potential soil-borne pathogens was proposed, a metabarcoding study was performed to have a first insight on fungal and oomycete communities associated with KD. Interestingly, *Phytopythium vexans* not only was found with a low relative abundance within diseased samples, but it was also recorded in healthy samples suggesting that the asymptomatic state of the plants might be linked also to the environmental conditions averse to the development of the pathogens. Metabarcoding analysis also suggested *Phytophthora sojae* and *Ilyonectria macrodidyma* as new potential pathogen candidates.

Results from this thesis provided several breakthroughs regarding the KD syndrome and defined the starting point for future studies. Indeed, not only the disease is now clearly associated to a combination of waterlogging conditions and soil-borne pathogens, but also a standardized protocol was setup to reproduce the disease. Moreover, new tools for in-field early disease detection are proposed and the first overview of fungal and oomycete community associated to KD is given for both root endosphere and rhizosphere compartments.

II. Conferences, Publications, Training activities and Teaching activities

PUBLICATIONS

Polano C, Martini M, **Savian F**, Moruzzi S, Ermacora P, Firrao G. 2019. Genome Sequence and Antifungal Activity of Two Niche-Sharing *Pseudomonas protegens* Related Strains Isolated from Hydroponics. *Microbial Ecology* **77**: 1025–1035.

Savian F, Ginaldi F, Musetti R, Sandrin N, Tarquini G, Pagliari L, Firrao G, Martini M, Ermacora P. Studies on the aetiology of kiwifruit decline: interaction between soil-borne pathogens and waterlogging. *submitted for publication: Plant and Soil*.

Prencipe S, **Savian F**, Nari L, Ermacora P, Spadaro D, Martini M. First Report of Phytopythium vexans causing decline syndrome of *Actinidia deliciosa* 'Hayward' in Italy. *submitted for publication: 'Plant Disease Note'*.

Savian F, Marroni F, Firrao G, Ermacora P, Martini M. A metabarcoding approach to investigate fungal and oomycete communities associated with kiwifruit decline in Italy. *under submission: Scientific Reports*.

Savian F, Martini M, Ermacora P, Paulus S, Mahlein A-K. Remote sensing data to assess and predict outbreaks of a new decline syndrome affecting Kiwifruit orchards. *under submission: Remote Sensing*.

SCIENTIFIC POSTER COMMUNICATION - POSTER

Savian F, Martini M, Borselli S, Saro S, Musetti R, Loi N, Firrao G. 2017. Studies on kiwifruit decline, an emerging issue even for Friuli Venezia Giulia (eastern italy). *Journal of Plant Pathology* 99: 18.

Valdevit F, **Savian F**, Pavan F, Danuso F. 2017. Modelling seasonal first appearence of *Scaphoideus titanus*. In: GRIMPP conference, Gruppo di Ricerca Italiano Modelli Protezione Piante. Brescia.

Martini M, Mesaglio A, **Savian F,** Loschi A, Loi N, Ermacora P. 2018. Identification of '*Candidatus* Phytoplasma fragariae' (16SrXII-E) infecting *Cornus sanguinea* in Friuli Venezia Giulia (north-eastern Italy). In: 5th Bois Noir Workshop. Ljubljana, Slovenia.

Savian F, Martini M, Ermacora P, Paulus S, Mahlein A-K. 2019. Unsupervised clustering of remote sensing data from kiwifruit (A. deliciosa var. Hayward) orchards affected by kiwifruit decline. In: Bornimer Agrartechnische Berichte. Bonn, 89–98.

Savian F, Musetti R, Sandrin N, Ermacora P, Martini M. 2019. Etiological studies over kiwifruit decline reveal the involvement of both flooding and biotic factors. In: XXV National Congress of Italian Phytopathological Society (SIPaV). Milano.

AGRICULTURAL MAGAZINE

Sorrenti G, Tacconi G, Tosi L, Vittone G, Nari L, **Savian F**, Saro S, Ermacora P, Graziani S, Toselli M. 2019. Avanza la "moria del kiwi": evoluzione e primi riscontri della ricerca. *Frutticoltura* **2**: 34–42.

Tacconi G, Giacopini A, Vittone G, Nari L, Spadaro D, **Savian F**, Ermacora P, Saro S, Morone C, Bardi L, *et al.* 2019. "Moria del kiwi": situazione disastrosa al nord, preoccupante nel resto d'Italia. *Kiwi informa* Aprile/Giugno: 32–37.

TRAINING ACTIVITIES

- **Data Analysis and Management in Applied Biology**. Coordinated by PhD school in Agricultural Science and Biotechnology of the University of Udine. Paluzza, UD (Italy) September 6th -10th, 2017
- **EMPHASIS SUMMER SCHOOL.** Emerging pests and diseases in horticultural crops: innovative solutions for diagnosis and management. Coordinated by Prof. Maria Lodovica Gullino, Grugliasco, University of Torino, Italy. July 2nd -6th 2018.
- **Translational aspects of plant microbiome research.** Coordinated by Prof. Vittorio Venturi ICGEB, Trieste, Italy, November 26th-30th 2018.
- **CISM-UniUD Joint Course on Systems Biology**. Coordinated by PhD school in Agricultural Science and Biotechnology of the University of Udine. Udine (Italy) 3rd – 7th September, 2018.
- **Academic Guest** from January 8th to 30th April 2019 at Prof. Anne Katrin Mahlein's remote sensing group. Institute of Sugar Beet Research (IfZ), associated institute with the University of Goettingen, Goettinghen, Germany.

TEACHING ACTIVITIES

- Lecture (in Italian) on “Study and identification methods for fungal disease detection”, for Professor Giuseppe Firrao, University of Udine.
- Practical lecture (in Italian) in the course on Post harvest disease management (2017, 2018 and 2019): isolation, DNA extraction and PCR technique for fungi identification, for Professor Marta Martini, University of Udine, Udine.

1 Introduction to kiwifruit pest.

Kiwifruit species (*Actinidia chinensis* and *A. deliciosa*) are among the best examples of the successful domestication and commercialisation of a new crop (Ferguson, 2011). Until the beginning of last century, it was simply a wild plant until seeds were sent to New Zealand, where the process of domestication of *A. deliciosa* was successfully initiated (Ferguson, 2016). Firstly, introduced in Italy in the late '60s, kiwifruit cultivation grew rapidly in importance in the '80s thanks to the promising profit prospective. In 1990 kiwifruit cultivation reached approximately 20.000 ha, mostly located in Veneto, Piemonte, Emilia-Romagna and Lazio (Regazzi & Stanzani, 2003). The Italian kiwifruit industry is certainly important in terms of international trade, making up by itself for more than 15% of global demand (FAOSTAT, 2016).

In the previous century, studies on kiwifruit were mostly focused on testing agronomical practices (training systems, irrigation, fertilization) rather than on plant pathology aspects. Since there were no major diseases affecting the kiwifruit, phytopathological research was limited to some abiotic aspects such as frost damages or nutritional disorders. The first large scale epidemic was the bacterial canker caused by *Pseudomonas syringae* pv. *actinidiae* (Psa) (EPPO, 2012), that since 2007/2008 has spread rapidly all over Italian kiwifruit growing areas. Even if the disease is still a concern, nowadays farmers have learned to control it with a correct agronomic management combining copper preventive treatments with removal of infected material from the orchards.

Immediately after the PSA emergency was contained and the farmers began to recover from production losses, two new major threats appeared: the brown marmorated stink bug *Halyomorpha halys*, and the disease being studied in this thesis named Kiwifruit Decline.

In Italy, the first detection of *H. halys* occurred in Emilia Romagna in 2012 (Cesari *et al.*, 2015). Being highly polyphagous and with an astonishing biotic potential, it quickly became a threat for several crops including kiwifruit (Candian *et al.*, 2018). Effective strategies are still missing, but the

use of exclusion nets can provide sufficient protection from the damage (Candian *et al.*, 2018) until new and more efficient treatments will be developed. Recently individuals of *Trissolcus japonicus,* a wasp native of east Asia and known for parasitizing *H. halys* eggs, were found in some Friuli Venezia Giulia orchards, strengthening the hope that the natural or man-made introduction of this hyperparasite will lead to a natural balance of the population of *H. halys.*

The last, but not least, threat to kiwifruit growers is Kiwifruit Decline (KD), a destructive disease causing the complete degradation of the root system, and consequently the sudden appearance of wilting and plant death. In comparison to the other two major diseases (PSA and *Halyomorpha halys*), KD is probably the one creating the higher concerns among all the kiwifruit stakeholders, since the etiological background is still unclear and therefore, no reliable countermeasures are actually available to limit the disease spreading. Furthermore, the disease completely precludes kiwifruit growth and production, forcing many farmers to explant and shift to other crops. Long term solutions must be searched in resistant rootstocks, which are currently under evaluation, but unfortunately it will require at least several years before giving consistent results. In the meantime, farmers who have to face KD can only try to reduce water stagnation within their fields, even if this strategy has not always been proved effective (Sorrenti *et al.*, 2019).

1.1 Kiwifruit Decline: background.

Kiwifruit decline was identified for the first time in the Verona province (Veneto, North-eastern of Italy), where several kiwifruit orchards (about 50 ha) suddenly started to wilt during the summer of 2012 (Tacconi *et al.*, 2014, 2015). In only few seasons, the disease rapidly spread reaching 400 ha in 2014 (Tacconi *et al.*, 2014), and more than 1200 ha in 2016 (Sorrenti *et al.*, 2016). In 2014-2015 other two outbreaks occurred in two regions of the Northern Italy, in Friuli Venezia Giulia (FVG) (Savian *et al.*, 2017) and in Piedmont (Sorrenti *et al.*, 2019) respectively. Unfortunately, to date the disease is

spreading also in Lazio (Central Italy) and in Calabria (Southern Italy), and it is currently affecting more than 25% (6600 ha ca.) of the total Italian kiwifruit growing area (Tacconi personal communication as update of Sorrenti *et al.*, 2019).

The very first step performed during this thesis was to assess the similarity of KD symptoms described in Veneto (Tacconi *et al.*, 2014, 2015; Tosi *et al.*, 2015; Sorrenti *et al.*, 2016) with those observed in Friuli Venezia Giulia (FVG, region were most of this thesis studies were performed). The identification of diseased orchards was carried out in collaboration with the regional territorial agency ERSA-FVG in a survey during 2015 and 2016 summers involving more than 20 orchards (Savian *et al.*, 2017). Symptoms in FVG corresponded indeed to those reported in Veneto: i) astonishing spreading speed and radius; ii) oil spot spreading pattern, iii) fast, sudden and irreversible wilting of the canopies; iv) almost complete decays of the white feeding roots; v) reddish discoloration and "rat-tail" symptoms on coarse roots. A comprehensive and more detailed description of the symptoms is given in Chapter 2. In order to have a preliminary overview on the feature characterising KD-affected orchards in FVG-region, farmer experiences were further investigated to know about first disease appearance, spreading patterns, agricultural practices and orchard characteristics. It was found that even if the biggest epidemic in FVG was observed in 2014 (Savian *et al.*, 2017), the first signs of the disease could be dated back to 2012. The consultation with the farmers highlighted that the disease was affecting both: i) *A. deliciosa* and *A. chinensis* orchards; ii) old and young plants; iii) organic and conventional farming; and iv) hormone-treated and -untreated orchards.

The involvement of waterlogging hypothesized in Veneto (Sorrenti *et al.*, 2016) was also confirmed in FVG, since the disease was mostly observed in poorly drained soil, usually with a high percentage of silt. Additionally, the spreading typically started from down-slope areas or soils dips where the waterlogging conditions occur most easily. Indeed, KD was quickly associated to flooding conditions by Tosi, Tacconi, Sorrenti and co-workers (Tosi *et al.*, 2015; Tacconi *et al.*, 2015; Sorrenti *et al.*,

2016). Furthermore, preliminary results of an experimental trial in Veneto were giving promising results, since it seemed possible to grow kiwifruit in KD-affected soils creating high raised bed (70 cm) and using accurate water management strategies (Sorrenti *et al.*, 2019). In the literature, the susceptibility of kiwifruit to waterlogging is well stated and believed to be able to produce root degradations similar to those observed in KD (Smith *et al.*, 1990; Reid *et al.*, 1991, 1992; Reid & Petrie, 1991). Considering theese aspects KD was initially addressed as an agronomical problem especially linked to wrong irrigation practices. Nevertheless, some aspects were in contrast with this hypothesis, especially in FVG region, where almost all the infected orchards were equipped with micro sprinkler irrigation systems, and several of them were characterised by loamy and/or well drained soils.

The hypothesis of the involvement of one or many soil-borne pathogens was never disregarded by the previous studies, but also never fully clarified (Tosi et al., 2015; Tacconi et al., 2015; Sorrenti et al., 2016). *Phytophthora*, *Phytium*, *Fusarium* and *Cylindrocarpon* were frequently isolated from infected plants (Tosi *et al.*, 2015; Tacconi *et al.*, 2015), and some of them (*Phytophthora cryptogea* and *Phytophthora citrophthora*) seems to be able to induce wilting on kiwifruit cuttings (Tacconi at al., 2015). Indeed, several features of KD seemed to suggest the involvement of a pathogen: i) the disease persisted even after extirpation, ploughing and replanting, ii) diseased plant did not recover from their weakened status once waterlogging conditions ceased, iii) the root rotting and the absence of new feeding root were observed even in not-flooded areas, and iv) the disease spread with an oil-spot pattern. On the contrary, the astonishing spreading speed and the wide spreading radius are quite unusual for a soil borne disease. Nevertheless, since no common pathogens were found in infected plants, the involvement of a soil-borne pathogen was initially overlooked, focusing the studies on waterlogging as the main cause of KD.

After gathering all these information, we started to develop our own hypothesis around KD aetiology, by summarising all pros and cons linked to the two most probable factors involved in the disease: flooding and soil-borne pathogens (see, Table 1). As result, before attempting any experiment, our general idea was that waterlogging and soil-borne pathogens should be both involved, since there were several evidences in favour and none clearly against the involvement of both factors.

Waterlogging cloud lead indeed to different situation: anoxia causing plant weakening, anaerobiotic pathogen proliferation, and soil structure degradation. The predisposing role played by waterlogging stresses in plant pathology is well renowned even if its impact vary across plant species (Bostock et al., 2014). Waterlogging mainly decrease the gas fluxes within the soil, reducing the dispersal of oxygen through the soil pore space around the root zone. The absence of oxygen induce a modification on the metabolic activities of the plant, by reducing: photosynthetic rate, stomatal conductance, hydraulic conductivity and translocation of photoassimilates (Taiz & Zeiger, 2010). In particular, the rapid decline of cell walls and protein synthesis occurring under waterlogging condition would seem to compromise the defence budget of the plant, rising the susceptibility to weakly aggressive facultative pathogens (Bostock et al., 2014). Waterlogging could also facilitate the proliferation of water-related microorganism or pathogen that may have the ability to grow under anoxic condition. For instance, oomycetes can not only grow under low oxygen pressure but also require water for formation, movement and accumulation of zoospore on susceptible roots (Toussoun et al., 1970). Finally, prolonged or repeated situation of waterlogging cause important and permanent effect on the physical properties of the soil, such as compaction and structural decline of soil aggregates (Manik et al., 2019). These aspects even if not directly involved in the root degradation processes, can decrease the root growth rate and increase the duration/frequencies of condition unfavourable to plant growth (Manik et al., 2019).

Among biotic stresses, we decide to focus our work on Fungi and Oomycetes based on the analysis of the KD symptoms and literature reports on root rot diseases. Indeed, wilting, root rot, decline and oil spot spreading patters are symptoms and features usually associated with these organisms. Moreover, reports of decline-like diseases on kiwifruit similar to KD were found for both Oomycetes (Latorre *et al.*, 1991; Lee *et al.*, 2001; Akilli *et al.*, 2011; Wang *et al.*, 2015; Çiftçi *et al.*, 2016) and Fungi (Homer, 1992; Erper *et al.*, 2011, 2013). Arthropods and nematodes were excluded from the study mainly because no feeding-related symptoms (chewing, piercing, holes, and galls) were found in KD diseased plants. Similarly, phytoplasmas and viruses were excluded since they are usually associated with symptoms which are mainly due to alteration in plant growth regulating hormones (witches'-broom, phyllody, virescence, yellowing and leaf curling), that are totally absent in KD. The exclusion of Bacteria from the study was initially made since, in kiwifruit, they had been usually associated with cancer, exudates, leaf spot and/or floral necrosis (Balestra *et al.*, 2011), rather than wilting and root rot alone. However, it was not possible to completely rule out Bacteria considering only KD symptomatology and ad hoc experiments should be performed to prove this statement. Nevertheless, the low occurrence rates of Bacteria obtained from the preliminary isolation tests seemed to confirm our hypothesis.

Table 1. Conceptual framework on Kiwifruit Decline features of the two most probable etiological causes before etiological studies reported on in this thesis (2016).

Features	Flooding		Pathogen	
	Pro	Con	Pro	Con
Soil properties				
High occurrence in poorly drained soils	✓			
Some occurrence in well drained soils		✓		
Agronomical practices				
Higher occurrence in flood irrigated orchards	✓			
Several occurrence in micro-irrigated orchards		✓		
Spreading pattern				
Higher occurrence in down slope areas	✓			
Soil dips are usually the initial spreading point	✓			
Sudden appearance of the disease in different pedo-climatic areas			✓	
Astonishing spreading speed and radius	✓			✓
Oil spot spreading pattern			✓	
No recovery after witlings appearance			✓	
Persistence of symptoms even plowing and replanting			✓	
Symptoms				
Rotting tissues on fine roots			✓	
Absence of feeding roots			✓	
Redness discoloration of the cortex	✓		✓	
Literature				
No common pathogen isolated	✓			✓
Raised bed and accurate irrigation allowed replanting	✓			
Susceptibility of kiwifruit to waterlogging	✓			
Susceptibility of kiwifruit to Oomycetes			✓	
Report on similar disease involving flooding and soil-borne pathogens	✓		✓	

1.2 Aim of the thesis

In Europe the kiwifruit is cultivated in Italy, Greece, France, Portugal, Spain, Turkey; beyond Europe in New Zealand, China, Iran, Chile, Argentina, California. Up to now, Kiwifruit Decline has only been reported in Italy, whereas in France and Portugal a similar situation seemed to be due to waterlogging alone occurred in particular situations (Tacconi, personal communication). Thus, the study of KD is important not only to solve a problem in Italy, but also to prevent its diffusion in other countries.

This thesis deals with the study of this emerging and unknown disease using an interdisciplinary approach. The work is divided into four main chapters, each of which responds to a specific topic regarding etiological and epidemiological questions over KD.

Firstly, the juggling between waterlogging and soil-borne pathogen involvement was resolved thanks to a greenhouse experiment. This work aimed to clarify the role played by the two main factors involved in the disease, integrating notions of climate analysis, plant physiology and plant pathology, including ultrastructural analysis and isolation of potential pathogens from diseased plants. (Chapter 2)

Secondly, a pathogenicity test was performed on the isolates that were most frequently obtained from diseased plants to fulfil the Koch's postulates. Among all the pathogenic candidates, *Phytopythium vexans* was selected because this species was not only found in diseased plants in the experimental trial described in Chapter 2, but it was also the most frequently isolated species from diseased plants in a survey carried out in Piedmont region. (Chapter 3).

The third main question we tried to address regarded the identification of heathy and diseased plants in the field before the wilting appearance, in order to improve the monitoring and sampling activities. Indeed, the feeding roots, core sample for all the etiological analysis, are usually completely degraded

when symptoms are visible on the canopy. Therefore, a remote sensing study was set up using multispectral and thermal imaging acquired with a UAV survey. Imaging data were clustered into homogeneous areas using an unsupervised machine learning approach. (Chapter 4)

Finally, the last part of the thesis was planned to describe the microbial community associated with asymptomatic and disease plants, within (endosphere) and outside (rhizosphere) the roots, in order to highlight microorganisms probably associated with the Kiwifruit Decline. Thus, a metabarcoding study was setup on samples collected from completely asymptomatic and infected orchards. Sampling areas in the infected site were previously identified in Chapter 4, via unsupervised clustering of remote sensing data.

References

Akilli S, Serçe ÇiU, Zekaİ Katircioğlu Y, Karakaya A, Maden S. **2011**. Involvement of *Phytophthora citrophthora* in kiwifruit decline in Turkey. *Journal of Phytopathology* **159**: 579–581.

Balestra GM, Renzi M, Ricci L, Taratufolo MC, Quattrucci A, Rossetti A, Mazzaglia A. **2011**. History of kiwifruit bacterial diseases in Italy. *Acta Horticulturae*: 457–460.

Bostock RM, Pye MF, Roubtsova TV. **2014**. Predisposition in plant disease: exploiting the nexus in abiotic and biotic stress perception and response. *Annual Review of Phytopathology* **52**: 517–549.

Candian V, Pansa MG, Briano R, Peano C, Tedeschi R, Tavella L. **2018**. Exclusion nets: a promising tool to prevent Halyomorpha halys from damaging nectarines and apples in NW Italy. *Bulletin of Insectology* **71**: 21–20.

Cesari M, Maistrello L, Ganzerli F, Dioli P, Rebecchi L, Guidetti R. **2015**. A pest alien invasion in progress: potential pathways of origin of the brown marmorated stink bug Halyomorpha halys populations in Italy. *Journal of Pest Science* **88**: 1–7.

Çiftçi O, Serçe ÇU, Türkölmez Ş, Derviş S. **2016**. First Report of Phytophthora palmivora causing crown and root rot of kiwifruit (Actinidia deliciosa) in Turkey. *Plant Disease* **100**: 210.

EPPO. **2012**. Final pest risk analysis for Pseudomonas syringae pv. actinidiae. *EPPO, Paris*.

Erper I, Agustí-Brisach C, Tunali B, Armengol J. **2013**. Characterization of root rot disease of kiwifruit in the Black Sea region of Turkey. *European Journal of Plant Pathology* **136**: 291–300.

Erper İ, Tunali B, Carlos A-B, Armengol J. **2011**. First Report of *Cylindrocarpon liriodendri* on Kiwifruit in Turkey. *Plant Disease* **95**: 76–76.

FAOSTAT. **2016**. Food and Agriculture Organization of the United Nations, Rome, Italy.

Ferguson AR. **2011**. Kiwifruit: Evolution of a Crop. *Acta Horticulturae*: 31–42.

Ferguson AR. **2016**. World Economic Importance. In: Testolin R, Huang H-W, Ferguson AR, eds. Compendium of Plant Genomes. The Kiwifruit Genome. Cham: Springer International Publishing, 37–42.

Homer IJ. **1992**. Epidemiology of armillaria root-rot of kiwifruit. *Acta Horticulturae*: 573–578.

Latorre BA, Alvarez C, Ribeiro OK. **1991**. Phytophthora root rot of kiwifruit in Chile. *Plant Disease* **75**: 949–952.

Lee Y-H, Jee H-J, Cha K-H, Ko S-J, Park K-B. **2001**. Occurrence of Phytophthora Root Rot on Kiwifruit in Korea. *The Plant Pathology Journal* **17**: 154–158.

Manik SMN, Pengilley G, Dean G, Field B, Shabala S, Zhou M. **2019**. Soil and Crop Management Practices to Minimize the Impact of Waterlogging on Crop Productivity. *Frontiers in Plant Science* **10**: 140.

Rao R, Li Y. **2003**. Management of Flooding Effects on Growth of Vegetable and Selected Field Crops. *HortTechnology* **13**: 610‑616.

Regazzi D, Stanzani N. **2003**. Il caso dell'actinidia in Italia: dall'esame del passato a indicazioni per il futuro. In: Actinida, la novitá frutticola del XX secolo. Verona: Societá Orticola Italiana, 11–28.

Reid JB, Petrie RA. **1991**. Effects of soil aeration on root demography in kiwifruit. *New Zealand Journal of Crop and Horticultural Science* **19**: 423–432.

Reid JB, Tate KG, Brown NS. **1992**. Effects of flooding and alluvium deposition on kiwifruit (*Actinidia deliciosa*). *New Zealand Journal of Crop and Horticultural Science* **20**: 283–288.

Reid JB, Tate KG, Brown NS, Cheah LH. **1991**. Effects of flooding and alluvium deposition on kiwifruit (Actinidia deliciosa): 1. Early vine decline. *New Zealand Journal of Crop and Horticultural Science* **19**: 247–257.

Savian F, Martini M, Borselli S, Saro S, Musetti R, Loi N, Firrao G. **2017**. Studies on kiwifruit decline, an emerging issue even for friuli venezia giulia (eastern italy). *Journal of Plant Pathology* **99**: 18.

Smith GS, Judd MJ, Miller SA, Buwalda JG. **1990**. Recovery of kiwifruit vines from transient waterlogging of the root system. *New Phytologist* **115**: 325–333.

Sorrenti G, Tacconi G, Tosi L, Vittone G, Nari L, Savian F, Saro S, Ermacora P, Graziani S, Toselli M. **2019**. Avanza la "moria del kiwi": evoluzione e primi riscontri della ricerca. *Frutticoltura* **2**: 34–42.

Sorrenti G, Toselli M, Reggidori G, Spinelli F, Tosi L, Giacopini A, Tacconi G. **2016**. Implicazioni della gestione idrica nella "Moria del kiwi" del veronese. *Frutticoltura* **3**: 1–7.

Tacconi G, Giacopini A, Tosi L. **2014**. La Moria Del Kiwi Nel Veronese. *Kiwi informa* **Aprile/Giugno**: 5–23.

Tacconi G, Paltrinieri S, Mejia JF, Fuentealba SP, Bertaccini A, Tosi L, Giacopini A, Mazzucchi U, Favaron F, Sella L, *et al.* 2015. Vine decline in kiwifruit: climate change and effect on waterlogging and phytophthora in north italy. *Acta Horticulturae*: 93–97.

Taiz L, Zeiger E. **2010**. *Plant physiology*. Sunderland, MA: Sinauer Associates.

Tosi L, Tacconi G, Giacopini A. **2015**. La moria del kiwi, situazione e prospettive. *L'Informatore Agrario* **44**: 67–70.

Toussoun TA, Bega RV, Nelson PE. **1970**. *Root Diseases and Soil-Borne Pathogens*. Berkeley: University of California Press.

Wang KX, Xie YL, Yuan GQ, Li QQ, Lin W. **2015**. First Report of Root and Collar Rot Caused by *Phytopythium helicoides* on Kiwifruit (*Actinidia chinensis*). *Plant Disease* **99**: 725.

2 Discrimination between the etiological role of waterlogging and soil-borne pathogen

2.1 Introduction to the study | Chapter 2

To better understand the Kiwifruit Decline, it was necessary to reproduce the disease in controlled environment, in order to inspect daily the disease progress and collect timely the tissue samples for the aetiological studies. Based on the differential analysis performed in chapter 1.1, we hypothesized that the disease could be reproduced in experimental condition only when taking into account two factors: water-logging and soil-borne pathogen(s). Thus, a simple yet original approach was used to discriminate between the role played by these two factors.

Different combinations of flooded or not flooded plants, potted in sterilized or unsterilized soil were created. While the inoculation of plants with potentially pathogenic microorganisms was an easy task solved with the collection of soil next to diseased plants, the setup of waterlogging condition required more attention. In the literature, several studies regarding susceptibility of kiwifruit to flooding conditions were found (Smith *et al.*, 1990; Reid & Petrie, 1991; Reid *et al.*, 1992) but, since none of them had addressed specifically plant-pathogen-flooding interactions, we preferred to mimic the conditions usually occurring in the field. Thus, an analysis on rainfall data series was performed for both the duration and the relative frequency of wet spells occurred after the first outbreak of KD in FVG region, and used to set up the flooding and drainage periods of the experiment.

Death rate, above/below biomass measurements, ultrastructural modification and isolation occurrence were the main results obtained from this experiment, giving for the first time, clear insights on the etiological role of waterlogging and soil-borne pathogens in KD. Even if this work does not completely solve the KD aetiology, it is the first that clearly demonstrates the need for both waterlogging and a soil-borne pathogen(s) to incite the disease. It also highlights the complexity of KD aetiology that need to be addressed via interdisciplinary approaches.

This work is currently submitted to the journal Plant and Soil.

References

Reid JB, Petrie RA. **1991**. Effects of soil aeration on root demography in kiwifruit. *New Zealand Journal of Crop and Horticultural Science* **19**: 423–432.

Reid JB, Tate KG, Brown NS. **1992**. Effects of flooding and alluvium deposition on kiwifruit (*Actinidia deliciosa*). *New Zealand Journal of Crop and Horticultural Science* **20**: 283–288.

Smith GS, Judd MJ, Miller SA, Buwalda JG. **1990**. Recovery of kiwifruit vines from transient waterlogging of the root system. *New Phytologist* **115**: 325–333.

2.2 Studies on the aetiology of kiwifruit decline: interaction between soil-borne pathogens and waterlogging

Francesco Savian[1#], Fabrizio Ginaldi[2#], Rita Musetti[1], Nicola Sandrin[1], Giulia Tarquini[1], Laura Pagliari[1], Giuseppe Firrao[1], Marta Martini[1*], Paolo Ermacora[1]

[1] Department of Agricultural, Food, Environmental and Animal Sciences (DI4A), University of Udine, Via delle Scienze 206, 33100 Udine, Italy

[2] CREA – Council for Agricultural Research and Economics, Research Centre for Agriculture and Environment, via di Corticella 133, 40128 Bologna, Italy

[#] These authors contributed equally to the work

[*] Corresponding author: Marta Martini: email: marta.martini@uniud.it

Keywords: *Actinidia deliciosa*, ITS sequencing, *Phytopythium* spp., Rainfall time series, Transmission electron microscopy, waterlogging.

ABSTRACT

Aims. In 2012, Italian kiwifruit orchards were hit by a serious root disease of unknown aetiology (kiwifruit decline, KD) that still causes extensive damage to the sector. While waterlogging was soon observed to be associated with its outbreak, the putative role of soil microbiota remains unknown. This work investigates the role of these two factors in the onset of the disease.

Methods. Historical rainfall data were analysed to identify changes that might explain KD outbreak and mimic the flooding conditions required to reproduce the disease in a controlled environment. A greenhouse experiment was thus designed, and vines were grown in either unsterilized (U) or sterilised (S) soil collected from KD-affected orchards, and subjected (F) or not (N) to artificial flooding. Treatments were compared in terms of mortality rate, growth, and tissue modifications.

Results. KD symptoms were only displayed by FU-treated vines, with an incidence of 90%. Ultrastructural observations detected tyloses and fibrils in the xylem vessels of all plants, irrespective of the treatment. Phytopythium vexans and Phytopythium chamaehyphon, isolated from roots of FU plants, emerged as the potential pathogens.

Conclusions. We succeeded in reproducing KD under controlled conditions and confirming its association with both waterlogging and pathogenic microorganism(s).

List of abbreviation

C treatment acronym for plants grown in sterilized peat and under optimal water condition.

CR cumulative rainfall (mm)

ET elapsing time between two consecutive rainfall

FD downpours causing flooding

FS treatment acronym for flooded plants grown in sterilized soil.

FU treatment acronym for flooded plants grown in unsterilized soil.

KD Kiwifruit decline

NU treatment acronym for non-flooded plants grown in unsterilized soil.

INTRODUCTION

Kiwifruit orchards cover 0.4% of Italy's agricultural land (around 26,400 ha), and the country is the second largest exporter, meeting over 15% of the global demand for this product (FAOSTAT, 2017). Bacterial canker caused by *Pseudomonas syringae* pv. *actinidiae* has always been a problem for the farmers, but since 2012, a new threat imperils Italian production (Tacconi et al., 2015). At the end of 2019, kiwifruit vine decline (KD) had destroyed over 25% of all kiwifruit orchards: Veneto 2000 ha, Piedmont 3500 ha, Lazio 1000 ha, Friuli Venezia Giulia 60 ha, and a few areas in Emilia Romagna and Calabria (Tacconi, personal communication updating Sorrenti et al., 2019). The fruit production decreased of about 200.000 tons in the last 4 years (from 550.000 tons in 2015 to 350.000 in 2018) mainly due to KD (Tacconi, personal communication). To our knowledge, the disease is still limited to Italy but there are several reports of similar vine decline disorders in other countries, which can probably be ascribed to KD: Turkey (Akilli et al., 2011; Kurbetli and Ozan, 2013, Polat et al., 2017), Japan (Huang and Qi, 1998), and New Zealand (Reid et al., 1992).

The most obvious sign of KD is a rapid, sudden and irreversible wilting of the plant. No symptoms in the canopy are displayed until the summer heat waves occur (July – August in the Northern hemisphere), then the affected vines usually die within a few weeks. Symptoms throughout the canopy are associated with extensive damage to the root system. Coarse roots usually display a reddish discoloration under the cortex and their external cylinder easily detaches from the core, giving them a "rat-tail" appearance (Online resource 1). The greatest damage directly caused by KD is the almost complete decay of the white feeding roots. When feeding roots do not deteriorate, they usually remain localized within the top 5-10 cm of the soil (Tacconi et al., 2015). Infested land has never shown sign of recovery, forcing several farmers to shift to other crops (Tacconi et al., 2019).

KD is most frequently observed in silty soils with poor drainage, which are more subjected to submersion (Sorrenti et al., 2019). Waterlogging is believed to be one of the main factors involved in

the disease (Tacconi et al., 2014; 2015; Tosi et al., 2015; Sorrenti et al., 2016, 2019), although cases of KD have been reported in well-drained soils where flooding is rare, as well as in orchards where raised bed farming techniques were employed (Sorrenti et al., 2019).

To date, most authors believe waterlogging to be the main cause of KD, and assume that pathogens play a role of little or no importance, given that no direct link has been established between symptom appearance and presence of a given microorganism (Tacconi et al., 2014; Sorrenti et al., 2016; Fontana, 2016). The involvement of a biotic stress factor in KD was first proposed by Tacconi et al. (2015), but to date, no ad hoc experiment has been performed to verify this theory. Moreover, agronomic approaches focusing only on irrigation and drainage practices have failed to explain why Italian farmers are suddenly faced with such a large-scale epidemic after 40 years of successfully kiwifruit cultivation.

This work aims at clarifying KD aetiology, investigating the role played by microorganisms and waterlogging in its onset under controlled conditions mimicking an open field environment.

MATERIAL AND METHODS

A preliminary analysis of historical rainfall data was performed to define a flooding and drying pattern that could reliably mimic the waterlogging conditions occurring in KD-affected areas. For this investigation, both the duration and relative frequency of wet spells immediately before and after the first outbreak of KD (2012) were taken into account.

The experiments then carried out included: i) greenhouse trials aimed at discriminating between the effect of flooding and soil-borne pathogens on both symptom appearance and plant growth; ii) ultrastructural observations to find signs of cell alteration brought about by to pathogen activity; iii) isolation of fungi and oomycetes to identify potential KD-associated pathogens.

A further analysis of historical rainfall data was subsequently carried out to investigate possible correlations in three local case-studies between disease outbreak and changes in rainfall patterns over the last two decades. In particular, the research focused on changes in seasonal trends, rainfall event concentration and number of floods in both diseased and unaffected sites.

Greenhouse experiments

A greenhouse trial was set up to test the role of waterlogging and/or biotic factors in the aetiology of KD under controlled conditions. Three experimental conditions provided for different water stress conditions (flooding and non-flooding) with and without soil sterilization, as summarised in Fig. 1. The treatments are defined as follows: NU are non-flooded (N) plants grown in unsterilized (U) soil; FU and FS are vines subjected to waterlogging (F), which were planted in non-sterile (U) and sterile (S) soil, respectively. FS-treated plants were considered as a negative control because preliminary investigations revealed that they displayed the same response as non-flooded vines growing in sterile soil in terms of mortality, canopy and root growth (details in Online resource 5 and 6).

Soil collection and plant material

Soil samples were collected near symptomatic plants in 3 sites of the Friuli Venezia Giulia region (FVG, North-eastern Italy) (Table 1). Topsoil (5 to 10 cm) was discarded, keeping only the soil surrounding the roots displaying “rat-tail” symptoms. The samples were then mixed together in equal proportions and 1/3 of the resulting mixture was autoclaved at 120°C for 20 minutes.

Eight-month-old micropropagated plantlets of *A. deliciosa* (A.Chev.) C.F.Liang & A.R.Ferguson cv. *Hayward* rooted in 250ml-large peat blocks were used for the experiment. Twenty vines were used for each experimental condition. Just before transplanting, 1/4 of the rooted peat block was sliced horizontally to induce the emission of new feeding roots and allow the entrance of potential pathogens. Plants were then transplanted into black plastic pots, 6.5 l in volume. Three additional

plants were potted into sterile peat and used as controls for the ultrastructural observations (C, ultrastructural control).

Table 1. Details of the experimental sites and relative soil properties.

Experimental orchards				
Location	San Giovanni di Casarsa	San Giorgio della Richinvelda	Cordenons	Udine
Latitude (°N)	45.93	46.06	46	46.03
Longitude (°E)	12.83	12.87	12.74	13.22
Stand age (years)	20	4	14	12
KD appearance	2015	2016	2015	Unaffected
Species	A. deliciosa	A. deliciosa, A. chinensis	A. chinensis	A. deliciosa
Reference weather station				
Location	Palazzolo	Vivaro	-	Udine
Latitude (°N)	45.8	46.08		46.03
Longitude (°E)	13.08	12.78		13.22
Soil properties				
Gravel (% w/w)	5	8	0	20
Sand (% w/w)	16	36	41	43
Silt (% w/w)	56	59	52	40
Clay (%w/w)	28	5	7	17
Water table depth	Superficial	None	None	None
MWC* (mm mm-1)	0.47	0.43	-	0.43
Flooding threshold# (mm d-1)	14.1	12.9	-	12.9

Water stress treatments

In the NU treatment, the soil moisture was kept slightly below field capacity, whereas both FU and FS plants were subjected to two flooding cycles. Each flooding cycle consisted of a number of flooding stages, made up of a flooding and a subsequent drainage step. Flooding was performed to induce symptom expression; the duration and frequency of this stage was estimated on the ground of the rainfall distribution recorded during the early vegetative season of kiwifruit vines in two KD-affected areas (Table 1, San Giovanni di Casarsa and San Giorgio della Richinvelda) between the

first outbreak of the disease (2012) and the start of trial (2016), (see Section 2.6 for details). The number of flooding stages in a flooding cycle was estimated on the ground of preliminary trials and set to 3, since most of plants died within this course of events (Online resource 6). A flooding cycle therefore had the following pattern: 3f-4d, 4f-4d and 5f-5d where #f is the number of consecutive days of flooding and #d is the duration of the following drainage step (Online resource 2). Flooding was mimicked by submerging the pots in buckets full of tap water with the water level maintained at least 1 cm above the soil surface. Only C plants were kept under optimal water condition for the entire duration of the trial.

Timeline

Following is a brief outline of the timeline for the operations, which is described in greater detail in Fig. 1. In late July 2017, kiwifruit plants were transplanted into sterilized or unsterilized soil collected one week beforehand. The vines were grown under optimal watering conditions until the beginning of the first flooding cycle (September 19th, 2017). Later on, FS and FU plants were flooded, while NU vines were watered regularly to keep the soil moisture just below field capacity, (Online resource 2). After the first flooding cycle, all plants were kept at optimal water conditions until bud breaking. Three weeks after this stage, the vines were irrigated so as to replicate the rainfall events recorded daily in an unaffected location (Udine): when daily rainfall was less than or equal to 15 mm/d, irrigation was applied in a single event, otherwise the plants were watered twice (morning and evening, see Online resource 2 for further details). Each irrigation supplied enough water to restore the maximum water holding capacity of the pot. At the end of July 2018, a second flooding cycle was carried out following the same schedule as the first one.

Plants were constantly monitored over the whole trial period and the canopy was examined daily during the flooding cycles to detect any sign of the disease. Sampling for ultrastructural observation and isolation was performed as outlined in Fig. 1.

Sampling protocols and data analysis

Mortality rate and dry biomass measurements. Mortality rate was measured daily during both flooding cycles, considering as dead those plants whose canopy was completely wilted. Leaf and root biomass were measured to assess the effect of each treatment and their interaction. Only roots that were directly in contact with the soil mixture, hence that had extended beyond the original peat block, were collected. These samples were then gently rinsed under running tap water to remove all soil residues. Roots and leaves were then oven-dried (60°C for 4 days) before weighting. One-way ANOVA using Rstudio (Team, 2013) was performed to compare the dry biomass and leaf/root ratio in the various treatments.

Ultrastructural observations were carried out to detect cellular modifications induced by treatments, and vascular pathogens or pathogen-specific changes in plant tissues. Fully-expanded leaves at the 6°-7° internode (60 cm height) were randomly harvested from three plants per each treatment. The three unstressed plants growing in sterile peat (C) were used as negative controls. Segments (3-4 mm in length) of leaf tissues including lateral veins and surrounding parenchyma cells were embedded in Epon-Araldite epoxy resin; ultrathin (60-70 nm) sections were cut with an ultramicrotome (Reichert Leica Ultracut E ultramicrotome, Leica Microsystems, Wetzlar, Germany) and collected on 200 mesh uncoated copper grids as described by Tarquini et al. (2019). Sections were then stained with UAR-EMS (uranyl acetate replacement stain) (Electron Microscopy Sciences, Fort Washington, PA, USA) and observed under a PHILIPS CM 10 (FEI, Eindhoven, The Netherlands) transmission electron microscope (TEM), operated at 80 kV, and equipped with a Megaview G3 CCD camera (EMSIS GmbH, Münster, Germany). Five non-serial cross-sections from each sample were analysed.

Fungi and oomycetes isolation and identification. Fungi and oomycetes were isolated from the roots of plants displaying KD symptoms. Only roots with a diameter of less than 5 mm were used.

The samples were rinsed under running tap water, surface sterilized in sodium hypochlorite 2% for 1 minute and rinsed twice in sterilized water for 2 minutes. The overall sterilization process was repeated twice. Eight slices of root tissue were cut 3-10 mm above the rotting/healthy tissue interface of each plant. The slices were placed into two 90 mm Petri dishes containing potato dextrose agar (PDA; Oxoid Ltd) and streptomycin (100 µg/ml; Sigma-Aldrich). The Petri dishes thus inoculated were incubated in a growth chamber and kept in the dark for 48 h at 24°C. Each fungal colony was sub-cultured at least five times.

After isolation, the colonies were grouped according to macroscopic morphological features (colour, margin shape and growth rate). For every plant, at least one colony per morphological group was selected for further molecular analyses. A maximum of 300 mg mycelia was collected by scraping the surface of 7- or 14-day-old colonies and stored at -20°C until DNA extraction. High-molecular-weight DNA was extracted using the procedure described by Lecellier and Silar (1994) with slight modifications (Martini et al., 2009). The nuclear rDNA internal transcribed spacer regions (ITS1 and ITS2) and the 5.8S rRNA gene were amplified by PCR using the universal primers ITS1 and ITS4 (White et al., 1990). Amplifications were performed with an automated thermal cycler (MJ Research DNA Thermal Cycler PTC-100) in a 25-µL solution containing 200 µM each of the four dNTPs, 0.4 µM of each primer, 1.5 mM MgCl2, 0.625 units of DNA polymerase, GoTaq-Flexy (Promega), and 1 µL of 2 ng/µL diluted DNA. The PCR programme consisted of: 2 minutes at 94 °C followed by 35 cycles of 40 s at 94 °C; 30 s at 56 °C, 50 s at 72 °C and a final extension cycle of 7 minutes at 72 °C. The PCR reaction was checked by performing a 1% agarose gel electrophoresis in 1X TAE (60 min). PCR products of isolates belonging to the less common morphological groups were directly Sanger sequenced, whereas the PCR products obtained from the more common ones were digested using Tru1I and HinfI enzymes (Fermentas Ltd). RFLP patterns were visualized on 2% agarose gel electrophoresis in 1X TBE, and compared within each morphological group to separate the isolates

into molecular groups. At least one isolate per molecular group was selected for Sanger sequencing using the ITS4 primer (Genechron laboratories, Ylichron S.r.l, Italy). Sequences were then compared with BLAST algorithms against NCBI GenBank database for taxonomical identification (Altschul et al., 1990).

Historical rainfall data analysis

Rainfall data from 1998 to 2018 recorded by the meteorological stations in Vivaro, Palazzolo and Udine (Friuli Venezia Giulia, FVG, north-eastern of Italy), were downloaded from the OMNIA regional weather database (Cicogna et al., 2015) (Table 1). The first orchards to be affected by KD were located near Vivaro and Palazzolo (2012-2014), whereas to date, Udine still seems to be free of the disease. The first case of KD was officially diagnosed in FVG in 2014 (Savian et al., 2017), but by combining farmers' accounts with Google Earth historical satellite data (Google LLC, 2019) we were able to trace the first outbreak back to 2012 (S. Saro, personal communication).

In order to verify a possible link between KD and waterlogging, we examined rainfall data during the early vegetative (March-May) and ripening (August-October) stages of kiwifruit vines, given that during those months: i) floods are usually more frequent; ii) the temperature allows microorganism development; iii) plants are not dormant, and iv) root decay is potentially more harmful. Indeed, kiwifruit vines only have one major rooting phase, i.e. in late summer/early autumn (Buwalda and Hutton, 1988). When roots deteriorate during or after this period, the plants tend not to restore the root system in the following vegetative season because of the strong competition of shoots and fruits.

We investigated the pattern of rainfall events in these two periods, taking into account the duration of wet spells, the average time span between two consecutive wet periods (ET, used as a proxy of rainfall concentration over time), cumulative rainfall evolution (CR) and the frequency of flood-causing downpours (FD).

The analysis of rainfall data in affected areas from the first outbreak of the disease (2012) to the beginning of the experiments (2016) allowed us to define the duration of the flooding and drainage steps used in the greenhouse trials. The number of wet spells (classified by length: 1, 2, ≥3 days) occurring during the early vegetative stage determined the reference duration of the flooding step, while mean ET determined that of the drainage step.

The rainfall time series over the last two decades was analysed to identify changes in trends, rain intensity and distribution that could explain the sudden and widespread diffusion of the disease after 2012, considering data from both diseased and unaffected locations.

A preliminary flat step analysis and piecewise regression was carried out on the cumulative rainfall time series to detect any change points (Mariani, 2008; Chiaudani et al., 2008). The first analysis splits a time series into stationary sub-periods identifying the transition point from one climatically homogeneous phase to another characterized by different mean values. The latter method detects the initial changing moment of the system, discerning internal trends of the series.

The Theil-Sen nonparametric method was applied to identify any linear trends in CR data (Helsel, 2005) and the Mann-Kendall test was subsequently used to assess the significance of the resulting slope (Mann, 1945; Kendall, 1975). The Theil-Sen estimator is based on the idea that if a simple slope estimate is computed for every pair of distinct measurements in a sample, the average of this series of slope values should approximate the true value.

Moreover, frequencies of FD and mean ET before and after the first outbreak of the disease (2012) were compared in every location using the Mann-Whitney-Wilcoxon test.

The estimation of frequency of FD and mean ET was based on the following assumptions: i) a day was considered rainy when more than 1 mm fell, and ii) a downpour causes flooding when the rain fallen exceeds soil saturation, which we estimated by multiplying root depth by the maximum water

content of the soil. Root depth was set at 30 cm from the soil surface, because this is the region where most of the superficial root system of kiwifruit resides. Maximum water content was estimated from soil texture composition using the SPAW models (Saxton and Willey, 2005). Soil properties (texture, maximum water content and saturation volume) are listed in Table 1. All the analyses were performed using R statistical software (Team, 2013).

RESULTS

Definition of flooding cycles

Analyses of the duration of rainy spells during the period 2012 to 2016 revealed that most rainfall events in the affected areas (Palazzolo, Vivaro) lasted 1-2 days, although more prolonged rainy periods (≥ 3 consecutive days) were not rare and occurred at least twice a year (Fig. 2a, b). The time elapsing between two consecutive events averaged 4.8 days (Fig. 2c, d). In the light of these data, flooding conditions for the greenhouse experiments were set with a reference combination of 3 days flooding followed by 4 days of drainage. This flooding/drainage combination was used in the first flooding stage of the cycle; in the following ones, the duration of the flooding step was progressively increased, so that each flooding cycle consisted of three stages, which can be summarized as follows: 3f-4d; 4f-4d; 5f-5d where #f is the number of consecutive days of flooding and #d is the duration of the following drainage step.

Symptoms, mortality rates, and biomass measurements

The experimental design proved successful in reproducing KD symptoms in a controlled environment. No signs of the disease were observed during the first flooding cycle in September 2017. Symptoms were first detected in July 2018 during the second flooding cycle, just after the first flooding stage (Fig. 3). Wilting always started from the basal leaves and quickly moved upwards, usually ending with the all leaves falling. Complete wilting occurred 7 to 10 days after the first symptoms appeared. The severity of wilting and the number of damaged plants increased as the flooding cycle progressed. No sign of recovery was ever observed once wilting began.

FS vines successfully colonized the entire pot, displaying healthy white feeding roots, whereas the roots of NU plants extended just a few centimetres beyond the peat block and, in a small number of cases, exhibited a partial rotting of the smaller feeding roots (Fig. 3f, g). On the other hand, FU plants displayed the classical KD symptoms: a serious deterioration of the feeding roots, rotting tissues in the smaller (<5 mm) coarse roots, a reddish discoloration beneath the cortex of coarse roots, and a rat-tail appearance (Fig. 3h).

By the end of the trial period, most (90%) FU plants revealed KD symptoms whereas FS and NU vines had none (Fig. 3). However, highly significant differences ($P<0.001$) were observed between both root dry weight and leaf dry weight of FS and NU plants, as well as in their ratio (Fig. 4); the dry weight of FU vines was not measured, given their severe reduction in secondary roots and abundant loss of leaves. FS plants had approximately double the amount of roots and leaves than NU-treated ones, and also had a more balanced leaf/root ratio, almost half that of NU vines.

Ultrastructural observations

Ultrastructural observations revealed tyloses and fibrils in the xylem vessels (Fig. 5) of all the treated vines (FS, NU and FU), but not the controls (C, non-flooded plants growing in sterile peat). Gums

adhering to the cell walls were found in all samples. Tyloses and fibrils appeared to be more abundant in FU vines than in NU and FS ones. No pathogen-related structures (hyphae, conidia) were found in the xylem and likewise, no pathogen-related symptoms (such as xylem cell wall deterioration) were observed. Finally, no unusual alteration of the parenchyma and phloem cells was detected.

Isolation results

128 Isolates were obtained from the roots of the 18 symptomatic FU-treated plants. A total of 21 morphological groups were identified on the ground of their macroscopic characteristics, and RFLP analysis made it possible to further characterize the major morphological groups (Online resource 3 and 4). After morphological and molecular grouping, 76 isolates were selected for Sanger sequencing of their ITS region. Identification revealed 42 unique sequences ascribable to 23 different species. Families with the highest occurrence were Hypocreaceae, Ceratobasidiaceae, Pythiaceae, and Nectriaceae (56, 67, 89 and 100%, respectively), but as regards the species, only *Fusarium solani* (78%), *Phytopythium chamaehyphon* (61%) and *Phytopythium vexans* (56%) were frequently found, Fig. 6. *F. solani* presented several sequence types (8 unique sequences) but none of them had a high frequency of occurrence (less than 22%). As regards *P. vexans*, only one sequence was slightly different (two SNPs) from all the others. All the sequences of *P. chamaehyphon* were identical. Information regarding isolation, including accession numbers of the isolates from this study, is reported in Online resource 8.

Historical rainfall data analysis

Descriptive statistics of rainfall time series revealed that the average cumulative rainfall (CR) during the early vegetative stage of kiwifruit vines differed quite extensively between the two diseased areas over the years 1998 to 2018: 281 mm in Palazzolo and 401 mm in Vivaro. As regards the ripening stage, the CR in the two areas was of 342 and 456 mm, respectively. The pluviometric regime in the unaffected area (Udine) had intermediated values, with an average of 350 mm during the early

vegetative stage and 437 mm in the fruit ripening one. In 2013, rainfall peaks during the early vegetative stage were noteworthy both in terms of cumulative rainfall (1012 mm in Palazzolo, 1052 mm in Vivaro and 1129 mm in Udine Fig. 7a-c) and wet spell duration (Fig. 7).

Change point analysis identified no significant transition points in the CR data series. Overall, slight negative trends were detected in the CR of both early vegetative and ripening stages (Fig. 7a-c), which were generally not significant, except in two cases (Palazzolo during the vegetative stage, Udine during ripening).

Frequency of flood-causing downpours (FD) in the two affected locations differed extensively (an average of 5.7 and 6.9 events in Palazzolo during the early vegetative and ripening stages, respectively, vs. 9.0 and 10.0 in Vivaro) but was very similar between Vivaro and the unaffected site (i.e. Udine, with 9.2 and 10.6 events, respectively, Fig. 7d-f and Fig. 7j-l).

As regards inter-event time, the mean elapsed time (ET) between two consecutive wet spells was similar for all the locations: 4.5 and 4.9 days in Vivaro during the early vegetative and ripening stages, respectively, 4.9 and 5.1 days in Udine, 5.4 and 5.6 days in Palazzolo (Fig. 7g-k and Fig. 7m-o).

No increase in flood-causing downpours was observed nor in the frequency of rainy events; no significant differences in mean FD (Fig. 7d-f and Fig. 7j-l) and mean ET (Fig. 7g-k and Fig. 7m-o) were detected before and after first outbreak of KD in 2012 (Mann-Whitney, $P > 0.15$, Online resource 7).

DISCUSSION

The aetiology of KD has been puzzling the Italian kiwifruit sector for the last seven years (Sorrenti et al., 2019). The swiftness with which this syndrome has spread across Northern Italy and the astonishingly rapid progress it has made throughout the affected areas would suggest the involvement of an aggressive, invasive alien pathogen, but the attempts to find the infective agent have failed.

The renowned susceptibility of kiwifruit vine to waterlogging (Savé and Serrano, 1986, Smith et al., 1990; Reid and Petrie, 1991; Reid et al., 1991; J. B. Reid et al., 1992), combined with the frequent occurrence of KD in poorly drained soils (Tacconi et al., 2014, 2015; Tosi et al., 2015; Sorrenti et al., 2016), misled the first researchers investigating its aetiology, who identified waterlogging as the main cause of KD. In particular, i) Smith et al. (1990) observed that flooding caused the cortex to separate from the central stele of the root, in a manner similar to that caused by KD; ii) a sudden plant wilting was described by Reid et al. (1991) right after floods caused by a cyclone; and iii) a reduction in root growth due to prolonged or transient flooding was reported by Savé and Serrano (1986) and Smith et al. (1990), respectively. Moreover, waterlogging changes the above/below ground biomass ratio, because shoots are only marginally affected whereas roots are strongly inhibited (Savé and Serrano, 1986).

The hypothesis of waterlogging as the causal agent of KD however, did not hold up against the analysis of rainfall data series, which, as reported previously, failed to highlight any change over the last two decades that could explain the outbreak of KD. Indeed, the cumulative rainfall trend during the most susceptible stages seemed to decrease in both affected and unaffected areas. The number of flood-causing downpours (FD) and their frequency (ET) displayed no particular pattern in either diseased or unaffected area, both before and after first disease outbreak (2012). Nonetheless, it is interesting to note that even if the first KD outbreak in FVG dates back to 2012, the disease escalated in 2014 (Savian et al., 2017) during a hot and dry vegetative season preceded by the rainiest year in

the last two decades (2013). Although the historical rainfall analysis approach used in this work did not employ soil water models to predict water stagnation, the indications were clear enough to discard the hypothesis of a major climatic change in rainfall distribution as the sole cause of the first outbreaks of KD.

For the first time, our results clearly reveal that waterlogging is a prerequisite for the deteriorations of feeding roots and the onset of the decline syndrome, but also that a soil-borne pathogen must be present to induce the disease.

The greenhouse experiments were successful in reproducing unequivocal symptoms of KD in both the roots and canopy of *A. deliciosa* cv. Hayward. These results were consistent with those of the trials performed in the field, both in terms of kiwifruit vine physiology and environmental conditions.

The vines were planted in August, so as to take full advantage of the most active period for rooting (Buwalda & Hutton, 1988). Moreover, the flooding cycles mimicked the rainfall conditions that usually occur in the Friuli-Venezia Giulia region. Moreover, three or more days of flooding have been reported as sufficient to weaken kiwifruit plants (Savé & Serrano, 1986; Smith et al., 1990). Our ultrastructural observation of the lumina of the xylem vessels revealing the presence of tyloses and fibrils, confirmed the stressing effect of the flooding conditions employed during the trial. Tyloses and fibrils are indeed unspecific plant stress responses (De Micco et al. 2016) that have been linked to both flooding condition (Davison and Tay 1987) and/or pathogen infection (Dimond 1955; Davison 2014; De Micco et al. 2016).

By prolonging the flooding step as the trial progressed, we promoted the progressive expression of KD symptoms, allowing a better characterization of the disease. As observed in the field (Tosi et al., 2015; Tacconi et al., 2015), flooded plants grown in unsterilized soil (FU) suddenly die during the second flooding cycle, and their death is associated with a greatly unbalanced leaf/root ratio and high environmental temperatures. The results of this investigation confirm those obtained during the

preliminary trial where, once again, 88% of the plants died when flooding was applied on unsterile soil (Online resource 5 and Online resource 6), thus strengthening the reliability of our protocol in reproducing KD.

Our results are consistent with a model where pathogen aggressiveness is enhanced by waterlogging. On one hand, our measurements revealed highly significant differences in the dry weight of roots and leaves (and in their ratio) harvested from plants growing in sterilised and non-sterile, indicating that the severe damage to the kiwifruit root system was caused by microorganism(s) present in soil. On the other, the evidence of obvious KD symptoms in FU vines and their absence in NU ones highlighted the dramatic effect of flooding and its ability to promote an unbalanced above/below ground biomass ration in the presence of pathogen infection. The reason for the marginal effect of waterlogging observed in plants grown in sterile soil can be ascribed to the flooding conditions employed, which were intentionally calibrated to induce bearable stress. Indeed, kiwifruit vines respond to root loss caused by transient waterlogging, i.e. lasting less than 5 days, by sprouting new roots (Smith et al., 1990). The hypothesis of a synergy between soil-borne pathogens and waterlogging is also supported by the larger amount of tyloses and fibrils found in the vessels of FU plants, as compared to the other treatments and the controls.

The results of the isolations provided a first idea of the potential soil-borne pathogens associated with KD. Given the frequency of their occurrence and the data yielded from ITS sequence analyses, the major candidates would appear to be *P. chamaehyphon* and *P. vexans*. *F. solani* was also consistently isolated but, considering the lower occurrence of the many sequence types found and that there is no record of its association with kiwifruit root rot, its role as the primary cause of KD appears unlikely, although there are some reports of its indirect involvement in decline-like diseases (Porta-Puglia & Corazza, 1985; Huang & Qi, 1998).

Conversely, Oomycetes have been frequently reported as causal agents of root rot in kiwifruit vines (Latham & Dozier, 1989; Conn et al., 1991; Latorre & Alvarez, 1991; Stewart & McCarrison, 1992; Akilli et al., 2011; Kurbetli & Ozan, 2013; Çiftçi et al., 2016). Polat et al. (2017) isolated *P. vexans*, a pathogen associated with root and collar rot, from kiwifruit in Turkey. The ITS region of one of these isolates (acc. KY24339) shared a high sequence similarity with that of the strains isolated by us. *P. chamaehyphon* has never been reported to be a potential pathogen for kiwifruit, although a closely related species, *Phytopythium helicoides*, has been previously associated with root and collar rot of kiwifruit in China (Wang et al., 2015). In this respect, it should be noted that neither the symptomatology nor the aggressiveness of the cases reported in the cited literature perfectly match those observed in Italy. No crown or trunk rotting has ever been observed in vines affected by KD; moreover this disease has rapid spread patterns within and between seasons, and the infected orchards never recover.

The results obtained allow us to speculate about the dynamics of the disease and the sudden appearance of the symptoms. The ability of kiwifruit vines to take up great amounts of water when available (Xiloyannis et al., 1993), together with the large size of its xylem vessels and the may pits, allows the plants to rapidly take up and relocate water where needed (Dichio et al., 1999, 2013). Kiwifruit vines can therefore endure consistent reductions in the size of their root system (up to 80%) before limiting their shoot growth rates (Black et al., 2011), as long as water is not a limiting factor. However, this can be a double-edged sword, since: i) the large vessels make kiwifruit more susceptible to vessel occlusion by tyloses and gums (De Micco et al., 2016), and ii) the great ability to take up and translocate water might mask a compromised root system. Therefore, Kiwifruit vines could have developed an abundant canopy in springtime even in the presence of severe root deterioration. When the first heat waves occur, transpiration rate could then easily exceed uptake capability of the root system, leading to the sudden wilting of the whole plant.

CONCLUSIONS

This is the first comprehensive approach to KD and the first demonstration of the synergic, necessary interaction between waterlogging and soil-borne pathogens for the onset of the disease. We have also defined a reliable protocol to reproduce KD in a controlled environment.

Several aspects require further investigations to clarify the dynamics of this new disease. A better understanding of the root deterioration processes is needed to improve sampling times and strategy in both controlled-environment trials and open-field systems. Detection methods need to be defined, in order to promptly evaluate the health status of the vines. In this respect, remote sensing technologies such as image analysis in non-visible spectra and/or transpiration rate measurements might prove helpful to reveal compromised plants and predict potential outbreaks of this disease.

Finally, a further characterization of the role played by each factor in root decay as well as pathogenicity tests to confirm Koch's postulates are necessary to fully clarify the aetiology and sustain our preliminary indications about the involvement of one or more oomycete species in KD.

AUTHOR CONTRIBUTION

All authors contributed to the experimental design and the writing of this paper, and more specifically: statistical analysis of rainfall series FG; interpretation of rainfall analysis FS, FG; TEM sample preparation, observation and interpretation FS, LP, RM; Isolation and identification of isolates FS, GT, MM, NS; Interpretation of greenhouse trial FS, PE, RM, MM, GF.

ACKNOWLEDGMENTS

Dr. Simone Saro, from ERSA- Phytosanitary Service of Friuli Venezia Giulia region (Italy), for his collaboration and support in field-scouting activities. Mr. Borselli Stefano and Mr. Alberto Loschi from University of Udine, for their professional advice and help when setting up the experiment and throughout the entire duration of the trial. Mr. Arrigo Toffolutti, from Toffolutti's nursery, for supplying kiwifruit plantlets.

REFERENCES

Akilli S, Serçe ÇiU, Zekaİ Katircioğlu Y, Karakaya A, Maden S. **2011**. Involvement of *Phytophthora citrophthora* in kiwifruit decline in Turkey. *Journal of Phytopathology* **159**: 579–581.

Black MZ, Patterson KJ, Minchin PEH, Gould KS, Clearwater MJ. **2011**. Hydraulic responses of whole vines and individual roots of kiwifruit (*Actinidia chinensis*) following root severance. *Tree Physiology* **31**: 508–518.

Buwalda JG, Hutton RC. **1988**. Seasonal changes in root growth of kiwifruit. *Scientia Horticulturae* **36**: 251–260.

Chiaudani A, Berti A, Borin M, Mariani L. **2008**. Piecewise and strucchange: test of two methods of change point analysis in agroclimatology. In: S.Michele all'Adige, Italy: Rivista Italiana di Agrometeorologia.

Cicogna A, Medeossi R, Bellan A, Gimona A, Stefanuto L, Micheletti S. **2015**. Omnia: a new tool for the management of meteorological data. *Italian journal of agrometeorology* **20**: 73–80.

Çiftçi O, Serçe ÇU, Türkölmez Ş, Derviş S. **2016**. First Report of *Phytophthora palmivora* causing crown and root rot of kiwifruit (Actinidia deliciosa) in Turkey. *Plant Disease* **100**: 210.

Conn KE, Gubler WD, Mircetich SM, Hasey JK. **1991**. Pathogenicity and relative virulence of nine *Phytophthora* spp. from kiwifruit. *Phytopathology* **81**: 974–979.

Davison EM. **2014**. Resolving confusions about jarrah dieback - don't forget the plants. *Australasian Plant Pathology* **43**: 691–701.

Davison EM, Tay FCS. **1987**. The effect of waterlogging on infection of eucalyptus margin at a seedlings by *Phytophthora cinnamomi*. *New Phytologist* **105**: 585–594.

De Micco V, Balzano A, Wheeler EA, Baas P. **2016**. Tyloses and gums: a review of structure, function and occurrence of vessel occlusions. *IAWA Journal* **37**: 186–205.

Dichio B, Baldassarre R, Nuzzo V, Biasi R, Xiloyannis C. **1999**. Hydraulic conductivity and xylem structure in young kiwifruit vines. *Acta Horticulturae*: 159–164.

Dichio B, Montanaro G, Sofo A, Xiloyannis C. **2013**. Stem and whole-plant hydraulics in olive (*Olea europaea*) and kiwifruit (*Actinidia deliciosa*). *Trees* **27**: 183–191.

Dimond AE. **1955**. Pathogenesis in the Wilt Diseases. *Annual Review of Plant Physiology* **6**: 329–350.

FAOSTAT. **2016**. Food and Agriculture Organization of the United Nations, Rome, Italy.

Fontana E. **2016**. La moria del kiwi avanza verso il nord-ovest. *www.freshplaza.it/article/4086587/la-moria-del-kiwi-avanza-verso-il-nord-ovest/*.

Google LLC. **2019**. *Google earth Pro*. Google LLC.

Huang Y, Qi P. **1998**. Studies on the cause of root rot of kiwifruit in Guangdong Province. *Journal of South China Agricultural University* **19**: 19–22.

Kurbetli İ, Ozan S. **2013**. Occurrence of *Phytophthora* Root and Stem Rot of Kiwifruit in Turkey. *Journal of Phytopathology* **161**: 887–889.

Latham AJ, Dozier WA. **1989**. Root Rot of Kiwi (*Actinidia chinensis*) Caused by *Pythium ultimum*. *Plant Disease* **73**: 938.

Latorre BA, Alvarez C, Ribeiro OK. **1991**. *Phytophthora* root rot of kiwifruit in Chile. *Plant Disease* **75**: 949–952.

Lecellier G, Silar P. **1994**. Rapid methods for nucleic acids extraction from Petri dish-grown mycelia. *Current Genetics* **25**: 122–123.

Mariani L. **2006**. Some methods for time series analysis in agrometeorology. *Rivista Italiana di Agrometeorologia*: 48–55.

Martini M, Musetti R, Grisan S, Polizzotto R, Borselli S, Pavan F, Osler R. **2009**. DNA-dependent detection of the grapevine fungal endophytes *Aureobasidium pullulans* and *Epicoccum nigrum*. *Plant Disease* **93**: 993–998.

Polat Z, Awan QN, Hussain M, Akgül DS. **2017**. First Report of *Phytopytium vexans* Causing Root and Collar Rot of Kiwifruit in Turkey. *Plant Disease* **101**: 1058.

Porta-Puglia A, Corazza L. **1985**. *Fusarium solani* (Mart.) Sacc. associato ad un marciume del colletto dell'Actinidia. *Rivista di ortoflorofrutticoltura italiana* **69**: 81–83.

Reid JB, Petrie RA. **1991**. Effects of soil aeration on root demography in kiwifruit. *New Zealand Journal of Crop and Horticultural Science* **19**: 423–432.

Reid JB, Tate KG, Brown NS. **1992**. Effects of flooding and alluvium deposition on kiwifruit (*Actinidia deliciosa*). *New Zealand Journal of Crop and Horticultural Science* **20**: 283–288.

Reid JB, Tate KG, Brown NS, Cheah LH. **1991**. Effects of flooding and alluvium deposition on kiwifruit (*Actinidia deliciosa*): 1. Early vine decline. *New Zealand Journal of Crop and Horticultural Science* **19**: 247–257.

Savé R, Serrano L. **1986**. Some physiological and growth responses of kiwi fruit (*Actinidia chinensis*) to flooding. *Physiologia Plantarum* **66**: 75–78.

Savian F, Martini M, Borselli S, Saro S, Musetti R, Loi N, Firrao G. **2017**. Studies on kiwifruit decline, an emerging issue even for Friuli Venezia Giulia (eastern Italy). *Journal of Plant Pathology* **99**: 18.

Saxton KE, Willey PH. **2005**. The SPAW model for agricultural field and pond hydrologic simulation. *Watershed models*: 400–435.

Smith GS, Judd MJ, Miller SA, Buwalda JG. **1990**. Recovery of kiwifruit vines from transient waterlogging of the root system. *New Phytologist* **115**: 325–333.

Sorrenti G, Tacconi G, Tosi L, Vittone G, Nari L, Savian F, Saro S, Ermacora P, Graziani S, Toselli M. **2019**. Avanza la "moria del kiwi": evoluzione e primi riscontri della ricerca. *Frutticoltura* **2**: 34–42.

Sorrenti G, Toselli M, Reggidori G, Spinelli F, Tosi L, Giacopini A, Tacconi G. **2016**. Implicazioni della gestione idrica nella "Moria del kiwi" del veronese. *Frutticoltura* **3**: 1–7.

Stewart A, McCarrison AM. **1992**. Pathogenicity and relative virulence of seven *Phytophthora* species on kiwifruit. *New Zealand Journal of Crop and Horticultural Science* **19**: 73–76.

Tacconi G, Giacopini A, Tosi L. **2014**. La Moria Del Kiwi Nel Veronese. *Kiwi informa* **Aprile/Giugno**: 5–23.

Tacconi G, Giacopini A, Vittone G, Nari L, Spadaro D, Savian F, Ermacora P, Saro S, Morone C, Bardi L, *et al.* 2019. "moria del kiwi": situazione disastrosa al nord, preoccupante nel resto d'italia. *Kiwi informa* **Aprile/Giugno**: 32–37.

Tacconi G, Paltrinieri S, Mejia JF, Fuentealba SP, Bertaccini A, Tosi L, Giacopini A, Mazzucchi U, Favaron F, Sella L, *et al.* 2015. Vine decline in kiwifruit: climate change and effect on waterlogging and *Phytophthora* in north italy. *Acta Horticulturae*: 93–97.

Tarquini G, Zaina G, Ermacora P, De Amicis F, Franco-Orozco B, Loi N, Martini M, Bianchi GL, Pagliari L, Firrao G, *et al.* 2019. Agroinoculation of Grapevine Pinot Gris Virus in tobacco and grapevine provides insights on viral pathogenesis. *PLoS ONE* **14**.

Team RC. **2013**. R: A language and environment for statistical computing.

Tosi L, Tacconi G, Giacopini A. **2015**. La moria del kiwi, situazione e prospettive. *L'Informatore Agrario* **44**: 67–70.

Wang KX, Xie YL, Yuan GQ, Li QQ, Lin W. **2015**. First Report of Root and Collar Rot Caused by *Phytopythium helicoides* on Kiwifruit (*Actinidia chinensis*). *Plant Disease* **99**: 725.

White TJ, Bruns T, Lee S, Taylor JL. **1990**. Amplification and direct sequencing of fungal ribosomal RNA genes for phylogenetics. *PCR protocols: a guide to methods and applications* **18**: 315–322.

Xiloyannis C, Massai R, Piccotino D, Baroni G, Bovo M. **1993**. Method and technique of irrigation in relation to root system characteristics in fruit growing. *Acta Horticulturae*: 505–510.

FIGURES CAPTIONS

Fig 1. Overview of the greenhouse trials and their timeline. The sequence of processes is depicted in grey; tick boxes indicate the processes carried out on the different treatments. Grey circles (1,2,3) are the flooding stages. FS (green) are flooded (F) plants grown in sterile (S) soil; FU (orange) are flooded (F) vines planted in non-sterile soil (U); NU (blue) are non-flooded (N) plants in non-sterile (U) soil. In yellow, observation period for symptoms of wilting. In purple, sample collection for ultrastructural observations; in red, for biomass evaluation; in light blue, for the isolation of fungi/oomycetes.

Fig. 2. Rainfall distribution parameters taken into account to define the flooding cycle. Rainfall data during the early vegetative stage (March-June) of kiwifruit vines growing in diseased areas (Palazzolo, a, c; Vivaro, b, d) from the first outbreak of KD (2012) to the beginning of the greenhouse trials (2016). The number of wet spells (a, b) is depicted in blue: the darkness of the shade is proportional to the duration of the rainy spell (1, 2, 3 days or more). In green, the average elapsed time (ET) between two consecutive rainfalls (c, d).

Fig. 3. Evolution of wilting symptoms during the second flooding cycle (July 2018). a) Watering regime (WR): blue triangles depict when NU (non-flooded, in non-sterile soil) vines were watered; light blue rectangles indicate for how many days the plants grown in sterile (FS) and non-sterile soil (FU) were waterlogged. b) Mean (red line), maximum and minimum (light red shaded area) air temperature values inside the greenhouse. c-e) Number of healthy (green) and wilted (orange) plants per treatment. f-h) Images of representative plants for each treatment at the end of the trial period.

Fig. 4. Comparison of dry biomass values. In the box plot: comparison of root (a) and leaf (b) dry biomass, and leaf/root ratio (c) between flooded vines grown in sterile soil (FS) and non-flooded ones in non-sterile soil (NU). All the parameters differed in a highly significant manner ($P<0.001$).

Fig. 5. TEM micrographs of xylem vessels of A. deliciosa cv. Hayward subjected to different combinations of water supply and soil sterilization conditions. Whole cells (a-d) and details (e-f) of xylem vessels (Xy). Sections of plants grown in non-sterile (FU; a, e) and sterile soil (FS; c, g) and subjected to flooding; not subjected to flooding, and growing in non-sterile soil (NU; b, f) and sterile peat (C; d, h). Tyloses (t) are visible in a), e) and b), fibrils (fi) in a), c) and e). Gum deposits (arrows) are visible in all samples (a-h). Scale bar = 2 μm.

Fig. 6. Isolation results from eighteen diseased plants grown in non-sterile soil and subjected to flooding. Occurrence of isolated Fungi and Oomycetes are shown at family (green), genus (blue) and species (light blue) levels.

Fig. 7. Statistical analysis of historical rainfall data over the last two decades (1998-2018) in Palazzolo, Vivaro and Udine (North-eastern Italy). In green, data relative to the early vegetative stage (March-May); in orange, relative to ripening (August-October). a-c) Cumulative rainfall (CR) and corresponding Theil-Sen trends (continuous lines) and observed data (dots and squares); the significance of the trend slopes is also shown ($P<0.05$). d-f, j-l) Number of flooding events (FD). g-i, m-o) elapsed time (ET) between two consecutive rainfalls; from light to dark, the 10th, 50th and 90th percentile. The light blue background highlights the time interval since the first appearance of kiwifruit decline in FVG.

SUPPLEMENTARY MATERIAL

Online Resource 1. Kiwifruit decline symptoms and spreading patterns. A) KD spreading pattern in a diseased orchard located in San Giorgio della Richinvelda, Friuli Venezia Giulia, Italy, from 2015 (A1), when the symptoms first appeared to 2017 A2); pictures downloaded from the Google Earth Archive. B) KD infection on the canopy2 years (B1) and 1 week (B2) after the first appearance of symptoms, respectively. C) Details of symptomatic roots and leaves. C1, "rat-tail" symptoms; C2, reddish discolouration under the cortex; C3 deterioration of the fine roots; C4, leaf deformation (wilting); C5 scorched leaves.

Online Resource 2. Weather trends and watering regime during the trial. a) Daily air temperature and rainfall trends recorded by the weather station in Udine (NE of Italy) during the trial period, i.e. June 2017-July 2018; b) and c) greenhouse temperature and watering regime during the flooding cycles in September 2017 (b) and July 2018 (c). In a): The gray background highlights periods with optimal water supply (OWC) for all the experimental treatments; the light blue background is rainfall-driven irrigation (RD) with red dashed line highlighting the 15 mm threshold set for the double irrigation; the green background underline is the period when flooding cycles were applied (FC). Blue bars are used for daily rainfall in a); red, orange, yellow, lines for maximum, average, and minimum temperature, respectively, in a), b) and c). the light blue rectangle in b) and c) shows the duration of the forced flooding in FU and FS treatments; the black arrows in b) and c) indicate when NU plants were irrigated.

Online Resource 3. RFLP patterns of isolates belonging to morphological groups 1 and 7. Numbers above the lanes correspond to the identification code ID_I of the single colonies as reported in Online Resource 8. Ladder lanes contain the phiX174 DNA/*BsuR*I-*Hae*III marker (Thermo Scientific™).

Online Resource 4. RFLP profiles of isolates belonging to morphological groups 10, 5, 9, 23 and 6. Numbers above the lanes correspond to the identification code ID_I of the single colonies as reported

in Online Resource 8. Ladder lanes contain the phiX174 DNA/*Bsu*RI-*Hae*III marker (Thermo Scientific™).

Online Resource 5. Wilting appearance during the preliminary trial in a controlled environment.

Online Resource 6. Frequencies of flooding downpours (FD) and mean elapsed time (ET) before and after disease outbreak (2012). The header reports the combination of all the experimental factors as described in Online Resources 5, whereas the table lists the number of wilted plants observed throughout the experiment. Wilting was only observed in flooded vines growing in non-sterile soil.

Online Resource 7. Identification of isolates from roots of symptomatic plants. Average values +/- standard deviation and *P* values (Mann-Whitney test) are reported for both early vegetative (March-June) and ripening (August-October) stages in all the sites.

Online Resource 8. Identification of isolates from roots of symptomatic plants. ID_I, identification code of each isolate. ID_P, Identification code of each plant (flooded on unsterile soil) from which the isolates were taken. ID_M, morphological group based on colony colour, shape and growth speed. ID_R, molecular group codes: each letter identifies a unique combination of two RFLP profiles obtained after HinfI and Tru1I digestion; "." samples that were not digested and directly sequenced. The NCBI sequence used as reference for isolate identification and the corresponding percentage of identity are reported in the NBCI result and Identity columns, respectively. The NCBI accession numbers of our sequences are listed in the last column. Sequences with uncertain identification were not submitted.

Fig. 1. Overview of the greenhouse trials and their timeline.

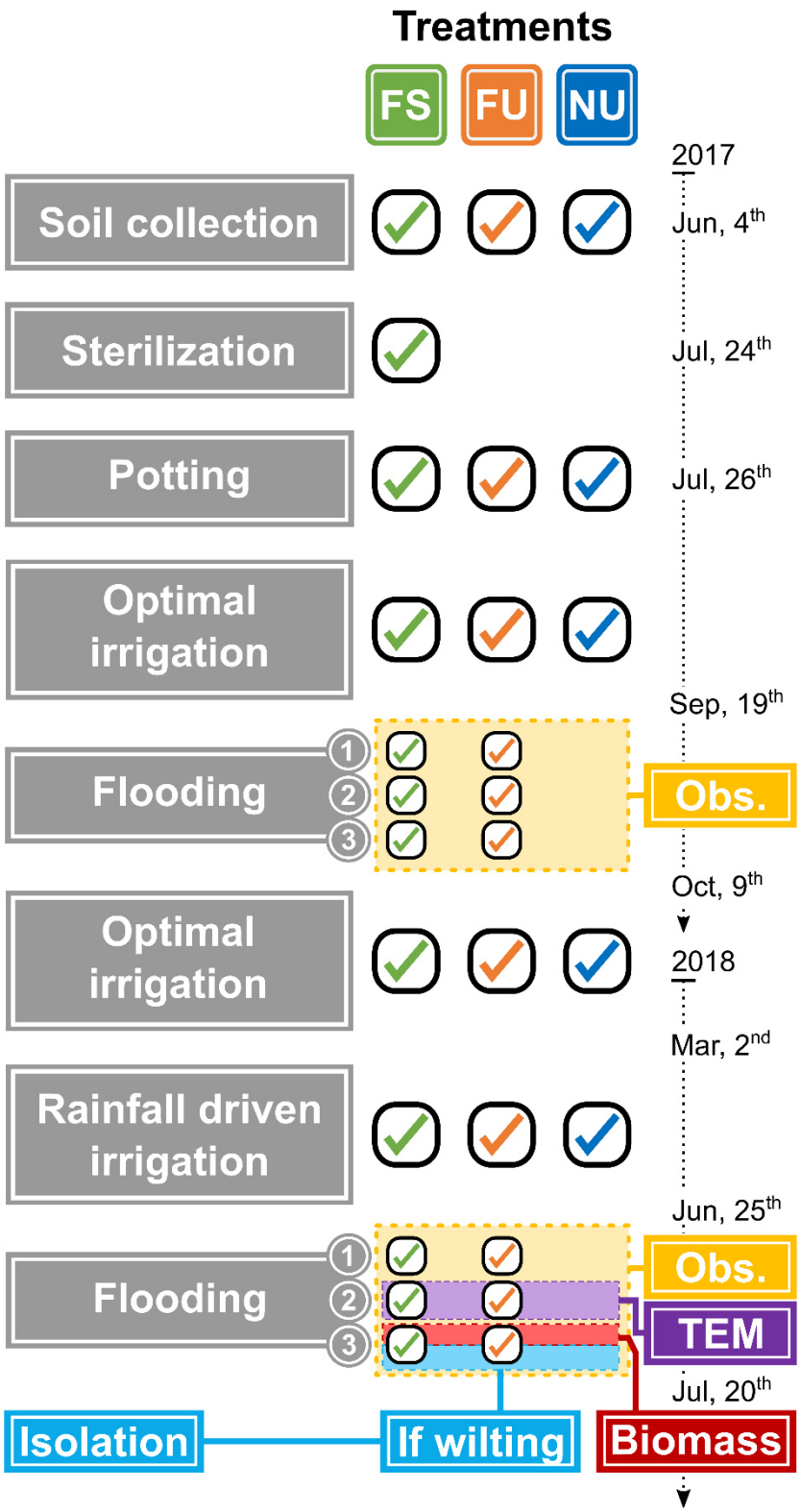

Fig. 2. Rainfall distribution parameters taken into account to define the flooding cycle.

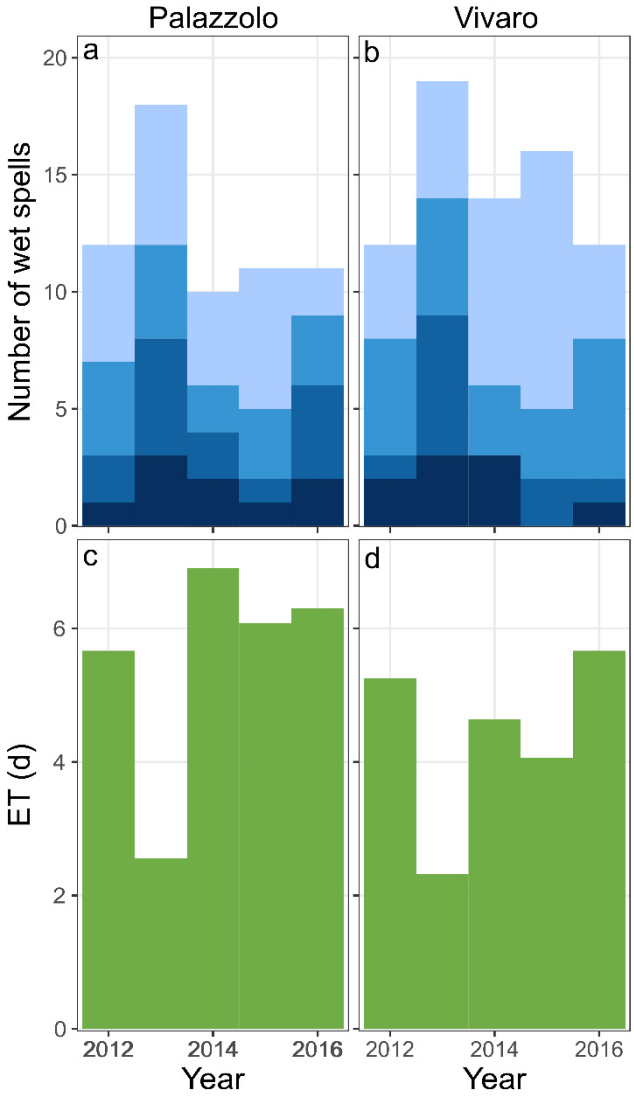

Fig. 3. Evolution of wilting symptoms during the second flooding cycle (July 2018).

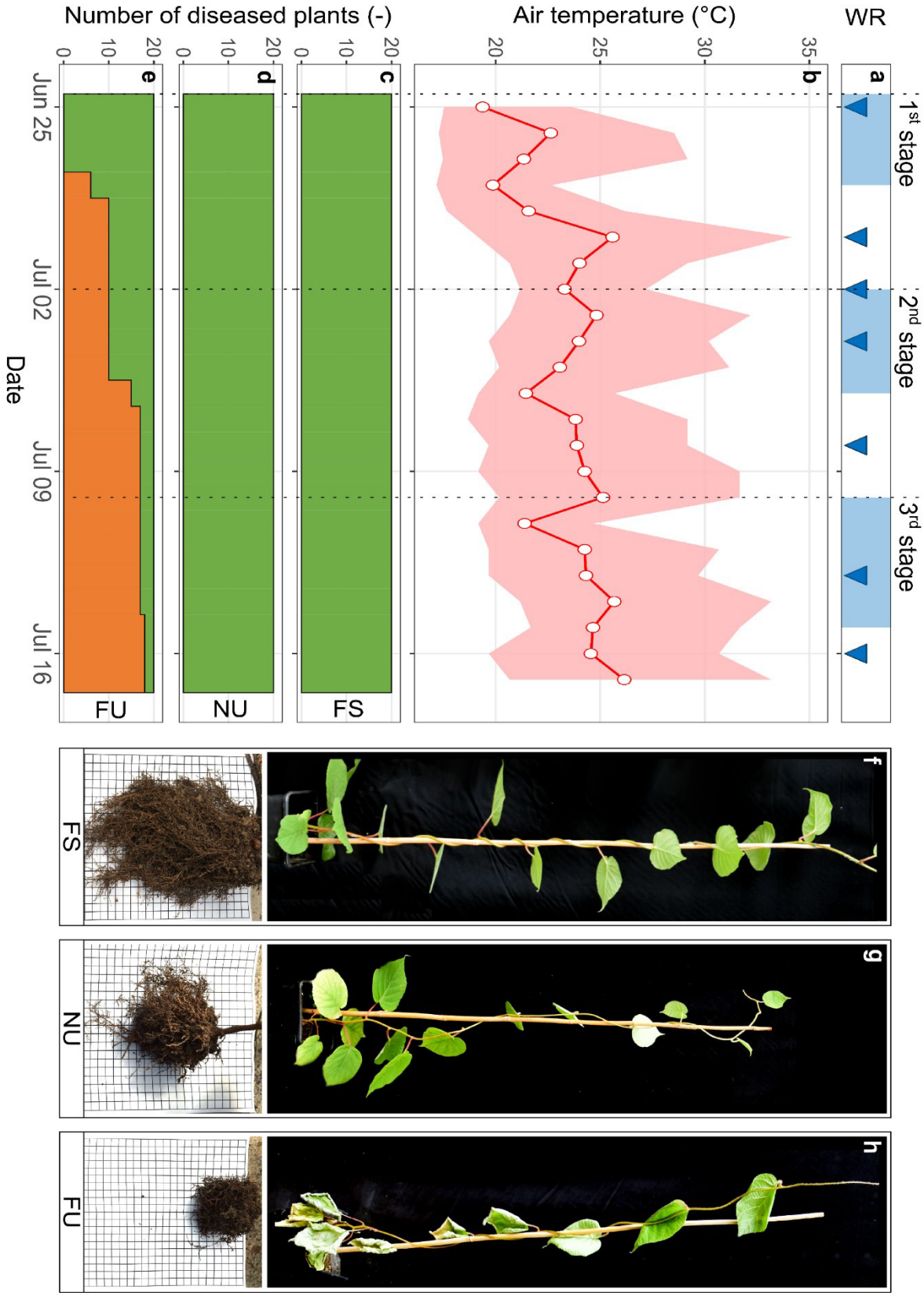

Fig. 4. Comparison of dry biomass values.

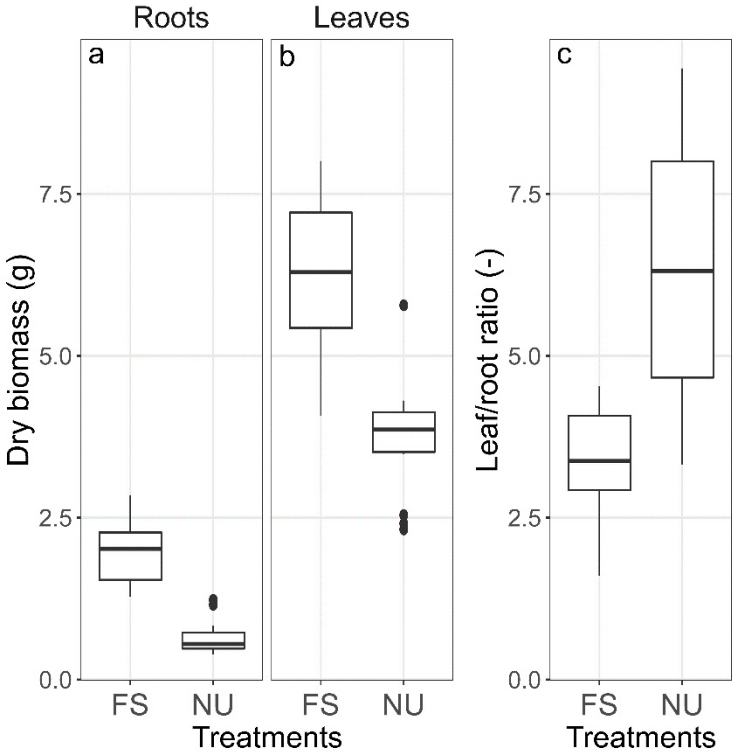

Fig. 5. TEM micrographs of xylem vessels of *A. deliciosa* cv. *Hayward* subjected to different combinations of water supply and soil sterilization conditions.

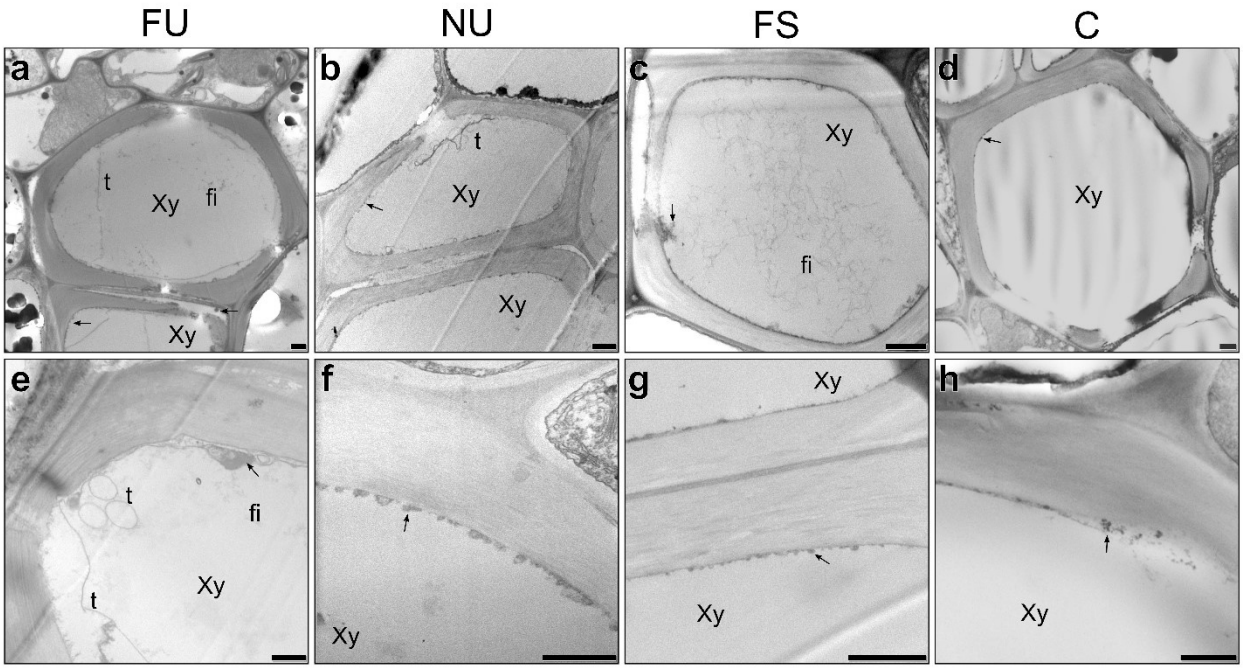

Fig. 6. Isolation results from eighteen diseased plants grown in non-sterile soil and subjected to flooding.

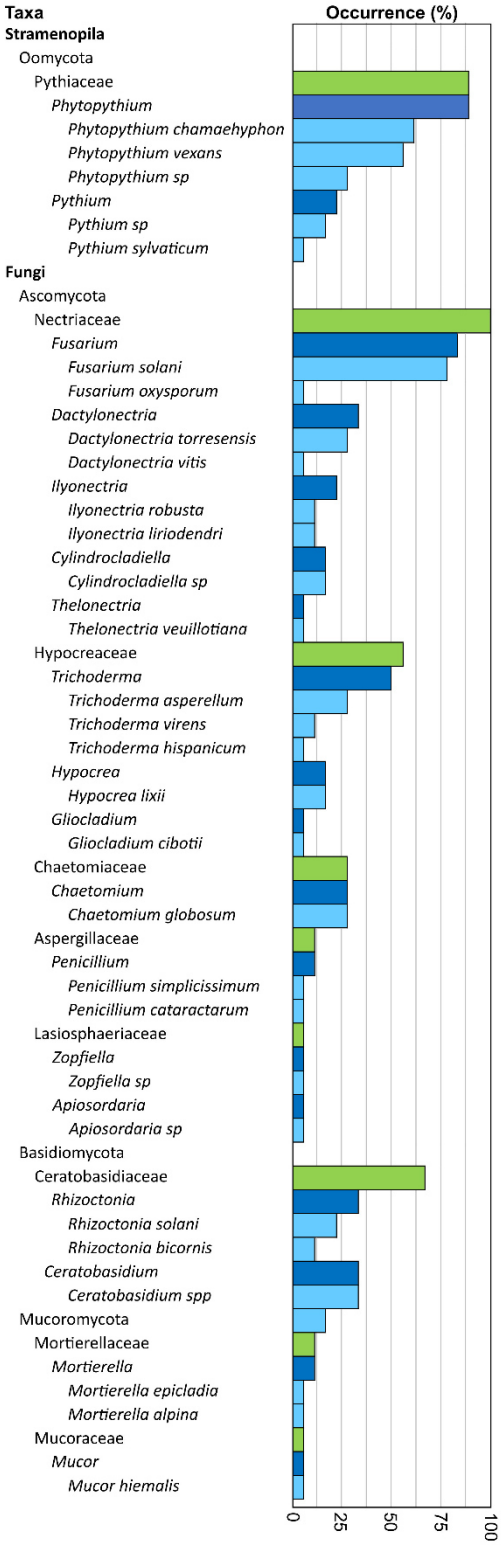

Fig. 7. Statistical analysis of historical rainfall data over the last two decades (1998-2018) in Palazzolo, Vivaro and Udine (North-eastern Italy).

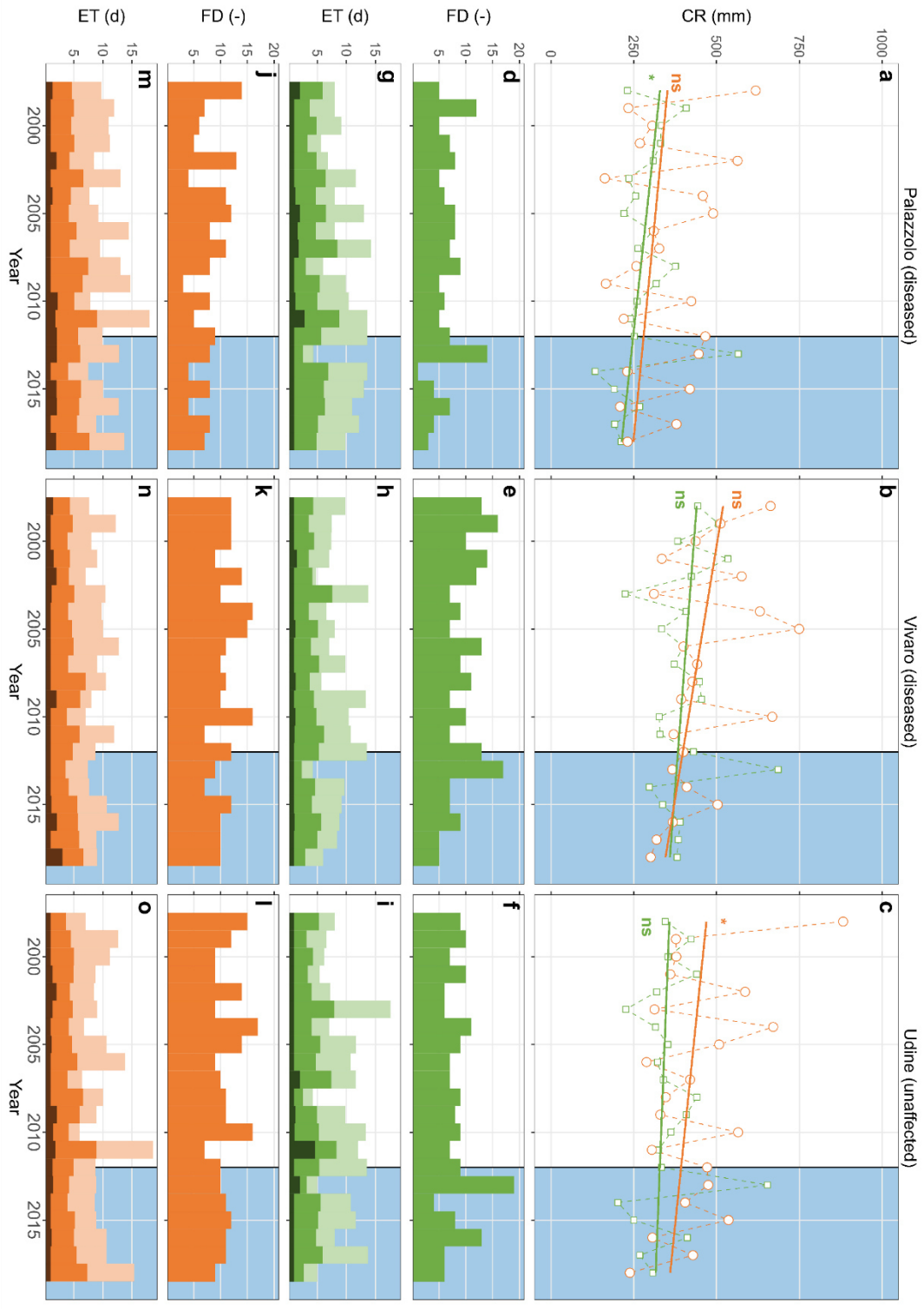

Online Resource 1. Kiwifruit decline symptoms and spreading patterns.

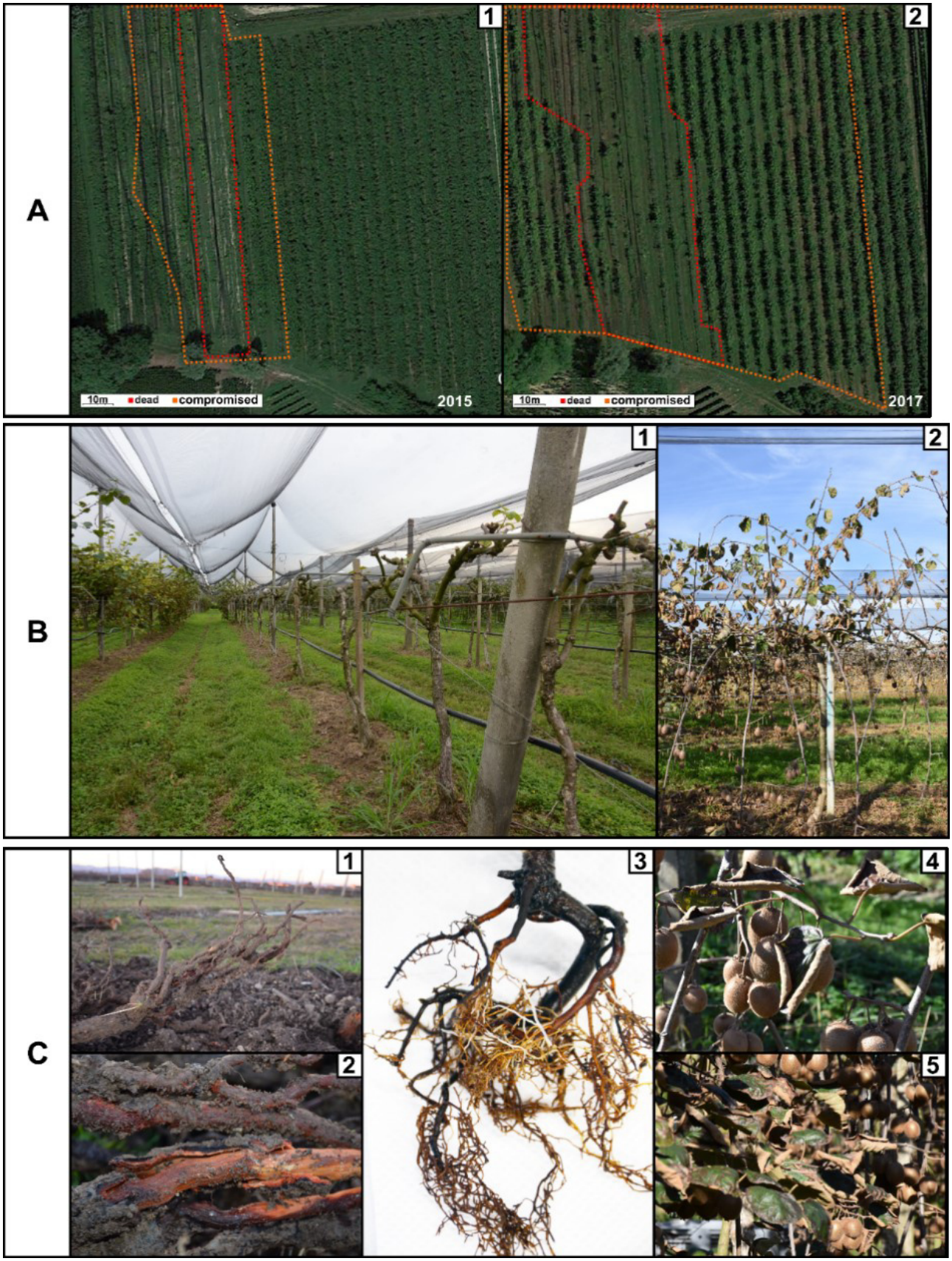

Online resource 2. Weather trends and watering regime during the trial.

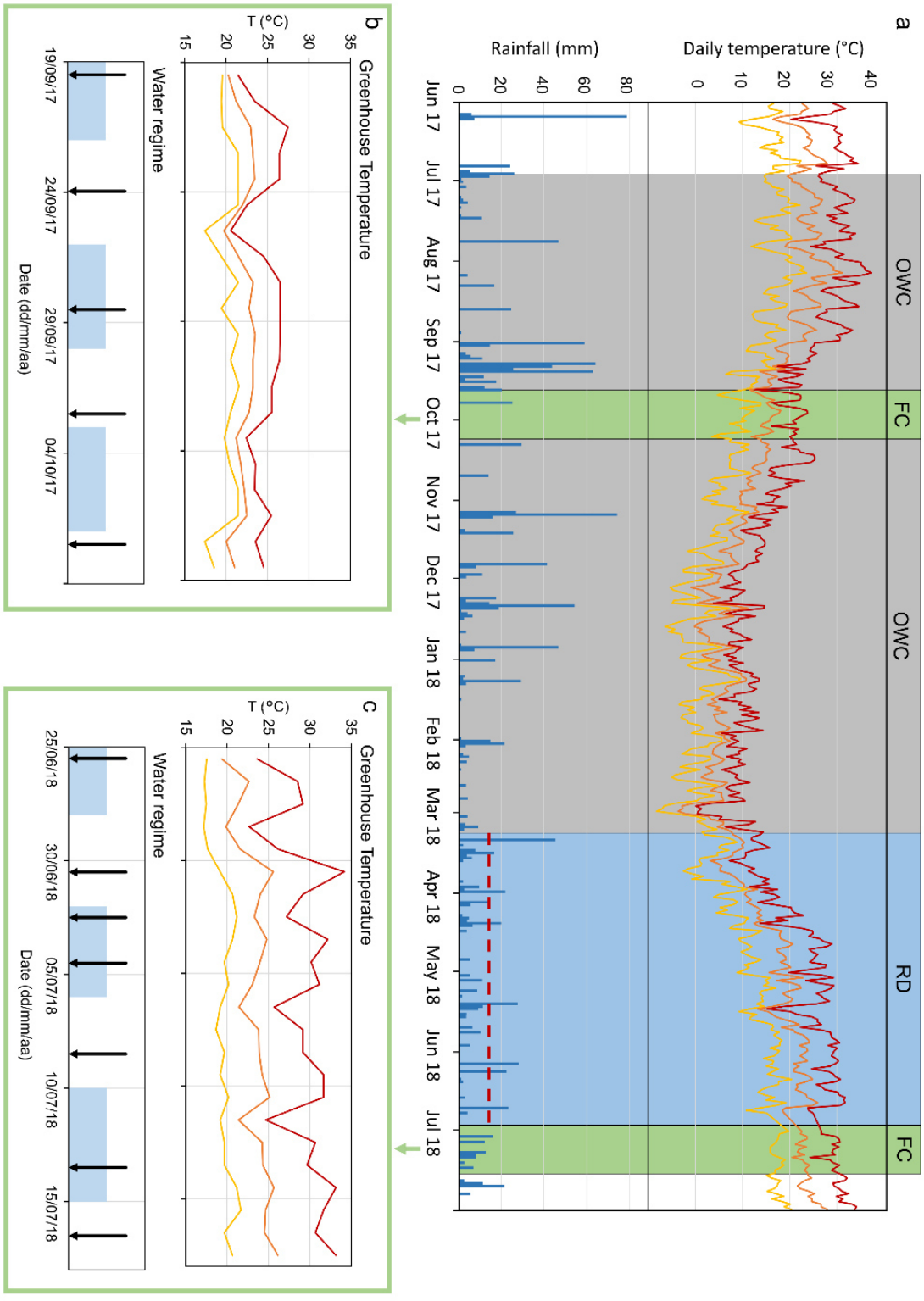

b

Online Resource 3. RFLP patterns of isolates belonging to morphological groups 1 and 7.

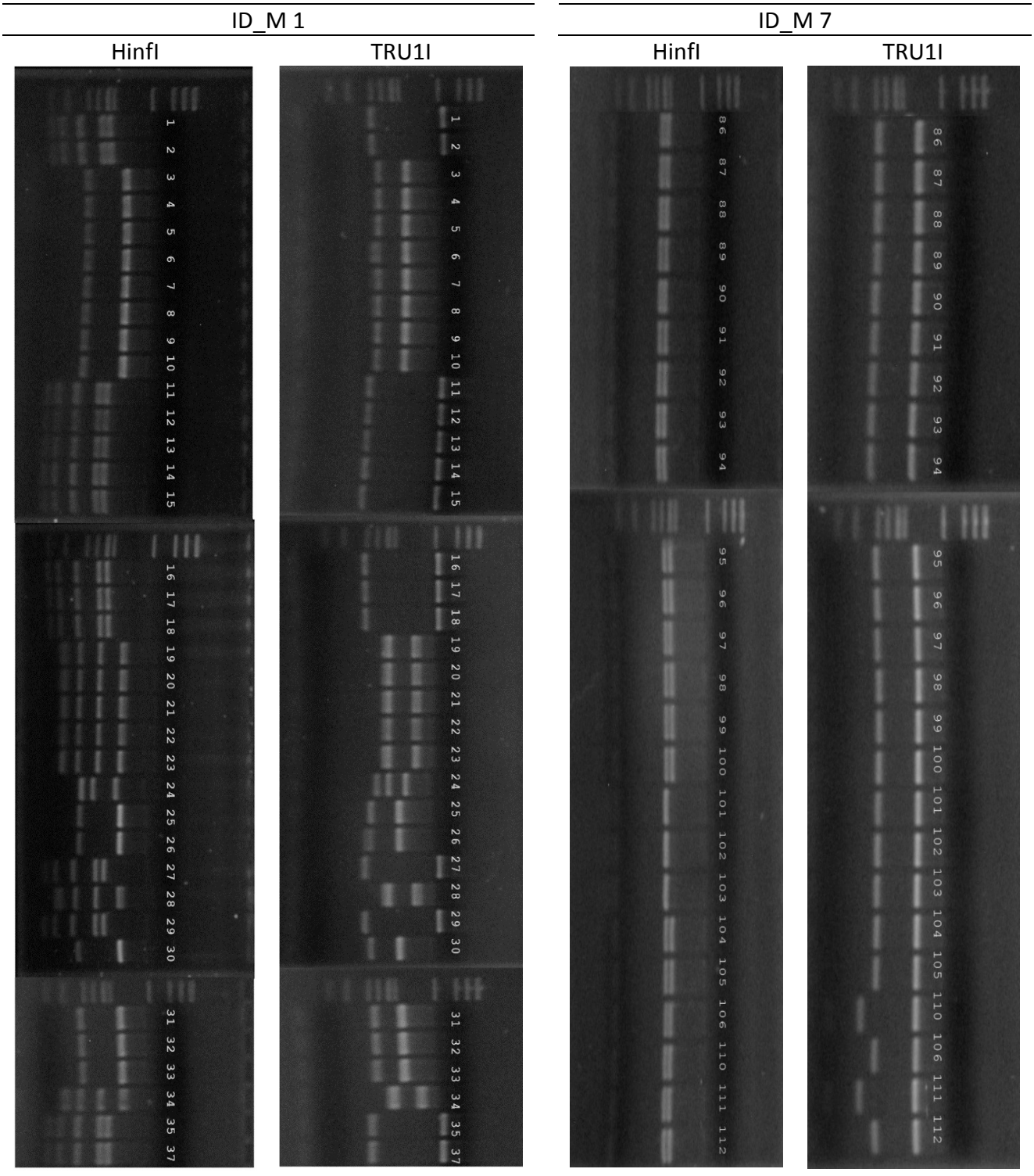

Online Resource 4. RFLP profiles of isolates belonging to morphological groups 10, 5, 9, 23 and 6.

ID_M 10

HinfI TRU1I

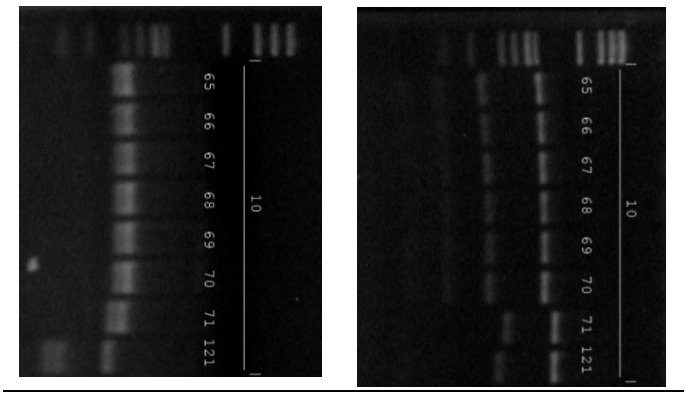

ID_M 5

HinfI TRU1I

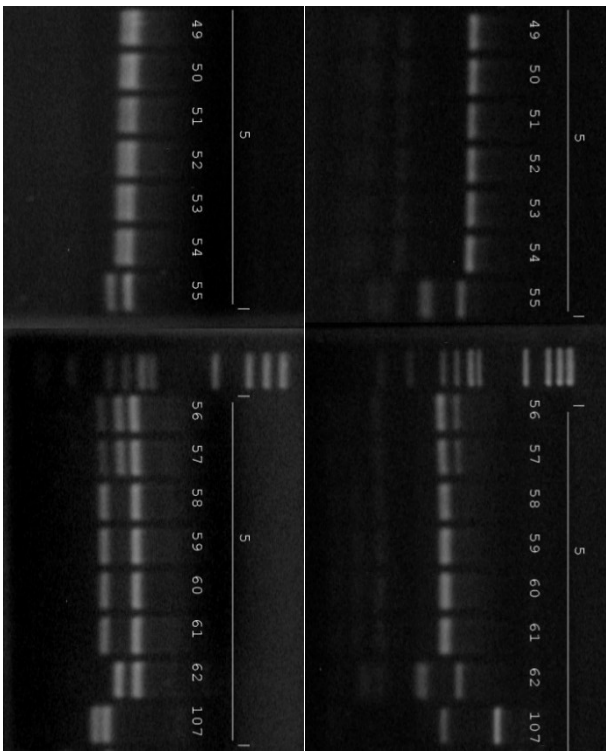

ID_M 9

HinfI TRU1I

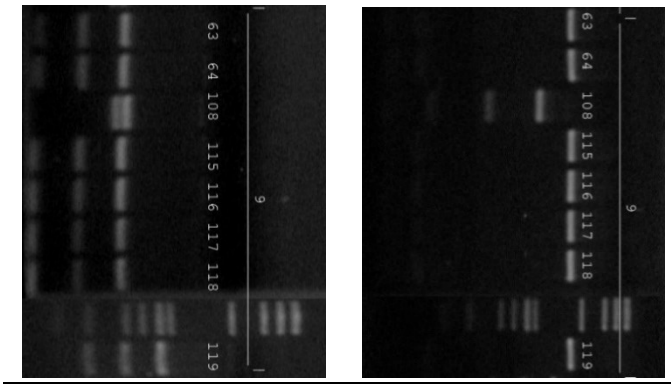

ID_M 23

HinfI TRU1I

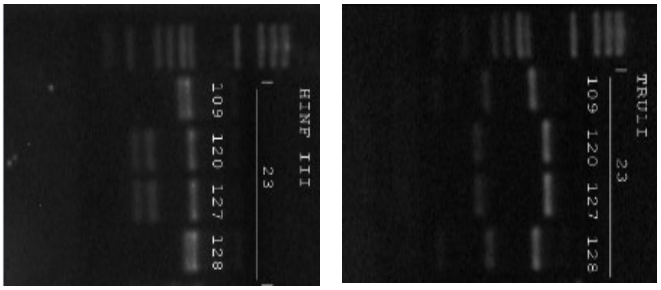

ID_M 6

HinfI TRU1I

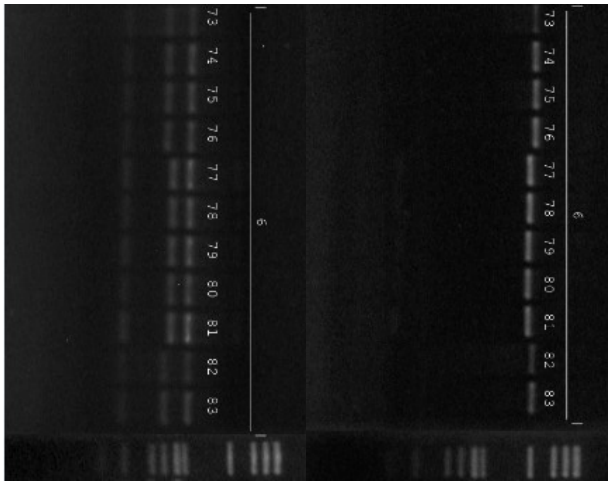

Online resource 5. Preliminary trial to reproduce Kiwifruit Decline in a controlled environment.

The preliminary experiment had a similar setup to that described in the main article. It combined 2 levels of water management (flooded, F / non-flooded, N) and two types of soil (sterilized, S / unsterilized, U), for a total of four experimental conditions: FS, NU, FU (as in the main trial) and NS. The soils used for the trial were collected from the three diseased orchards as described in the article (section 2.2).

The main differences were: the overall duration of the trial (from May to July), the date of soil sampling and plant potting (May 2017), the preparation of the soils, which were not mixed together, and the number of vines tested. A total of 9 plants per treatment were tested, 3 for each soil sample.

The canopy was monitored for symptoms from the day of transplanting, while root observation was only performed at the end of the trial. Wilting symptoms only appeared on FU vines, while root deterioration was present in both NU and FU plants, but more severe in FU. The number of dead plants throughout the flooding cycle is reported in the Table S1. NS and FS plants displayed no symptoms of KD, neither in the canopy nor in the roots, independently of water supply. Moreover, it seems that root growth in sterilised soils was unaffected by the flooding cycle.

Online Resource 6. Wilting appearance during the preliminary trial in a controlled environment.

Soil	**Sterilized**						**Unsterilized**					
Water	**Non-flooded**			**Flooded**			**Non-flooded**			**Flooded**		
Treatment	**NS**			**FS**			**NU**			**FU**		
Site*	**SGC**	**SGR**	**Cor**	**SGC**	**SGR**	**Cor**	**SGC**	**SGR**	**Cor**	**SGC**	**SGR**	**Cor**
before flooding	0	0	0	0	0	0	0	0	0	0	0	0
1st stage	0	0	0	0	0	0	0	0	0	2	0	0
2nd stage	0	0	0	0	0	0	0	0	0	0	1	2
3rd stage	0	0	0	0	0	0	0	0	0	1	2	0
Total	**0/3**	**0/3**	**0/3**	**0/3**	**0/3**	**0/3**	**0/3**	**0/3**	**0/3**	**3/3**	**3/3**	**2/3**

* Experimental orchards where soils were collected: SGC, San Giovanni di Casarsa; SGR San Giorgio della Richinvelda; Cor, Cordenons (Friuli Venezia Giulia Region, NE of Italy).

Online resource 7. Frequencies of flooding downpours (FD) and mean elapsed time (ET) before and after disease outbreak (2012).

Climatic Variable	Site	Period	Before	After	*P*
FD*	Palazzolo	Early	6.86 ± 2.03	5.71 ± 4.23	0.16
		Late	8.21 ± 3.49	6.86 ± 2.04	0.52
	Udine	Early	8.21 ± 1.58	9.29 ± 5.15	0.82
		Late	11.64 ± 3.08	10.57 ± 0.98	0.70
	Vivaro	Early	10.36 ± 2.92	9.00 ± 4.47	0.27
		Late	11.79 ± 2.67	10.00 ± 1.73	0.15
ET*	Palazzolo	Early	5.39 ± 1.71	5.35 ± 1.42	0.71
		Late	5.47 ± 1.44	5.88 ± 1.09	0.31
	Udine	Early	5.04 ± 1.77	4.65 ± 1.25	0.97
		Late	5.06 ± 1.38	5.13 ± 1.11	0.63
	Vivaro	Early	4.6 ± 1.16	4.27 ± 1.24	0.91
		Late	4.79 ± 0.96	5.17 ± 1.09	0.48

* Both FD and ET are expressed in days

Online Resource 8. Identification of isolates from roots of symptomatic plants.

ID_I	ID_P	ID_R	ID_R	Genera	Species	Authority	NCBIref	Identity	Accession number
2	24	1	A	Phytopythium	chamaehyphon	(Sideris) Abad, de Cock, Bala, Robideau, Lodhi & Lévesque	MF375471.1	99.68	MN535819
13	32	1	A	Phytopythium	chamaehyphon	(Sideris) Abad, de Cock, Bala, Robideau, Lodhi & Lévesque	MF375471.1	99.68	MN535819
15	34	1	A	Phytopythium	chamaehyphon	(Sideris) Abad, de Cock, Bala, Robideau, Lodhi & Lévesque	MF375471.1	99.68	MN535819
27	23	1	A	Phytopythium	chamaehyphon	(Sideris) Abad, de Cock, Bala, Robideau, Lodhi & Lévesque	MF375471.1	99.68	MN535819
35	33	1	A	Phytopythium	chamaehyphon	(Sideris) Abad, de Cock, Bala, Robideau, Lodhi & Lévesque	MF375471.1	99.68	MN535819
11	25	1	A	Phytopythium	chamaehyphon	.	.	.	.
12	30	1	A	Phytopythium	chamaehyphon	.	.	.	.
14	33	1	A	Phytopythium	chamaehyphon	.	.	.	.
16	39	1	A	Phytopythium	chamaehyphon	.	.	.	.
17	91	1	A	Phytopythium	chamaehyphon	.	.	.	.
18	128	1	A	Phytopythium	chamaehyphon	.	.	.	.
29	23	1	A	Phytopythium	chamaehyphon	.	.	.	.
37	34	1	A	Phytopythium	chamaehyphon	.	.	.	.
1	21	1	A	Phytopythium	chamaehyphon	(Sideris) Abad, de Cock, Bala, Robideau, Lodhi & Lévesque	MF375471.1	99.68	MN535819
19	23	1	B	Phytopythium	sp	.	.	.	.
23	38	1	B	Phytopythium	sp	.	.	.	.
20	28	1	B	Phytopythium	sp	Abad, de Cock, Bala, Robideau, A.M. Lodhi & Lévesque	MK326408.1	82.35	.
21	34	1	B	Phytopythium	sp	Abad, de Cock, Bala, Robideau, A.M. Lodhi & Lévesque	MK326408.1	82.35	.
22	36	1	B	Phytopythium	sp	Abad, de Cock, Bala, Robideau, A.M. Lodhi & Lévesque	MK326408.1	82.35	.
3	26	1	C	Phytopythium	vexans	.	.	.	.
5	32	1	C	Phytopythium	vexans	.	.	.	.
7	38	1	C	Phytopythium	vexans	.	.	.	.
8	39	1	C	Phytopythium	vexans	.	.	.	.
9	128	1	C	Phytopythium	vexans	.	.	.	.
26	26	1	C	Phytopythium	vexans	.	.	.	.
30	24	1	C	Phytopythium	vexans	.	.	.	.
31	30	1	C	Phytopythium	vexans	.	.	.	.
32	31	1	C	Phytopythium	vexans	.	.	.	.
6	36	1	C	Phytopythium	vexans	(de Bary) Abad, de Cock, Bala, Robideau, Lodhi & Lévesque	KT337684.1	100	MN535820
4	31	1	C	Phytopythium	vexans	(de Bary) Abad, de Cock, Bala, Robideau, Lodhi & Lévesque	KT337684.1	100	MN535820

ID_I	ID_P	ID_R	ID_R	Genera	Species	Authority	NCBIref	Identity	Accession number
25	21	1	C	Phytopythium	vexans	(de Bary) Abad, de Cock, Bala, Robideau, Lodhi & Lévesque	KT337684.1	100	MN535820
33	38	1	C	Phytopythium	vexans	(de Bary) Abad, de Cock, Bala, Robideau, Lodhi & Lévesque	KT337684.1	100	MN535820
10	24	1	C	Phytopythium	vexans	(de Bary) Abad, de Cock, Bala, Robideau, Lodhi & Lévesque	MK567962.1	100	MN535818
24	128	1	D	Pythium	sp	Pringsh.	KU665819.1	98.58	.
28	23	1	D	Pythium	sp	Pringsh.	KU665819.1	98.58	.
34	34	1	D	Pythium	sp	Pringsh.	KU665819.1	98.58	.
41	33	4	.	Pythium	sylvaticum	W.A. Campb. & F.F. Hendrix	KU665814.1	100	MN535854
40	33	4	.	Pythium	sylvaticum	W.A. Campb. & F.F. Hendrix	KU665814.1	100	MN535854
45	31	15	.	Penicillium	cataractarum	Visagie, Malloch & Seifert	NR_158822.1	99.61	MN535826
122	26	15	.	Penicillium	simplicissimum	(Oudem.) Thom	MH856014.1	99.43	MN535827
123	26	15	.	Penicillium	simplicissimum	(Oudem.) Thom	MH856014.1	99.43	MN535827
83	24	6	E	Trichoderma	hispanicum	(Jaklitsch & Voglmayr) Jaklitsch & Voglmayr	NR_138451.1	99.63	MN535843
73	29	6	E	Trichoderma	asperellum	.	.	.	.
75	33	6	E	Trichoderma	asperellum	.	.	.	.
76	38	6	E	Trichoderma	asperellum	.	.	.	.
74	31	6	E	Trichoderma	asperellum	Samuels, Lieckf. & Nirenberg	KC479809.1	100	MN535839
82	30	6	E	Trichoderma	asperellum	Samuels, Lieckf. & Nirenberg	KC479809.1	100	MN535839
78	34	6	F	Hypocrea	lixii	Rifai	KY031340.1	99.82	MN535840
81	128	6	F	Hypocrea	lixii	Pat.	AY605747.1	99.82	MN535842
80	33	6	F	Trichoderma	virens	(J.H. Mill., Giddens & A.A. Foster) Arx	MH864402.1	99.82	MN535841
79	38	6	F	Trichoderma	virens	(J.H. Mill., Giddens & A.A. Foster) Arx	MH864402.1	99.82	MN535841
77	36	6	F	Hypocrea	lixii	Pat.	AY605747.1	99.82	MN535842
126	29	19	.	Thelonectria	veuillotiana	(Sacc. & Roum.) P. Chaverri & C. Salgado	MK594388.1	99.79	MN535832
124	25	13	.	Cylindrocladiella	sp	Boesew.	MF444907.1	100	MN535831
36	30	18	.	Cylindrocladiella	sp	Boesew.	MF444907.1	100	MN535831
0	25	24	.	Cylindrocladiella	sp	.	.	.	.
84	25	24	.	Cylindrocladiella	sp	Boesew.	MF444907.1	100	MN535831
125	26	13	.	Cylindrocladiella	sp	Boesew.	MF444907.1	99.79	MN535831
65	36	10	G	Dactylonectria	torresensis	.	.	.	.
66	128	10	G	Dactylonectria	torresensis	.	.	.	.
68	23	10	G	Dactylonectria	torresensis	.	.	.	.
69	29	10	G	Dactylonectria	torresensis	.	.	.	.

ID_I	ID_P	ID_R	ID_R	Genera	Species	Authority	NCBIref	Identity	Accession number
70	36	10	G	Dactylonectria	torresensis	.	.	.	.
67	37	10	G	Dactylonectria	torresensis	(A. Cabral, Rego & Crous) L. Lombard & Crous	MH865183.1	99.79	MN535821
121	32	10	H	Dactylonectria	vitis	(A. Cabral, Rego & Crous) L. Lombard & Crous	MH865179.1	99.57	MN535823
42	27	8	.	Fusarium	oxysporum	Schltdl	MK432913.1	100	MN535849
43	27	8	.	Fusarium	oxysporum	Schltdl	MK432913.1	100	MN535849
86	24	7	J	Fusarium	solani	.	.	.	.
88	91	7	J	Fusarium	solani	.	.	.	.
90	32	7	J	Fusarium	solani	.	.	.	.
91	33	7	J	Fusarium	solani	.	.	.	.
92	33	7	J	Fusarium	solani	.	.	.	.
93	30	7	J	Fusarium	solani	.	.	.	.
95	21	7	J	Fusarium	solani	.	.	.	.
96	24	7	J	Fusarium	solani	.	.	.	.
97	21	7	J	Fusarium	solani	.	.	.	.
98	33	7	J	Fusarium	solani	.	.	.	.
100	23	7	J	Fusarium	solani	.	.	.	.
94	24	7	J	Fusarium	solani	(Mart.) Sacc.	JX435204.1	100	MN535845
112	31	7	J	Fusarium	solani	(Mart.) Sacc.	JX435204.1	100	MN535845
89	32	7	J	Fusarium	solani	(Mart.) Sacc.	KJ562369.1	99.8	MN535855
87	128	7	J	Fusarium	solani	(Mart.) Sacc.	KU939051.1	100	MN535833
99	30	7	J	Fusarium	solani	(Mart.) Sacc.	KU939051.1	100	MN535833
105	37	7	J	Fusarium	solani	(Mart.) Sacc.	KU939051.1	100	MN535833
104	39	7	J	Fusarium	solani	(Mart.) Sacc.	KY381843.1	100	MN535847
107	23	7	J	Fusarium	solani	(Mart.) Sacc.	MF993094.1	100	MN535838
106	23	7	J	Fusarium	solani	(Mart.) Sacc.	MF993094.1	100	MN535838
111	34	7	K	Fusarium	solani	(Mart.) Sacc.	AY904064.1	100	MN535848
110	91	7	K	Fusarium	solani	(Mart.) Sacc.	AY904064.1	100	MN535848
101	29	7	L	Fusarium	solani	.	.	.	.
103	29	7	L	Fusarium	solani	.	.	.	.
102	29	7	L	Fusarium	solani	(Mart.) Sacc.	MH300495.1	100	MN535846
71	36	10	M	Fusarium	solani	(Mart.) Sacc.	MH855035.1	99.8	MN535822
113	36	30	.	Fusarium	solani	(Mart.) Sacc.	MH855035.1	99.8	MN535822

ID_I	ID_P	ID_R	ID_R	Genera	Species	Authority	NCBIref	Identity	Accession number
72	32	20	.	Fusarium	solani	(Mart.) Sacc.	KU939051.1	100	MN535833
108	38	9	N	Ilyonectria	liriodendri	(Halleen, Rego & Crous) Chaverri & C. Salgado	MH861308.1	100	MN535834
128	128	23	O	Ilyonectria	liriodendri	.	.	.	.
109	38	23	O	Ilyonectria	liriodendri	(Halleen, Rego & Crous) Chaverri & C. Salgado	MH861308.1	100	MN535834
0	128	21	.	Ilyonectria	liriodendri	.	.	.	.
114	128	21	.	Ilyonectria	liriodendri	(Halleen, Rego & Crous) Chaverri & C. Salgado	MH861308.1	100	MN535834
127	25	23	P	Ilyonectria	robusta	.	.	.	.
120	24	23	P	Ilyonectria	robusta	(A.A. Hildebr.) A. Cabral & Crous	MH865181.1	100	MN535824
85	25	12	.	Ilyonectria	robusta	(A.A. Hildebr.) A. Cabral & Crous	MH865181.1	100	MN535824
46	28	16	.	Gliocladium	cibotii	J.F.H. Beyma	DQ825981.1	99.77	MN535828
63	38	9	Q	Chaetomium	globosum	J.N. Rai & J.P. Tewari	MH860809.1	99.6	MN535850
64	128	9	Q	Chaetomium	globosum	.	.	.	.
116	37	9	Q	Chaetomium	globosum	.	.	.	.
117	38	9	Q	Chaetomium	globosum	.	.	.	.
115	24	9	Q	Chaetomium	globosum	J.N. Rai & J.P. Tewari	MH860809.1	98.26	MN535850
118	31	9	Q	Chaetomium	globosum	J.N. Rai & J.P. Tewari	MH860809.1	98.26	MN535850
119	24	9	R	Chaetomium	globosum	J.N. Rai & J.P. Tewari	MH860809.1	98.26	MN535850
47	32	17	.	Apiosordaria	striatispora	(Furuya & Udagawa) Guarro & Cano	MH861043.1	92.41	MN535829
48	32	17	.	Zopfiella	macrospora	Guarro & Calvo	MH861958.1	91.65	MN535830
55	28	5	S	Rhizoctonia	bicornis	(J. Erikss. & Ryvarden) Oberw., R. Bauer, Garnica & R. Kirschner	MG515375.1	100	MN535836
62	36	5	S	Rhizoctonia	bicornis	(J. Erikss. & Ryvarden) Oberw., R. Bauer, Garnica & R. Kirschner	MG515375.1	96.76	MN535836
56	37	5	T	Ceratobasidium	sp	.	.	.	.
57	37	5	T	Ceratobasidium	sp	D.P. Rogers	HQ680957.1	84.2	.
58	38	5	U	Rhizoctonia	solani	.	.	.	.
61	25	5	U	Rhizoctonia	solani	.	.	.	.
60	128	5	U	Rhizoctonia	solani	J.G. Kühn	HF912173.2	100	MN535837
59	39	5	U	Rhizoctonia	solani	J.G. Kühn	HF912173.2	100	MN535837
49	26	5	V	Ceratobasidium	sp	.	.	.	.
51	29	5	V	Ceratobasidium	sp	.	.	.	.
53	32	5	V	Ceratobasidium	sp	.	.	.	.
54	33	5	V	Ceratobasidium	sp	.	.	.	.

ID_I	ID_P	ID_R	ID_R	Genera	Species	Authority	NCBIref	Identity	Accession number
50	27	5	V	Ceratobasidium	sp	D.P. Rogers	DQ278941.1	98.66	MN535835
52	29	5	V	Ceratobasidium	sp	D.P. Rogers	DQ278941.1	98.66	MN535835
39	31	3	.	Mortierella	alpina	Peyronel	JX976038.1	100	MN535853
38	31	2	.	Mortierella	epicladia	W. Gams & Emden	NR_111571.1	100	MN535852
44	28	14	.	Mucor	hiemalis	Wehmer	MH859159.1	100	MN535825

3 Pathogenicity tests of *Phytopythium vexans.*

3.1 Introduction to the study | Chapter 3

The study reported in Chapter 2 allowed us to have a first insight on the potential pathogen involved in the disease, suggesting some Oomycetes species as most probable pathogenetic candidates. Among those, *Phytopythium vexans* not only frequently occurred in diseased plants of our trial, but it was also frequently found in Piedmont region.

Reports of Oomycetes infecting kiwifruit are not uncommon and are often associated with flooding conditions (Latorre *et al.*, 1991; Lee *et al.*, 2001; Akilli *et al.*, 2011; Wang *et al.*, 2015; Çiftçi *et al.*, 2016). Most of the pathogenicity tests reported in the literature used a 5-mm cork bore to produce an injury in the stem of 1 years old plants, successively inoculated inserting an infected agar plug (Akilli *et al.*, 2011; Wang *et al.*, 2015; Polat *et al.*, 2017). Nevertheless, the methods used in these studies were not considered representative for KD which mainly affects feeding roots, so we decided to leave root crown and stems unharmed.

This work was developed in collaboration with Prof. Davide Spadaro and Dr. Simona Prencipe from the University of Turin (Italy) and is currently submitted to "Plant disease Note".

References

Akilli S, Serçe ÇiU, Zekaİ Katircioğlu Y, Karakaya A, Maden S. **2011**. Involvement of *Phytophthora citrophthora* in kiwifruit decline in Turkey. *Journal of Phytopathology* **159**: 579–581.

Çiftçi O, Serçe ÇU, Türkölmez Ş, Derviş S. **2016**. First Report of *Phytophthora palmivora* causing crown and root rot of kiwifruit (*Actinidia deliciosa*) in Turkey. *Plant Disease* **100**: 210.

Latorre BA, Alvarez C, Ribeiro OK. **1991**. *Phytophthora* root rot of kiwifruit in Chile. Plant Disease **75**: 949–952.

Lee Y-H, Jee H-J, Cha K-H, Ko S-J, Park K-B. **2001**. Occurrence of *Phytophthora* Root Rot on Kiwifruit in Korea. *The Plant Pathology Journal* **17**: 154–158.

Polat Z, Awan QN, Hussain M, Akgül DS. **2017**. First Report of *Phytopytium vexans* Causing Root and Collar Rot of Kiwifruit in Turkey. *Plant Disease* **101**: 1058.

Wang KX, Xie YL, Yuan GQ, Li QQ, Lin W. **2015**. First Report of Root and Collar Rot Caused by *Phytopythium helicoides* on Kiwifruit (*Actinidia chinensis*). *Plant Disease* **99**: 725.

3.2 First Report of *Phytopythium vexans* causing decline syndrome of *Actinidia deliciosa* 'Hayward' in Italy

S. Prencipe[1,*], F. Savian[2,*], L. Nari[3], P. Ermacora[2], D. Spadaro[1,4], M. Martini[2, †]

[1] Dept. Agricultural, Forestry and Food Sciences (DISAFA) – University of Torino, 10095 Grugliasco (TO), Italy

[2] Dept. Agricultural, Food, Environmental and Animal Sciences (DI4A) – University of Udine, 33100 Udine (UD), Italy

[3]AGRION, Fondazione per la ricerca l'innovazione e lo sviluppo tecnologico dell'agricoltura piemontese, 12030 Manta (Cn), Italy

[4] Centre of Competence for the Innovation in the Agroenvironmental Sector – University of Torino, 10095 Grugliasco (TO), Italy

* these two authors contributed equally to this work

† corresponding author: marta.martini@uniud.it

FIRST REPORT

A decline syndrome of kiwi (*A. deliciosa*) has been reported in Italy since 2012 and currently affects an estimated 12% of the country's kiwifruit production area (Sorrenti et al. 2019). The disease usually occurs in poorly drained soils prone to waterlogging, and it causes root rot, reduction of plant vigor, leaf curling, and sudden decline. During 2016 and 2018, 18 vineyards of the Piedmont region (NW Italy) were monitored in Jun-Oct and symptomatic vines were sampled in Oct-Dec. Experimental trials were set up in Friuli Venezia Giulia (NE Italy) to reproduce the disease in a controlled environment by applying waterlogging to kiwifruit plants grown in 6.5-l pots, filled with sterilized and unsterilized soil from the diseased vineyards. Root rot and decline appeared in 90% of the plants when flooding conditions on unsterilized soil were used, whereas symptoms were not observed on plants grown on flooded sterilized soil, suggesting the involvement of a pathogen.

Roots of the diseased plants, both from the field survey and the greenhouse experiment, were surface-disinfected with 1% sodium hypochlorite for 30 s, rinsed in sterile water and cultured on corn meal agar amended with pimaricin, ampicillin, rifampicin and pentachloronitrobenzene. Representative isolates were transferred onto V8 juice agar and morphological observations were performed according to de Cock et al. (2015). After 3 days, colonies showed typical mycelia of a *Pythium* species. Older cultures showed subglobose non-papillate sporangia (11.25 to 18.47 µm in diameter), bell-shaped antheridia, and smooth oogonia of *Phytopythium vexans* (de Bary A.) (de Cock et al. 2015). Species identification was confirmed by sequencing DNA fragments amplified from the rDNA gene internal transcribed spacer (ITS) (sequence length 606 bp), the large subunit (LSU) rDNA (682 bp) and cytochrome oxidase I (COI) region (666 bp) using primers ITS1/ITS4 (White et al. 1990), NL1/NL4 (Baten et al. 2014) and FM85mod/OomCOILevup (Robideau et al. 2011), respectively. The DNA sequence for each region of two isolates was deposited in GenBank (Accession N° from MN510423 to MN510428). BLAST-searches showed the isolates had 99 to 100% sequence homology with strains of *P. vexans* (Accession N° AY598713, HQ665090 and GU133476).

Pathogenicity of *P. vexans* isolates was tested on 1-year-old plants of *A. deliciosa* cv. 'Hayward': 6 plants per treatment grown in 3-l pots of sterilised agriperlite-peat mixture. Inoculum of sequenced *P. vexans* was grown for 7 days on a wheat and hemp mixture (100g and 50g respectively, plus 170 ml of water) and used to infest the soil: 6 g/l (fresh weight) of the inoculum per pot. Similarly, controls were inoculated with a sterile wheat and hemp mixture. All the plants were kept in a greenhouse at 32±3°C. To induce waterlogging stress, three rounds of flooding (72, 96, 120 hrs) and drainage (96, 96, 120 hrs) were applied to all the plants, including the controls, as described by Savian et al. (submitted for publication). Root rot, leaf curling and decline occurred after 14-24 days in all the inoculated plants, while controls remained symptomless. To fulfil Koch's postulates, re-isolations were performed from the roots of all the tested plants. Molecular identification of the isolates

confirmed *P. vexans* presence only in the inoculated plants. This is the first report of *P. vexans* causing kiwifruit decline syndrome in Italy, although its association with a similar disease was observed in Turkey (Polat et al. 2017).

ACKNOWLEDGMENTS

This research was partially founded by ERSA, Plant Protection Service, Pozzuolo del Friuli (UD), Italy.

REFERENCES

Baten MdA, Asano T, Motohashi K, Ishiguro Y, Rahman MZ, Inaba S, Suga H, Kageyama K. **2014**. Phylogenetic relationships among *Phytopythium* species, and re-evaluation of *Phytopythium fagopyri* comb. nov., recovered from damped-off buckwheat seedlings in Japan. *Mycological Progress* **13**: 1003.

de Cock AWAM, Lodhi AM, Rintoul TL, Bala K, Robideau GP, Abad ZG, Coffey MD, Shahzad S, Lévesque CA. **2015**. *Phytopythium*: molecular phylogeny and systematics. *Persoonia - Molecular Phylogeny and Evolution of Fungi* **34**: 25–39.

Polat Z, Awan QN, Hussain M, Akgül DS. **2017**. First Report of *Phytopytium vexans* Causing Root and Collar Rot of Kiwifruit in Turkey. *Plant Disease* **101**: 1058.

Robideau GP, De Cock AWAM, Coffey MD, Voglmayr H, Brouwer H, Bala K, Chitty DW, Désaulniers N, Eggertson QA, Gachon CMM, *et al.* 2011. DNA barcoding of oomycetes with cytochrome c oxidase subunit I and internal transcribed spacer. *Molecular Ecology Resources* **11**: 1002–1011.

Sorrenti G, Tacconi G, Tosi L, Vittone G, Nari L, Savian F, Saro S, Ermacora P, Graziani S, Toselli M. **2019**. Avanza la "moria del kiwi": evoluzione e primi riscontri della ricerca. *Frutticoltura* **2**: 34–42.

White TJ, Bruns T, Lee S, Taylor JL. **1990**. Amplification and direct sequencing of fungal ribosomal RNA genes for phylogenetics. *PCR protocols: a guide to methods and applications* **18**: 315–322.

4 See the unseen: empowering field monitoring activities with remote sensing data.

4.1 Introduction to the study | Chapter 4

Before this work, the monitoring of KD was limited to the observation of wilting appearance associated with rotted root and to the estimation of death rates. Indeed, no warning signs are usually visible before the first appearance of the symptoms and it is impossible to predict the evolution or the spread of the disease by observing the canopy with the naked eye. The only way to assess the disease presence is to look for rat tail symptoms and root rotting, but this sampling is highly unfeasible, time consuming and hard-working. Nevertheless, the intensive degradation of the roots caused by KD, should produce a considerable modification in the physiological response of the plants, especially regarding transpiration rates (Sorrenti *et al.*, 2016).

Meroni *et al.*, (2010) provided a comprehensive description of the effects of stressors on a plant's physiology and of how remote sensing technologies can be used to detect changes induced by them. Thermal infrared (TIR, 3 to 15 μm) and short wavelength infrared (SWIR, 1100 to 2500 nm) are the ones mostly suited to estimate leaf water content and transpiration rates, near infrared wavelength (NIR, 700–1,100 nm) respond to the leaf structure modifications, internal scattering processes, and on the absorption by leaf water, while visible range (VIS, 400 to 700 nm) is mostly related to pigment composition (Martinelli *et al.*, 2015; Mahlein, 2015).

This study evaluates the use of thermal and multispectral data to assess and predict the KD spreading, using k-means clustering algorithms to identify homogeneous areas within the field. K-means is an unsupervised approach for structuring the data when labelled reference data are not available (Behmann *et al.*, 2015). Our results suggest that plant vigour can correctly predict and therefore quickly evaluate the disease spread within a field, while temperature data instead provided enough accuracy to be considered reliable in predicting future disease outbreaks within infected orchards.

This work was developed in collaboration with Prof. Anne-Katrin Mahlein and Dr Stefan Paulus, Ph.D., at the Institut für Zuckerrübenforschung (IfZ), Gottingen, Germany, and is going to be submitted to "Remote Sensing".

References

Behmann J, Mahlein A-K, Rumpf T, Römer C, Plümer L. **2015**. A review of advanced machine learning methods for the detection of biotic stress in precision crop protection. *Precision Agriculture* **16**: 239–260.

Mahlein A-K. **2015**. Plant Disease Detection by Imaging Sensors – Parallels and Specific Demands for Precision Agriculture and Plant Phenotyping. *Plant Disease* **100**: 241–251.

Martinelli F, Scalenghe R, Davino S, Panno S, Scuderi G, Ruisi P, Villa P, Stroppiana D, Boschetti M, Goulart LR, *et al.* 2015. Advanced methods of plant disease detection. A review. *Agronomy for Sustainable Development* **35**: 1–25.

Meroni M, Rossini M, Colombo R. **2010**. Characterization of leaf physiology using reflectance and fluorescence hyperspectral measurements. In: Remote Sensing Optical Observation of Vegetation Properties. Research Signpost, Trivandrum, 165–177.

Sorrenti G, Toselli M, Reggidori G, Spinelli F, Tosi L, Giacopini A, Tacconi G. **2016**. Implicazioni della gestione idrica nella "Moria del kiwi" del veronese. *Frutticoltura* **3**: 1–7.

4.2 Remote sensing data to assess and predict outbreaks of a new decline syndrome affecting Kiwifruit orchards.

Francesco Savian[1], Marta Martini[1], Paolo Ermacora[1], Stefan Paulus[2] and Anne-Katrine Mahlein[2]

[1] Department of Agricultural, Food, Environmental and Animal Sciences (DI4A), University of Udine, Via delle Scienze 206, 33100 Udine, Italy

[2] Institute of Sugar Beet Research (IfZ), Göttingen, Germany.

Keywords: Disease detection, Outbreaks prediction, Sensor fusion, unsupervised clustering, multispectral imagery, thermal imagery.

ABSTRACT:

Backgrounds. After 7 years from the first record in Italy, Kiwifruit Decline (KD), a destructive disease causing root rot, has already affected more than 25% of the Italian kiwifruit cultivation area. Disease plants are characterized by a severe decay of the fine roots and sudden wilting of the canopy visible only after the first heat waves of the season (July-August).

Aims. The aim of this work was to study the feasibility of thermal and multispectral imagery for the detection of KD, using an unsupervised classifier.

Methods. RGB, Multispectral and Thermal data were acquired simultaneously over one field with diseased plants for two consecutive growing seasons (2017-2018) using a UAV platform. Data reduction was applied on the clipped areas and K-mean algorithm was used on the reduced data to cluster multispectral and thermal data of 2017 survey. Vigour class and health shifts between 2017 and 2018 were estimated via expert assessment and used as ground truth for clusters interpretation.

Results. Multispectral data showed high correlation with plant vigour, while temperature data seems to have good potential for health shift predictions especially for highly vigorous plants that were asymptomatic in 2017 and became symptomatic in 2018. Accuracy for vigour assessment was above 73% when using multispectral data, while clustering of temperature data allowed to predict one year in advance the disease outbreak with an accuracy of 71%.

Conclusions. Based on our results the unsupervised clustering of remote seeing data can be considered a reliable tool for the identification of sampling areas and will greatly improve the etiological studies on this new disease.

INTRODUCTION

Kiwifruit is an important, if yet relatively minor, crop easily recognized by consumers throughout the world. The total world production of cultivated kiwifruit is approximately 3 million tons and most of it is covered by China, New Zealand and Italy (Ferguson, 2016). Italy is one of the two major producers and exporters worldwide, covering alone the 15% of the total world demand (FAOSTAT, 2016). Since 2012, a new major disease known as kiwifruit decline (KD) is threatening the future of kiwifruit production in Italy (Tacconi et al., 2015). Up to now, the KD has already destroyed more than 25% (~6600ha) of the kiwifruit growing areas, (Tacconi, personal communication updating Sorrenti et al., 2019; Tacconi et al., 2019). To our knowledge, KD is limited to Italy but similar diseases were also described in other countries: New Zealand (Reid *et al.*, 1992), Japan (Huang & Qi, 1998), and more recently in Turkey (Akilli *et al.*, 2011; Kurbetli & Ozan, 2013; Polat *et al.*, 2017). The main damage caused by KD is the almost complete degradation of white feeding roots. Coarse roots usually show redness discoloration under the cortex and the external cylinder easily detach from the center creating the so called "rat tail" symptom (Tacconi *et al.*, 2014, 2015; Sorrenti *et al.*, 2016, 2019). Diseased plants go through an irreversible and fast wilting processes, suddenly visible late in the season (July, August- North hemisphere) when the first heat waves arrive (Savian et al., 2017). Diseased plants usually lose all the leaves and die in a few weeks after the appearance of the first wilting. In the following years, those plants that manage to survive reduce considerably the canopy vigour and never recover from their weakened condition (Sorrenti et al., 2019). KD spreads following and oil-spot pattern with and astonishing speed that can compromised the whole orchard in only one or two seasons (Tacconi et al., 2015).

Currently, the studies on KD are mostly focused on understanding the aetiology of the disease, which has not yet been fully clarified. Recent work demonstrated the necessary interaction between waterlogging and soil-borne pathogens to incite the disease (Savian *et al.*, 2019). Indeed, the role of

waterlogging was soon associated with KD, due to the high occurrence of the disease in poorly drained soils and because symptomatic plants are usually located in down slope areas where flooding occurs more easily (Tacconi *et al.*, 2014, 2015; Sorrenti *et al.*, 2016, 2019). The involvement of microorganisms in KD was introduce firstly by Tacconi et al. (Tacconi *et al.*, 2015) and more recently confirmed by Savian et al. (2019), but a common pathogen between diseased plants has not yet been found.

The lack of knowledge on the dynamics of root degradation, severely compromises the quality of sampling activities that cannot be properly scheduled. Timing and positioning of the sampling are indeed key factors for all etiological studies. In particular for KD, the core samples for laboratory analysis (feeding roots) are usually irreversibly deteriorated and almost useless for etiological investigations when symptoms appear (Savian *et al.*, 2019). Currently there are no efficient methods to scout orchards. Field survey presents indeed several limitations, mostly linked to the obstruction of the inter-row space by shoots, that reduce the field of view (1 to 3 meters only depending on plants vigour) and increase the time required even for the sole observation of the canopies. In addition, there are no methods to predict the disease outbreaks since the wilting appear suddenly even in healthy plants apparently devoid of any warning signs (Tosi *et al.*, 2015; Tacconi *et al.*, 2015; Sorrenti *et al.*, 2016). Currently, the only way to confirm the presence of the disease before plant dieback is the observation of the symptoms on the roots (rotting of fine roots and/or "rat-tail" symptoms in coarse roots) (Tacconi *et al.*, 2015), but this strategy is highly unfeasible: firstly, because there are no reliable methods to select which plant must be uprooted, and secondly because it is time consuming and hard-working.

Nevertheless, the high impact of the disease on plant vigour, if addressed properly, can be exploited to quickly assess KD spreading. Moreover, considering that feeding root decay is the main symptom of KD, the physiological response of the plant should be similar to the one induced by a drought

stress. It has been reported that in response to drought condition (Gucci *et al.*, 1993), severe root pruning (Black *et al.*, 2011) and even waterlogging condition (Savé & Serrano, 1986; Smith *et al.*, 1990), kiwifruit vines quickly close the stomata and reduce transpiration rates, leading to an increasing of the leaf temperature (Nuzzo *et al.*, 1996; Mills *et al.*, 2009).

Remote sensing can be a real support to scouting activities, especially for open field monitoring. Among remote sensing technologies, drone-based surveys provide several advantages for KD studies: firstly, they generate high resolution images which can be merged to picture the whole field and quickly evaluate the health status of the plants; secondly they can be equipped with different sensors, collecting data in non-visible wavelengths, such as the region of the near infrared (NIR) and thermal infrared.

Indeed, far infrared wavelength (TIR, 3 to 15 μm) has been wildly use to estimate water status of several plants (Jones & Schofield, 2008; Maes & Steppe, 2012; Mangus *et al.*, 2016), as well as indicator for early detection of several plant diseases that influence, directly or indirectly, leaf stomatal conductance and transpiration rates (Calderón *et al.*, 2013; Ortiz-Bustos *et al.*, 2017; Zarco-Tejada *et al.*, 2018). Also multispectral imagery has been widely used for evaluation of canopy vigour indices (Xue & Su, 2017), drought stress indexes (Li *et al.*, 2014) and plant pathogen detection (Sankaran *et al.*, 2010). In kiwifruit, thermal imaging has been previously adopted for the early detection of *Pseudomonas syringae* pv. *actinidiae* (Maes *et al.*, 2014), while multispectral data from satellite images were used to predict dry matter content of fruit (Mills *et al.*, 2018). Both multispectral and thermal images have been widely used for their correlation with plant physiological traits, but while thermal imagery reflects mostly water and gas exchange status of the plants, multispectral sensors (in particular NIR, 850–1700 nm) seem to be associated with internal structure modifications and water absorption by tissues (Mahlein, 2015).

To the best of our knowledge, the presented study is the first one which introduces remote sensing as a tool to guide etiological studies of unknown disease. Therefore, this work aimed to understand the feasibility and reliability of thermal and multispectral imagery in predicting and assessing disease outbreaks via an unsupervised classification approach.

MATERIALS AND METHODS

Experimental site

UAV based surveys were performed over one hectare of *Actinidia deliciosa* (A. Chev.) CF Liang et AR Ferguson var. *'Hayward'* in San Giorgio della Richinvelda (Friuli Venezia Giulia, NE Italy). The orchard was 20 years old, 5x5m T-bar plantation without anti-hail net, with micro-irrigation system (micro-sprinkler, 20 mm/hour) and with the following soil properties: 8% of gravel, 36% sand, 59% silt, 5% clay, 1.04 % organic matter (%w/w). First symptoms of kiwifruit decline were recorded in 2015 after an irrigation pipe broke in the central rows of the orchards. Later in 2016, the disease rapidly spread towards the border compromising approximately 30% of the field. From 2017, the field was regularly inspected to check the disease spreading patterns. In 2017, the disease affected almost the entire orchard compromising approximately 70% of the total areas, and in 2018 only few plants rows in the eastern border were still apparently healthy. Since the first appearance of the disease the orchard was irrigated following the usual agronomic practices. For instance, irrigation practices during the hotter period (June-August) consisted of one irrigation event every 4 days supplying a maximum of 30 mm of water.

Images acquisition

The UAV surveys were carried out on August 8th 2017, and July 18th 2018 during a sunny and hot day, between 10.00 and 11.00. The timing of the flight was based on a previous report suggesting this time frame as the one maximising the differences between well-fed and drought-stressed plants

(Nuzzo *et al.*, 1996). The flights were positioned respectively two days after an irrigation event in 2017 and three days after a heavy rainfall (20mm) in 2018, to exclude water deficit from the variables influencing canopy temperature and to make sure that the soil water content was not a limiting factor. The gravimetric soil moisture was measured the day before the flight in 9 points of the surveyed area. Three sampling areas were acquired inside an apparently healthy area, three in a heavily compromised area and three in a transition area between these two. The surveys were performed if the soil humidity was between 70 and 80% of the field capacity, optimal condition for kiwifruit growth (Huang, 2016). The field capacity was derived from the soil texture using SPAW models (Saxton & Willey, 2005).

Sensors specifics

The UAV flights were performed using a SAPR hexa-copter using RTK-GPS and a gimbal system on two axes (Adorn-technologies srl. - Italy). Thermal-Multispectral-RGB images were acquired simultaneously at a height of 35 m over the canopy. In 2017, the acquisition combined the three sensors reported in Table 1, while in 2018 the RGB and multispectral sensors were changed on behalf of Sequoia^{+} sensors (Parrot s.a.- France). For detailed information about the used sensors see Table 1.

Table 1. Characteristics of sensors used for clustering and expert assessment evaluation.

Flight year	Sensor type	Sensor name	Wavelength[1]			Spatial res.[2]	Use in this study
2017	RGB	GoPro 4	RED	0.66	0.40-0.70	1	Vigour and Plant health shifts assessment
			GREEN	0.55	0.40-0.70		
			BLUE	0.47	0.40-0.70		
	Multisp.	Tetracam ADC snap	NIR	0.79	0.52-0.90	4	Clustering
			RED	0.66	0.52-0.90		
			GREEN	0.55	0.52-0.90		
	Thermal	Thermal Capture 2.0 640	FIR	10.00	7.5-13.5	7	Clustering
2018	RGB	Sequoia+	RED	0.66	0.40-0.70	1	Vigour and Plant health shifts assessment
			GREEN	0.55	0.40-0.70		
			BLUE	0.47	0.40-0.70		

[1] wavelength central band and range in µm; [2] spatial resolution in cm/pixels with a flight height of at 35m

Pre-processing: creation of orthomosaic and alignment checking

For this study data from 2017 survey and RGB data from 2018 have been used. Before the stitching Multispectral data were scaled in a range from 0 to 1 with Pix4D (Pix4D s.a. - Switzerland), and temperature values (°C) were derived from the TIR wavelengths (Thermal Capture 2.0 640, FLIR system Inc., USA) using FLIR-studio (FLIR System Inc. – USA). Stitching, georeferencing and orthocorrection were processed independently for each combination of sensor x year. Acquisition, stitching and orthocorrection were performed by Adorn technology srl (Friuli Venezia Giulia - Italy). The four orthomosaics (multispectral and thermal of 2017; RGB of 2017 and 2018) were overlapped in Qgis software (Team, 2016) and planting line were drawn separately over each orthomosaics to check for alignment. A visualization of the workflow is presented in Figure 1.

Post-processing: clustering and reference data

Single-band orthomosaics were extracted from the multispectral orthomosaic and tested for band correlation. Green and red bands were de-correlated from the NIR band using the formula $R_{adj} = R_{ini} - R_{NIR} \times 0.8$, where R_{adj} is the corrected wavelength value, R_{ini} is the initial band value and R_{NIR} is the wavelength value in the NIR spectrum. This correction reduced the R^2 correlation to 0.64 between red and NIR band and from to 0.81 between green and NIR band. Temperature and RGB values were not modified after the stitching.

Identification of stump positions and determination of plant canopy size is hardly achievable when performing on-field UAVs surveys over kiwifruit, since: i) T-bar or pergola training system create a flat and dense canopy preventing stump identification; ii) the canopy of two neighbour plants usually overlap due to the disordered growth of shoots. For those reasons, a rough segmentation algorithm was applied to RGB, thermal and to each single-band multispectral orthomosaics. As first attempt, the segmentation has been made by cropping the orthomosaics with circular mask that progressively

moves along each planting line. The mask centres were placed 1.5 apart from each other and the masking radius was set to 1 m. The overlapping areas between two consecutive masks were evenly split before clipping. The circular shape was selected to reduce the border effect, while distance between mask centres and mask dimension were set to minimize interference from background pixels of the inter-row grass and reduce the occurrence of canopy overlapping.

After segmentation, multispectral and thermal data were used for unsupervised clustering, while RGB data from 2017 and 2018 surveys were used to estimate reference values for plant vigour and plant health shifts via expert assessment.

Mean values of thermal and multispectral data were evaluated within each masked areas. Mean values were stored in a matrix and associated with the coordinates of the masking centres. K-means clustering was then performed separately for multispectral (NIR and red bands) and thermal data, using a number of clusters between two and four.

The reference values for each clipped area were evaluated via expert assessment, rating the RGB data of 2017 and 2018. Clips derived from segmentation process, were singularly evaluated and ranked in four classes based on canopy vigour. Since it is impossible to assess the disease in field before symptoms appearance, the vigour shifts and the death rates between years are the only available features to estimate the plant health status. The assessment of plant vigour considered: leaf symptoms (yellowing, scorching wilting), disease severity (percentage of canopy with symptoms), and soil coverage (details in Table 2). The plant health shifts were then evaluated comparing plant vigour in 2017 and 2018. Only the shifts occurred on highly vigorous plants (apparently asymptomatic) were considered, since they were the most relevant for etiological studies (see Table 3). Indeed, reduction of the vigour can be caused by several aspects that might be unrelated to the disease under study.

Table 2. Criteria for expert assessment evaluation of vigour reference classes.

Plant vigour assessment				
Vigour class	V4	V3	V2	V1
Symptoms	None	None	Wilting ; yellowing; scorch	No leaf; wilting; yellowing; scorch
Disease severity[1]	0	0	25-50%	75-100%
Soil coverage	80-100%	60-80%	20-50%	0-20%
definition	High vigour	Medium vigour	Low vigour or irreversibly compromised	Dead or nearly dead

Table 3. Criteria for expert assessment evaluation of vigour reference classes.

Plant health shifts assessment				
Vigour in 2017	V4	V4	V4	V4
Vigour in 2018	V4	V3	V2	V1
Health shifts	S1	S2	S3	S4

Cluster interpretation

Finally, clustering results were compared with the reference classes of plant vigour in 2017, and plant health shifting between 2017 and 2018, via a two-step analysis: i) firstly, mosaic plots were used to visualize and explore possible correlation between clusters and reference data; ii) secondly predictive statistics were evaluated based on confusion matrices considering the result of correlation analysis.

Mosaic plot can display the relationship between categorical variables using rectangles whose areas represent the proportion of cases for any given combination of the multivariate categorical data [32]. Pared with residual analysis, such as Pearson X^2, the significance of that correlation can be estimated

[33]. A cluster can be considered representative of a reference class if it is positively correlated with only one class and negatively correlated with all the others.

Predictive statistics (sensitivity, accuracy, precision and F1-score) were then evaluated for those combinations (reference x cluster) whose correlation was significant ($p>0.05$) and meaningful. Therefore, vigour was compared to clusters from multispectral data, while thermal data were used for disease outbreak prediction. If the number of clusters was inferior to the number of reference classes, the latter was reduced to match the former, aggregating classes of the reference data. Reclassification was performed by merging classes reported in Table 2 only if: i) they were correlated (or at least highly represented) with the same cluster, ii) the overall accuracy of the confusion matrix increased after class aggregation, and iii) the new aggregated-classes preserved an internal logic. Therefore, the four reference classes for vigour (Table 2) were reduced to three and two merging V3 and V2 classes (weakened plants) and V4, V3 and V2 classes (plant with leaves) respectively. The new aggregated reference data for vigour were then compared with multispectral clustering with three or two clusters respectively.

The same criteria adopted for the aggregation of vigour classes were applied also for plant heath shifts, that were compared with two clusters derived from temperature data. Plants that remained asymptomatic without changing their vigour in 2018 (S1) were merged with those that reduced slightly their vigour without showing symptoms on the leaves (S2), creating a new class characterized by plants that remained unharmed; whereas plants that in 2018 died (S4) or were heavily compromised (23), were grouped in a new class composed by plants that most probably were already diseased in 2018.

All processing regarding decorrelation, segmentation, clustering and statistics of clusters were performed with RStudio (Team, 2013).

RESULTS

Correlation with reference data.

Multispectral data were mostly correlated with plant vigour (Figure 3a-c), but it was not a good predictor for disease outbreaks (Figure 3d-f). Spatial distribution of multispectral clusters resembles, indeed, those of reference data for vigour classes (Figure 2c-d and 2a, respectively). Overall it was possible to associate a meaningful interpretation to all the clusters, beside the number of clusters used.

With four clusters it was possible to correctly estimate all the vigour classes needed for the evaluation of the disease; with three, the weakened plants were separated from the asymptomatic and the dead ones; while with two clusters, plants with leaves were separated from those already dead.

When four clusters were used to classify multispectral orthomosaics (Figure 3a), each cluster was positively correlated with only one vigour class, and negatively correlated with all the others. Almost all the correlations were significant or highly significant suggesting that cluster M4 can be used for the detection of apparently asymptomatic plants with high vigour (V4), M3 for those asymptomatic but with low vigour (V3), M2 for plants heavily compromised but still alive (V2), and M1 for dead plants (V1).

Using three clusters (Figure 3b) on multispectral data, the extreme vigour classes V4 and V1 were still well discriminated by M3 and M1 respectively, while the cluster M2 was mostly correlated to the classes V2 and V3 corresponding to plants with a weakened status. Considering this association, errors can occur when assuming that cluster M3 is completely associated to the highly vigorous plants V4.

Finally, with two clusters only (Figure 3c), the plants with an asymptomatic canopy (V4 and V3) were clearly separated from the dead plants (V1) and correlated with clusters M2 and M1 respectively.

Major errors occur in the classification of the disease but still alive plant (V3), that seemed to be more correlated to the cluster M1.

Thermal data were mostly correlated with health shifts (Figure 3j-l), but could not be associated to any vigour class (Figure 3g-h). The hotter area within the orchards happened to be the one with the highest disease incidence in 2018 (Figure 2b and 2f-h). Canopy temperature ranged between 22 and 30°C, with the centre of the clusters between 23 and 26°C depending on the number of clusters used. Overall mosaic plots suggested that temperature data were able to predict disease outbreak by clustering the plants into two groups: one that will show disease symptoms (S3 and S4) and one that will remain asymptomatic (S1 and S2). Indeed, among the tested combinations the one with two clusters was showing the best discrimination between the plant health shift classes.

Nevertheless, the plants that died in 2018 (S4) have always been positively associated with the hottest clusters regardless of the number of clusters used (Figure 3j-l).

In the same way, plants that were heavily compromised but still alive in 2018 (S3), were usually abundant in hotter cluster, although not always with a significant correlation for all the numbers of clusters tested (Figure 3j-l).

Finally, the colder cluster T1 has always been positively associated with plants that maintained a high vigour also in 2018 (S1) and negatively correlated with those plants that became diseased (S3 and S4) (Figure 3j-l).

Clustering inference

Based on the mosaic plot results, the accuracy for estimating vigour classes or plant health shifts was tested via confusion matrix. Dead plants (V1) were the class with the highest predictive statistics for all the numbers of clusters tested, obtaining the best score set when four clusters were used. Reducing the number of clusters, the precision dropped to a minimum of 60%, but the sensitivity increased

greatly (91%). The same behaviour was observed for plants with high vigour (V4) that were correctly classified by clusters M4 and M3 when data were grouped into four or three clusters, respectively.

Clustering the data into four clusters was the approach that showed the best association with vigour of the plants and with the reference data. Each cluster was associated to a single class with an accuracy above 73% (Figure 4a). In particular, the extreme classes (V1 and V4) were precisely identified (precision above 78%) with a low number of false positives. Misclassification errors mostly occurred between neighbour classes, mostly due to false positives occurred in the association of cluster M3 with the vigour class V3. Reducing the number of clusters to three, the central cluster M2 was associated to weakened plants with an accuracy of 73% and a precision above 82% (Figure 4b). Finally, using only two clusters, it was possible to distinguish between dead plants with no canopy and plants with leaves (Figure 4c).

The predictive capability of thermal data was tested for health shifts occurred in plants that were highly vigorous in 2017 (Figure 4d). The best predictive capability on disease spreading was observed when clustering was performed with only two clusters, which allowed to discriminate plants that will show wilting from those that will not (accuracy and precision above 70%).

DISCUSSION

Our results suggested that these remote sensing technologies can indeed be useful tools for scouting activities at field scale and can highly improve monitoring activities. For instance, the sole observation of RGB map is highly useful because it allows us to quickly evaluate the conditions of the entire field.

Multispectral data can be used to speed up the assessment of the disease thanks to their correlation with plant vigour. By identifying dead or highly compromised plants, it was certainly possible to precisely delimit and monitor the spread of the disease, while the detection of very vigorous plants made it possible to identify homogeneous areas where other analyses could be focused for the prediction of disease outbreaks. Our results are in agreement with those of many other works that used NIR(850–1700 nm), green (495−570 nm), and red (620–750 nm) wavelengths to developed vegetation indices for the estimation of plant biophysical traits (Thenkabail *et al.*, 2000; Boelman *et al.*, 2003; Xue & Su, 2017; Quirós Vargas *et al.*, 2019).

The lack of ability to predict by multispectral data can be offset by that of thermal data. The canopy temperature was found to be a reliable predictor of plant health status, able to foresee the spread of the disease one year before. It is interesting to note that the best prediction metrics were obtained precisely for plants that were completely asymptomatic in 2017, far exceeding the predictive capably of any expert. Indeed, these plants were still apparently healthy in October 2017 and even in the first half of the vegetative season (March-June) of 2018 they produced a wide canopy, but suddenly after the first heat waves of July they showed scorches, leaves falling and in the worst cases complete defoliation. Results obtained from clustering of thermal data confirmed that plant responses to KD might be similar to those induced by drought stresses. Indeed, similarly to abiotic factors, pathogens may affect the stomata response by regulating the temperature gradient between the plant tissue and the air (Oerke *et al.*, 2014).

It could be speculated that the multispectral data fail to predict disease outbreaks, probably because the KD does not cause internal structure modifications until a critical point is reached, in which the root system can no longer support the transpiration rates (Sorrenti *et al.*, 2016). Indeed, it seems that kiwifruit has an excessive root:canopy ratio (Reid & Petrie, 1991; Black *et al.*, 2011), and can cope with a substantial (80%) loss of the root system before the growth of shoots and leaves is affected (Black *et al.*, 2011). Conversely, a justification on the predictive capability of canopy temperature may reside in the physiological response of kiwi vine to the drought stress or the root loss, which induce a rapid reduction of gas exchange fluxes and consequently an increase in leaf temperature (Gucci *et al.*, 1993; Xiloyannis *et al.*, 1993; Black *et al.*, 2011). It should also be noted that even flooding conditions can induce a reduction in the transpiration rate, therefore the water content of the soil cannot be overlooked during temperature data acquisition.

Given these results, the use of unsupervised clustering can be a reliable method for quickly explore and identify sampling areas that are suitable for etiological studies. To the best of our knowledge, unsupervised clustering has never been used for forecasting purposes, although it has been used for the assessment of cotton root rot (Yang *et al.*, 2015), for structuring the aggressiveness of fungal infection on peas (Setti *et al.*, 2009) and for the segmentation of plant background for weed detection (Tang *et al.*, 2000).

The biggest drawback of unsupervised classification methods is the need of an expert to assign meaning to each clustering. The use of supervised machine learning algorithms might be a solution to directly classify plant health status, but when the etiological background is not clear (such as in the KD syndrome), the development of a reliable training dataset is difficult because no tests are available to discriminate between diseased and healthy plants. Therefore, an unsupervised clustering is the only chance to see/find groups within unknown data when labelled data are not available, especially when

we do not know what kind of sensor data is needed to find patterns and groups (Behmann *et al.*, 2015).

Several improvements can be performed to the proposed approach. A better segmentation algorithm, which leverages on sensor fusion processes and perfect overlaps of the orthomosaics, is needed to remove background noise. For instance, the fusion of thermal, fluorescence and optical hyperspectral airborne data has been successfully used to assess olive plants infected by *Verticillum* wilt (Calderón *et al.*, 2013). Moreover, sensor fusion advantages are already evident in fruit safety and quality control studies (Blasco et al., 2007; Gowen et al., 2007; Sighicelli et al., 2009). In our case study, low-cost multispectral sensor precluded the possibility to correctly segment the grass of the inter-row from the kiwifruit canopy. Nevertheless, it allowed a correct classification of the plant vigour. A better understanding of the relationship between temperature and plant health status is also needed. To use temperature as reliable predictor, models able to predict leaf temperature using data from weather stations (e.g. air temperature, air relative humidity, radiation, soil water content) should be developed to set more objective thresholds for discriminating healthy plants from diseased ones. Studies on spectral resolution are also needed to identify the best wavelength for the disease detection. In particular, it would be interesting to study the correlations between KD appearance and short-wave infrared wavelength (1,100 to 2,500 nm), due to their correlation with the composition of leaf chemicals and with water content (Jacquemoud & Ustin, 2001; Carter & Knapp, 2001).

CONCLUSIONS

The proposed study is the very first one that managed to predict the spread of kiwifruit decline using remote sensing technologies. Our results suggested that the unsupervised clustering can be a reliable algorithm to characterize the disease in its early stages to identify homogenous areas within the fields. Multispectral data can be used to discriminate the symptomatic plants from the asymptomatic ones allowing a quick estimation of the disease spreading. On the other hand, thermal data has been shown

to be effective in predicting future outbreaks of the disease providing an informative tool for directing sampling activities for etiological and epidemiological studies.

REFERENCES

Akilli S, Serçe ÇiU, Zekaİ Katircioğlu Y, Karakaya A, Maden S. **2011**. Involvement of *Phytophthora citrophthora* in kiwifruit decline in Turkey. *Journal of Phytopathology* **159**: 579–581.

Behmann J, Mahlein A-K, Rumpf T, Römer C, Plümer L. **2015**. A review of advanced machine learning methods for the detection of biotic stress in precision crop protection. *Precision Agriculture* **16**: 239–260.

Black MZ, Patterson KJ, Minchin PEH, Gould KS, Clearwater MJ. **2011**. Hydraulic responses of whole vines and individual roots of kiwifruit (*Actinidia chinensis*) following root severance. *Tree Physiology* **31**: 508–518.

Blasco J, Aleixos N, Gómez J, Moltó E. **2007**. Citrus sorting by identification of the most common defects using multispectral computer vision. *Journal of Food Engineering* **83**: 384–393.

Boelman NT, Stieglitz M, Rueth HM, Sommerkorn M, Griffin KL, Shaver GR, Gamon JA. **2003**. Response of NDVI, biomass, and ecosystem gas exchange to long-term warming and fertilization in wet sedge tundra. *Oecologia* **135**: 414–421.

Calderón R, Navas-Cortés JA, Lucena C, Zarco-Tejada PJ. **2013**. High-resolution airborne hyperspectral and thermal imagery for early detection of *Verticillium* wilt of olive using fluorescence, temperature and narrow-band spectral indices. *Remote Sensing of Environment* **139**: 231–245.

Carter GA, Knapp AK. **2001**. Leaf optical properties in higher plants: linking spectral characteristics to stress and chlorophyll concentration. *American Journal of Botany* **88**: 677–684.

FAOSTAT. **2016**. Food and Agriculture Organization of the United Nations, Rome, Italy.

Ferguson AR. **2016**. World Economic Importance. In: Testolin R, Huang H-W, Ferguson AR, eds. Compendium of Plant Genomes. The Kiwifruit Genome. Cham: Springer International Publishing, 37–42.

Gowen A, Odonnell C, Cullen P, Downey G, Frias J. **2007**. Hyperspectral imaging – an emerging process analytical tool for food quality and safety control. *Trends in Food Science & Technology* **18**: 590–598.

Gucci R, Massai R, Piccotino D, Xiloyannis C. **1993**. Gas exchange characteristics and water relations of kiwifruit vines during drought cycles. *Acta Horticulturae*: 213–218.

Huang H. **2016**. *Kiwifruit: The Genus ACTINIDIA*. Academic Press.

Huang Y, Qi P. **1998**. Studies on the cause of root rot of kiwifruit in Guangdong Province. *Journal of South China Agricultural University* **19**: 19–22.

Jacquemoud S, Ustin SL. **2001**. Leaf optical properties: A state of the art. In: 8th International Symposium of Physical Measurements & Signatures in Remote Sensing. 223–332.

Jones H, Schofield P. **2008**. Thermal and other remote sensing of plant stress. *General and Applied Plant Physiology* **34**.

Kurbetli İ, Ozan S. **2013**. Occurrence of *Phytophthora* Root and Stem Rot of Kiwifruit in Turkey. *Journal of Phytopathology* **161**: 887–889.

Li L, Zhang Q, Huang D. **2014**. A Review of Imaging Techniques for Plant Phenotyping. *Sensors* **14**: 20078–20111.

Maes WH, Minchin PEH, Snelgar WP, Steppe K. **2014**. Early detection of Psa infection in kiwifruit by means of infrared thermography at leaf and orchard scale. *Functional Plant Biology* **41**: 1207.

Maes WH, Steppe K. **2012**. Estimating evapotranspiration and drought stress with ground-based thermal remote sensing in agriculture: a review. *Journal of Experimental Botany* **63**: 4671–4712.

Mahlein A-K. **2015**. Plant Disease Detection by Imaging Sensors – Parallels and Specific Demands for Precision Agriculture and Plant Phenotyping. *Plant Disease* **100**: 241–251.

Mangus DL, Sharda A, Zhang N. **2016**. Development and evaluation of thermal infrared imaging system for high spatial and temporal resolution crop water stress monitoring of corn within a greenhouse. *Computers and Electronics in Agriculture* **121**: 149–159.

Mills L, Flemmer R, Flemmer C, Bakker H. **2018**. Prediction of kiwifruit orchard characteristics from satellite images. *Precision Agriculture*.

Mills TM, Li J, Behboudian MH. **2009**. Physiological Responses of Gold Kiwifruit (*Actinidia chinensis*) to Reduced Irrigation. *Journal of the American Society for Horticultural Science* **134**: 677–683.

Nuzzo V, Dichio B, Montanaro G, Xiloyannis C. **1996**. Risposta di piante di actinidia in piena produzione alle limitate disponibilità idriche del suolo. Atti del Convegno Nazionale. In: Faenza.

Oerke E-C, Mahlein A-K, Steiner U. **2014**. Proximal Sensing of Plant Diseases. In: Gullino ML, Bonants PJM, eds. Plant Pathology in the 21st Century. Detection and Diagnostics of Plant Pathogens. Dordrecht: Springer Netherlands, 55–68.

Ortiz-Bustos CM, Pérez-Bueno ML, Barón M, Molinero-Ruiz L. **2017**. Use of Blue-Green Fluorescence and Thermal Imaging in the Early Detection of Sunflower Infection by the Root Parasitic Weed Orobanche cumana Wallr. *Frontiers in Plant Science* **8**: 833.

Polat Z, Awan QN, Hussain M, Akgül DS. **2017**. First Report of *Phytopytium vexans* Causing Root and Collar Rot of Kiwifruit in Turkey. *Plant Disease* **101**: 1058.

Quirós Vargas JJ, Zhang C, Smitchger JA, McGee RJ, Sankaran S. **2019**. Phenotyping of Plant Biomass and Performance Traits Using Remote Sensing Techniques in Pea (*Pisum sativum*, L.). *Sensors (Basel, Switzerland)* **19**.

Reid JB, Petrie RA. **1991**. Effects of soil aeration on root demography in kiwifruit. *New Zealand Journal of Crop and Horticultural Science* **19**: 423–432.

Reid JB, Tate KG, Brown NS. **1992**. Effects of flooding and alluvium deposition on kiwifruit (*Actinidia deliciosa*). *New Zealand Journal of Crop and Horticultural Science* **20**: 283–288.

Sankaran S, Mishra A, Ehsani R, Davis C. **2010**. A review of advanced techniques for detecting plant diseases. *Computers and Electronics in Agriculture* **72**: 1–13.

Savé R, Serrano L. **1986**. Some physiological and growth responses of kiwi fruit (*Actinidia chinensis*) to flooding. *Physiologia Plantarum* **66**: 75–78.

Savian F, Martini M, Borselli S, Saro S, Musetti R, Loi N, Firrao G. **2017**. Studies on kiwifruit decline, an emerging issue even for Friuli Venezia Giulia (eastern Italy). *Journal of Plant Pathology* **99**: 18.

Savian F, Musetti R, Sandrin N, Ermacora P, Martini M. **2019**. Etiological studies over kiwifruit decline reveal the involvement of both flooding and biotic factors. In: XXV National Congress of Italian Phytopathological Society (SIPaV). Milano.

Saxton KE, Willey PH. **2005**. The SPAW model for agricultural field and pond hydrologic simulation. *Watershed models*: 400–435.

Setti B, Bencheikh M, Henni J, Neema C. **2009**. Comparative Aggressiveness of *Mycosphaerella pinodes* on Peas from Different Regions in Western Algeria. *Phytopathologia Mediterranea* **48**.

Sighicelli M, Colao F, Lai A, Patsaeva S. **2009**. Monitoring post-harvest orange fruit disease by fluorescence and reflectance hyperspectral imaging. *Acta Horticulturae*: 277–284.

Smith GS, Judd MJ, Miller SA, Buwalda JG. **1990**. Recovery of kiwifruit vines from transient waterlogging of the root system. *New Phytologist* **115**: 325–333.

Sorrenti G, Tacconi G, Tosi L, Vittone G, Nari L, Savian F, Saro S, Ermacora P, Graziani S, Toselli M. **2019**. Avanza la "moria del kiwi": evoluzione e primi riscontri della ricerca. *Frutticoltura* **2**: 34–42.

Sorrenti G, Toselli M, Reggidori G, Spinelli F, Tosi L, Giacopini A, Tacconi G. **2016**. Implicazioni della gestione idrica nella "Moria del kiwi" del veronese. *Frutticoltura* **3**: 1–7.

Tacconi G, Giacopini A, Tosi L. **2014**. La Moria Del Kiwi Nel Veronese. *Kiwi informa* **Aprile/Giugno**: 5–23.

Tacconi G, Giacopini A, Vittone G, Nari L, Spadaro D, Savian F, Ermacora P, Saro S, Morone C, Bardi L, *et al.* 2019. "moria del kiwi": situazione disastrosa al nord, preoccupante nel resto d'Italia. *Kiwi informa* **Aprile/Giugno**: 32–37.

Tacconi G, Paltrinieri S, Mejia JF, Fuentealba SP, Bertaccini A, Tosi L, Giacopini A, Mazzucchi U, Favaron F, Sella L, *et al.* 2015. Vine decline in kiwifruit: climate change and effect on waterlogging and *Phytophthora* in north italy. *Acta Horticulturae*: 93–97.

Tang L, Tian LF, Steward BL. **2000**. Color image segmentation with genetic algorithm for in-field weed sensing. *Transactions of the ASAE* **43**.

Team RC. **2013**. R: A language and environment for statistical computing.

Team QD. **2016**. QGIS geographic information system. *Open Source Geospatial Foundation Project*.

Thenkabail PS, Smith RB, De Pauw E. **2000**. Hyperspectral Vegetation Indices and Their Relationships with Agricultural Crop Characteristics. *Remote Sensing of Environment* **71**: 158–182.

Tosi L, Tacconi G, Giacopini A. **2015**. La moria del kiwi, situazione e prospettive. *L'Informatore Agrario* **44**: 67–70.

Xiloyannis C, Massai R, Piccotino D, Baroni G, Bovo M. **1993**. Method and technique of irrigation in relation to root system characteristics in fruit growing. *Acta Horticulturae*: 505–510.

Xue J, Su B. **2017**. Significant Remote Sensing Vegetation Indices: A Review of Developments and Applications. *Journal of Sensors* **2017**: 1–17.

Yang C, Odvody GN, Fernandez CJ, Landivar JA, Minzenmayer RR, Nichols RL. **2015**. Evaluating unsupervised and supervised image classification methods for mapping cotton root rot. *Precision Agriculture* **16**: 201–215.

Zarco-Tejada PJ, Camino C, Beck PSA, Calderon R, Hornero A, Hernández-Clemente R, Kattenborn T, Montes-Borrego M, Susca L, Morelli M. **2018**. Previsual symptoms of *Xylella fastidiosa* infection revealed in spectral plant-trait alterations. *Nature Plants* **4**: 432.

AUTHOR CONTRIBUTIONS:

Conceptualization, FS, MM, PE and SP; methodology, FS, SP, MM, PE and AKM; formal and analysis and data curation, FS and SP; writing—original draft preparation, FS; writing—review and editing, SP, MM, PE and AKM; supervision, AKM.

ACKNOWLEDGMENTS:

Simone Saro, from ERSA- Phytosanitary Service of Friuli Venezia Giulia region (Italy), for his collaboration and support in field-scouting activities. Luca Zuliani, form Adron technology srl, for his help in the pre-processing of the images and generation of the orthomosaics.

FIGURE CAPTIONS

Figure 1. Processing pipeline. Processes are represented in darker background, while data are in light background. In green scale, data and processing used as input for the unsupervised classification; in blue scale, the ones used for reference data estimation; in yellow scale, the ones in common between the two processing pipelines. Abbreviations: ROI, region of interest; GeoRef, georeferenced

Figure 2. Spatial distribution of the results obtained after clustering and the references used for the interpretation. a) in blue scale, expert assessment of ratings for the vigour classes (V4 high, V3 medium, V2 weak, V1 dead). b) in brown scale, plant health shifts between 2017 and 2018 (S1 asymptomatic plant that preserved high vigour, S2 asymptomatic but weakened plant, S3 diseased plant but still alive, S4 plant that died in 2018). c-e) in green scale, clustering derived by multispectral bands. f-h) in red scale, clusters resulting from the analysis of thermal images: triangles indicate the temperature of the clusters' centres. In b) and f-h) white colour is used for plants that were not highly vigorous in 2017 and therefore were discarded for plant heath shifts analysis. Purple dotted circles identify the hottest area within the orchard that happened to be the one with the highest disease incidence.

Figure 3. Correlation between clusters and reference data. a-c) and d-e) correlation of multispectral clusters with vigour classes and plant health shifts respectively. g-i) and j-l) correlation of thermal clusters with vigour classes and plant heath shifts. White colour is used for not significantly correlated combinations. Positive and negative correlations are highlighted in blue and red respectively, and shaded in relation to their confidence level (Pearson test): 95% confidence in brighter colors, 99% in darker tones. The bases of the rectangles are proportional to the total number of images within each reference class (numbers at the bottom of the graph), whereas heights are the proportion of reference data within the specific cluster.

Figure 4. Predictive statistics for disease assessment (vigour) and outbreak prediction (plant heath shifts). a-c), performance of multispectral clustering to assess disease spreading (plant vigour) using 4, 3 or 2 clusters. Reference data were merged if the number of clusters was inferior to the number of reference classes: for 3 clusters, a class was created aggregating healthy plants (V3+V4); for 2 clusters, the three vigour classes in regards to plants with leaves (V4+V3+V2) were grouped together. d), performance of thermal clustering with 2 clusters in predicting disease outbreak occurred in plants highly vigorous in 2017. Plants that remained highly vigorous in 2018 or did not show wilting symptoms were separated from those that wilted or died.

Figure 1. Processing pipeline.

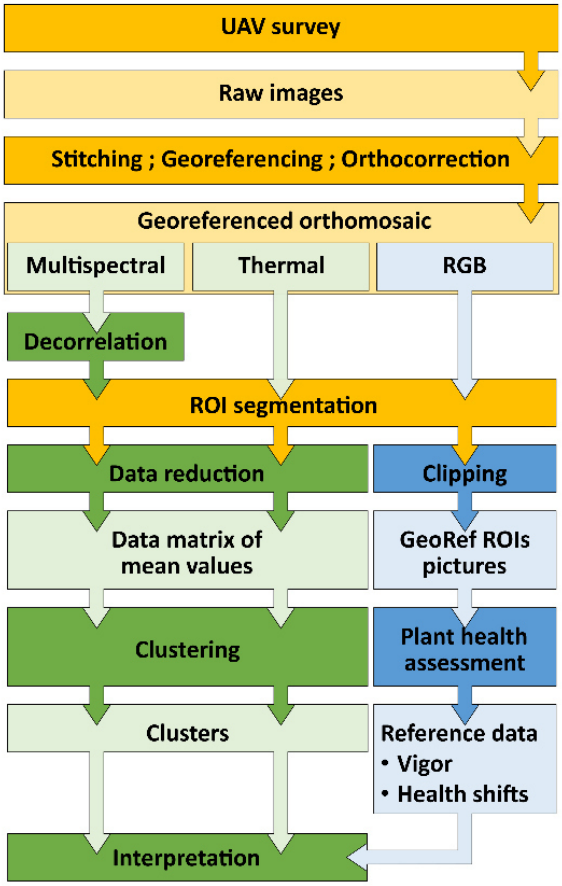

Figure 2. Spatial distribution of the results obtained after clustering and the references used for the interpretation.

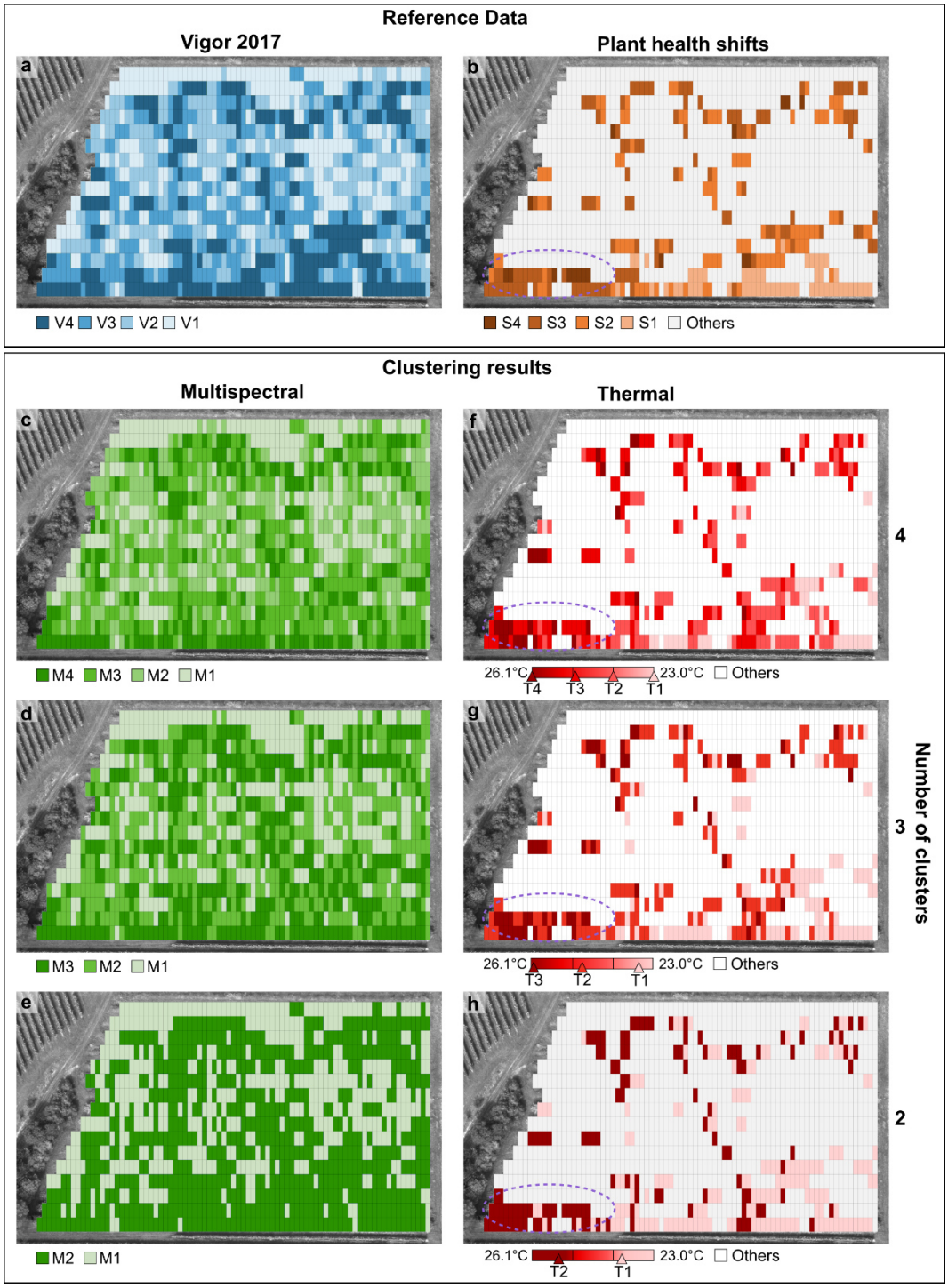

Figure 3. Correlation between clusters and reference data.

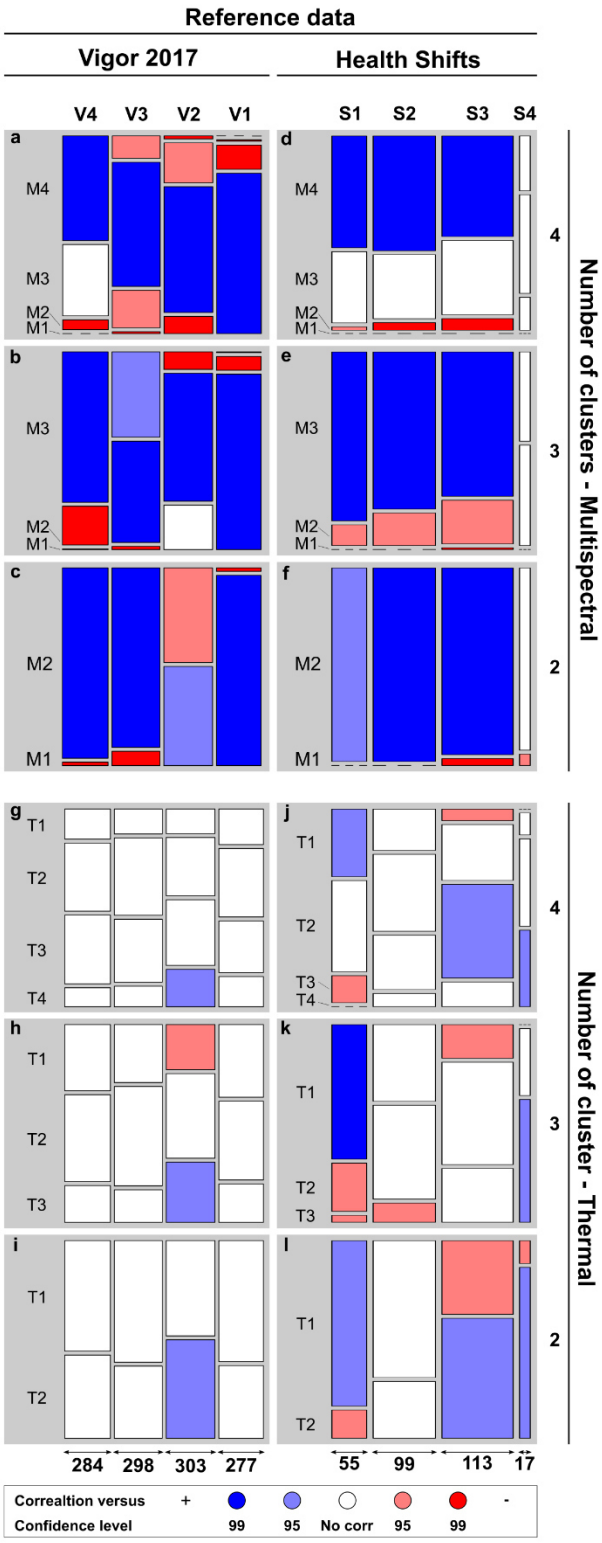

Figure 4. Predictive statistics for disease assessment (vigour) and outbreak prediction (plant heath shifts).

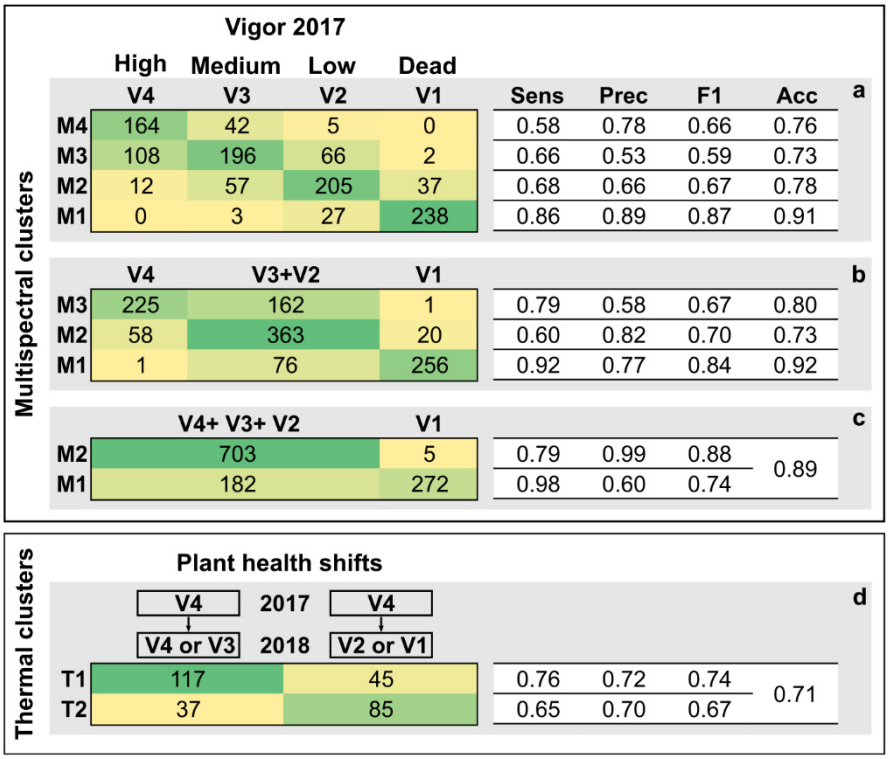

5 Exploring the whole community: metabarcoding approach applied to emerging diseases.

5.1 Introduction to the study | Chapter 5

The High Throughput Sequencing (HTS), or Next Generation Sequencing (NGS), methods are probably the most significant advances in molecular biology since the advent of the PCR process in the early 1980s (Adams *et al.*, 2018). Among the omics techniques, metabarcoding based on Illumina sequencing has been widely used in ecology due to the high sequencing depth and relatively low cost per read (Tedersoo *et al.*, 2019). This method allows to identify thousands of taxa per sample from hundreds of samples simultaneously, without the need of culturing the targeted microorganisms. Metabarcoding relies on the sequencing of one or more short fragments (barcode genes) of DNA from standardized regions of the genome to identify different species (Hebert *et al.*, 2003). These barcode genes can be defined as any fragment of DNA that: (i) contains significant species-level genetic variability (ii) possesses conserved, but taxa specific, flanking sites that can be used to design universal PCR primers to selectively amplify the desired microorganisms (Abdelfattah *et al.*, 2018). Updated and extensive reviews on metabarcoding techniques and practical advices on experimental set-up, bioinformatics analysis, and primer selection are given in Tedersoo *et al.*, (2018), Tedersoo *et al.*, (2019); Nilsson *et al.*, (2019); Calle, (2019).

Since metabarcoding provides a comprehensive picture of the genetic diversity present in a sample, it can be a valuable tool for identifying putative causal agents responsible for complex diseases or disease syndromes. In this regard, the concept of a "pathobiome" is emerging and is receiving greater discussion (Abdelfattah *et al.*, 2018). This concept takes into consideration the pathogen and its interactions within the whole microbial community and it has been used, for example, to study the microbial community associated with Acute Oak Decline Syndrome enabling the detection of some putative causal agents (Sapp *et al.*, 2016)

At the same way in the context of kiwifruit decline, this technology can provide useful information on microbial communities including all putative plant pathogens; thus, potentially revealing unknown association also with taxa that are non-culturable or that require specific protocols to be efficiently isolated. Although no confirmation on pathogenicity can be retrieved, this analysis is a powerful tool especially if used at the beginning of etiological studies since it can provide helpful information to correctly setup experiments and protocols.

In this work, we studied the oomycete and fungal communities sequencing the ITS2-region using an Illumina Myseq technology, to have the first comprehensive overview on taxa associated with KD.

This study will be submitted to "Scientific Reports".

References

Abdelfattah A, Malacrinò A, Wisniewski M, Cacciola SO, Schena L. **2018**. Metabarcoding: A powerful tool to investigate microbial communities and shape future plant protection strategies. *Biological Control* **120**: 1–10.

Adams IP, Fox A, Boonham N, Massart S, De Jonghe K. **2018**. The impact of high throughput sequencing on plant health diagnostics. *European Journal of Plant Pathology* **152**: 909–919.

Calle ML. **2019**. Statistical Analysis of Metagenomics Data. *Genomics & Informatics* **17**.

Hebert PDN, Cywinska A, Ball SL, deWaard JR. **2003**. Biological identifications through DNA barcodes. *Proceedings. Biological Sciences* **270**: 313–321.

Nilsson RH, Anslan S, Bahram M, Wurzbacher C, Baldrian P, Tedersoo L. **2019**. Mycobiome diversity: high-throughput sequencing and identification of fungi. *Nature Reviews Microbiology* **17**: 95–109.

Sapp M, Lewis E, Moss S, Barrett B, Kirk S, Elphinstone JG, Denman S. **2016**. Metabarcoding of Bacteria Associated with the Acute Oak Decline Syndrome in England. *Forests* **7**: 95.

Tedersoo L, Drenkhan R, Anslan S, Morales- Rodriguez C, Cleary M. **2019**. High-throughput identification and diagnostics of pathogens and pests: Overview and practical recommendations. *Molecular Ecology Resources* **19**: 47–76.

Tedersoo L, Tooming-Klunderud A, Anslan S. **2018**. PacBio metabarcoding of Fungi and other eukaryotes: errors, biases and perspectives. *The New Phytologist* **217**: 1370–1385.

5.2 A metabarcoding approach to investigate fungal and oomycete communities associated with kiwifruit decline in Italy

Francesco Savian[1], Fabio Marroni[1], Giuseppe Firrao[1], Paolo Ermacora[1], Marta Martini[1]

[1]Department of Agricultural, Food, Environmental and Animal Sciences (DI4A), University of Udine, 33100 Udine, Italy.

Keywords**:** Oomycetes, Fungi, microbiota, ITS2 Illumina sequencing, Actinidia.

ABSTRACT

Background. In the last 7 years a new disease known as Kiwifruit decline (KD) is severely compromising all the major kiwifruit growing areas in Italy. KD causes a decay of the fine roots, causing a sudden wilting and the plant death. The disease aetiology is still under study but a recent work has demonstrated the necessary interaction between waterlogging and a soil-borne pathogen(s).

Aim. This work aims to describe the oomycete and fungal communities associated with KD and to identify key taxa potentially involved in the disease, analysing root endosphere and rhizosphere via a metabarcoding approach.

Methods. Root and rhizosphere samples were collected based on a two-year survey (2017-2018) from kiwifruit plants in an area within a control site considered "healthy" (CC1) and in three areas of a diseased site: i) one which remained asymptomatic until 2018 (AA2), ii) one which became diseased during 2018 (AD2), and iii) the last one that was already diseased in 2017 (DD). Total genomic DNA was extracted from root endosphere a rhizosphere separately and amplified with a nested PCR to amplify the fungal and oomycetes communities. The communities were compared in term of alpha- and beta-diversities, and key taxa were identified using univariate differential abundance tests.

Results. Major differences in taxa distribution were found between samples from "healthy" and diseased site, rather than between asymptomatic (CC1 and AA) and diseased areas (AD2 and DD2). *Phytophthora sojae* and *Ilyonectria macrodidyma* were found as the key taxa characterising the diseased site and supposed to be involved in the diseases (putative plant pathogens). Other species previously linked to decline-like disease were found mostly correlated to diseased areas, such as *Phytopythium vexans*.

Conclusions. Our work seems to confirms the role of Oomycetes in Kiwifruit Decline, suggesting a scenario where several potential pathogens of this class might be involved in the disease.

INTRODUCTION

Italy is the second worldwide producer of kiwifruit (*Actinidia deliciosa* and *Actinidia chinesnis* C.F. Liang & A.R. Ferguson) with 26,650 ha of cultivated area and a production of approximately 571,020 tons/year which meets over 15% of the global demand for this product (FAOSTAT, 2016). A anomalous disease named kiwifruit decline (KD), characterized by root rot and plant dieback, has been reported in Italy since 2012 and currently affects 25% (6600 ha) of Italian kiwifruit production area Veneto 2000 ha, Piedmont 3500 ha, Lazio 1000 ha, Friuli Venezia Giulia 60 ha, and a few areas in Emilia-Romagna and Calabria (Tacconi, personal communication updating Sorrenti *et al.*, 2019). To our knowledge, the disease is still limited to Italy but similar vine decline disorders, which can probably be ascribed to KD, have been reported in other countries: Turkey (Akilli *et al.*, 2011; Kurbetli & Ozan, 2013; Polat *et al.*, 2017), Japan (Huang & Qi, 1998), and New Zealand (Reid *et al.*, 1992).

KD affects orchards of both green (*A. deliciosa*)- and yellow (*A. chinensis*)-fleshed kiwifruits and often proceeds from down slope areas or dips, compromising the entire orchard even in just one season (Sorrenti *et al.*, 2019). KD heavily damage the root system destroying most of the feeding roots and compromising the integrity of the coarse roots. Typical symptoms visible on the roots are rotting tissues on smaller roots (diameter less than 5 mm c.a) and lack of cohesion between the central cylinder and core of coarse roots defined as “rat-tail” symptom (Sorrenti *et al.*, 2016). Diseased plants remain asymptomatic till the arrival of the first heat waves in the summer, when suddenly scorches and leaves defoliation become visible.

While waterlogging was soon observed to be associated with its outbreak, the putative role of soil microbiota remained unknown until a recent work by Savian et al. (submitted for publication, Chapter 2) that investigated the role of these two factors in the onset of the disease.

Savian et al. (submitted for publication, Chapter 2) succeeded in reproducing KD under controlled conditions and clearly demonstrated that waterlogging is a prerequisite for the deteriorations of feeding roots and the onset of the decline syndrome, but also that a soil-borne pathogen must be present to induce the disease. The results of the isolations suggested that major candidates as potential soil-borne pathogens appear to be the Oomycetes *Pythopythium chamaehyphon* and *P. vexans*. Furthermore, the pathogenicity of some *P. vexans* isolates has been demonstrated through the fulfilment of Koch's postulates by Polat in Turkey (Polat *et al.*, 2017) and more recently for KD-associated isolates by Principe et al. (Prencipe et al, submitted for publication, Chapter 3). Taking into account these results by Savian et al. (submitted for publication, Chapter 2), the evidence from Tacconi et al. (2015), together with i) the role of free water in Oomycetes infections, ii) the role of waterlogging in KD and iii) the official reports on Oomycetes associated with decline-like diseases (Conn *et al.*, 1991; Huang & Qi, 1998; Latorre & Pak, 2003; Akilli *et al.*, 2011; Wang *et al.*, 2015; Çiftçi *et al.*, 2016), it seems that one or more oomycete species could be involved in the disease. In addition, little is known about the relationship between diversity of soil-borne microbial community in healthy kiwifruit orchards and much less about the one related to Kiwifruit Decline.

Since metabarcoding provides a comprehensive picture of the genetic diversity present in a sample through the amplification and high-throughput sequencing of a specific barcode region, it can be a valuable tool for assessing the diversity of soil microbiota and for identifying putative causal agents responsible in the context of complex diseases or disease syndromes like kiwifruit decline (Abdelfattah *et al.*, 2018). This approach has been used for example to study the microbial community associated with Acute Oak Decline Syndrome and enabled the detection of a set of putative causal agents (Sapp *et al.*, 2016).

The main objective of our work was to assess, describe and compare the structure and composition of fungal and oomycete communities in the root and rhizosphere of kiwifruit affected by kiwifruit decline, using a metabarcoding approach.

To reach our main objective, the following specific objectives were addressed: i) to compare the fungal and oomycete diversity in four groups of kiwifruit plants differing for health status in relation to KD; ii) to identify key taxa which might be related to kiwifruit decline. These results should contribute to a better understanding of the influence of soil microbial communities on the spreading of KD and to the identification of important fungal and oomycete taxa related to KD in Italy.

MATERIAL AND METHODS

Sites description

In order to minimize the influence of environmental conditions and plant phenological and physiological states on plant-associated microbial communities, samples were collected at the same time from plants of the same age, grown and managed with identical agronomical practices in two commercial orchards (Fig. 1 and Table 1) located in San Giorgio della Richinvelda (Pordenone province, Friuli-Venezia Giulia region, North-eastern Italy). Survey activities for the observation of KD symptoms on both canopy and roots started in October 2016 and continued since 2019. The two sites considered were: i) an orchard that was monitored since 2017 and remained asymptomatic in both canopy and root since 2019 (Site 1, Fig. 1b); ii) , an orchard 3 km away from Site 1 (Site 2, Fig. 1c), which showed the first symptoms of kiwifruit decline in 2015 after the break of an irrigation pipe. The irrigation pipe broke in June 2015 and was repaired 7 days later, causing waterlogging for at least 9-10 days. Later in July, KD symptoms appeared mostly on the planting row that had been

flooded. Since then, the disease spread rapidly and at the end of 2018 most of the field was already compromised excluding few plants in the north-eastern corner.

In Site 1, plants remained symptomless in both root and canopy along the entire duration of the surveys: complete absence of wilting in all the plants and healthy roots with complete absence of rat tail symptoms even in the deepest layer of soil. Plants of this site were still symptomless in 2019, confirming that they were most probably healthy even in 2018 (group CC1).

In Site 2, three main areas were identified based on plant health shifts occurred between 2017 and 2018 characterized by: i) plants showing no symptoms of kiwifruit decline at the canopy and root levels either in 2017 or in 2018 (group AA2), ii) plants showing symptoms only in 2018 (group AD2) and iii) plants that were symptomatic in both years 2017 and 2018 (group DD2). Observation in 2019 was impossible in site 2 because the orchard was explanted.

Root samples were collected on August 1st, 2018, from the four sampling areas: one from Site1 and three from Site 2. Details on sampling areas and group naming are given in Table 1.

Table 1. Characteristics of sampling sites and naming of sample groups. Sample group codes derive by the combination of Health status in 2017 x Health status in 2018 x Site x Compartment. The first 2 letter identify the health status in 2017 and 2018 respectively: "A" for asymptomatic and "D" for diseased. The control site health status was identified with "CC". The numbers "1" and "2" represent the sampling site, while "Rh" and "RE" stay for rhizosphere and root endosphere compartments, respectively.

Sampling sites:				
Site name	Site 1	Site 2		
Latitude[1]	46.0395	46.0389		
Longitude[1]	12.8649	12.8654		
Stand age[2]	17	21		
Year of first outbreak	None	2015		
Sampling areas				
Site	1	2	2	2
Health status in 2017	Asymptomatic	Asymptomatic	Asymptomatic	Diseased
Health status in 2018	Asymptomatic	Asymptomatic	Diseased	Diseased
Soil properties[3]				
Gravel	68	52	38	3
Sand	43	45	42	30
Silt	47	49	53	65
Clay	10	6	5	5
C org	-	1.22	-	0.89
Sample group's names:				
Compartment				
Root endosphere	CC1-RE	AA2-RE	AD2-RE	DD2-RE
Rhizosphere	CC1-Rh	AA2-Rh	AD2-Rh	DD2-Rh

[1] decimal degree, [2] years, [3] percentage (w/w)

Sample collection and separation of root endosphere and rhizosphere.

From each sampling area the roots from 10 plants were up-taken and processed to separate the rhizosphere from root endosphere following the protocol of Simmons *et al.*, (2018) with some

modifications. The two plant compartments were indicated with Rh for the rhizosphere and RE for the root endosphere (Table 1).

Fine roots and roots with a diameter less than 1cm were taken from approximately a depth of about 10-20 cm, along the row on both sides at a distance of approximately less than 100 cm from the trunk. Samples from symptomatic plants were collected as closed as possible to the “rat-tail” symptoms. After the uprooting the samples were kept at 4°C until the following step.

In the laboratory samples were observed to find areas with decayed tissue. Then roots of D<0.5 mm were cut from the main root and put into a 50 ml falcon tubes containing 30 ml of epiphyte removal buffer (6.75 g of KH_2PO_4, 8.75 g of K_2HPO_4, and 1 mL of Triton X-100, to 1 L of sterile water) without removing the rhizosphere. For each sample approximately 6-10 gr of roots plus soil were collected.

The samples were than sonicated at 600 Hz with a cycle of 30 sec sonication 30 sec without sonication for 10 minutes at 4°C. Root tissues were then transferred into 30 ml of chilled (4°C) sterile water.

The tubes containing buffer and rhizosphere, were centrifuged at 4000 x g for 10 min at 4 °C to let the rhizosphere deposit at the bottom of the tube. The supernatant was removed and the rhizosphere fraction (400 mg-1200 mg) was transferred into a 2 ml tube, centrifuged at 6000 x g for 2 minutes to remove excess of epiphytic buffer, before the immersion in liquid nitrogen and the storage at -20 °C.

The root in sterilised distilled water were vortexed till all residual soil particles were removed from the surface. Depending on the soil texture and humidity, 5-10 washes were necessary for completely cleaning of the root. The clean roots were then put on a sterilised glass petri dish and cut into pieces before the immersion in liquid nitrogen and the storage at -20°C. When the roots were cut, the portion next to the rotting tissue was preferred and particular care was payed to collect tissue from roots of different sizes. A total amount of 1 g of root tissue was sampled for each plant.

DNA extraction

Total genomic DNA from 200 mg of rhizosphere of each individual sample was obtained using the *Quick*-DNA™ Fecal/Soil Microbe Miniprep kit (Zymo Research Corp.), following the manufacturer's recommendations.

Total genomic DNA from root endosphere was obtained, after grinding with liquid nitrogen, using a modified Doyle & Doyle procedure (Martini *et al.*, 2009).

Concentration and quality of the DNA samples were verified using the NanoDrop ND-1000 spectrophotometer (ThermoFisher Scientific, Inc., Wilmington, DE, USA); successively DNA samples were diluted to 20 ng/µl.

Fungal and oomycete ITS amplicon library preparation, and sequencing

A nested PCR approach was used to amplify fungal and oomycete ITS region from 6 samples per each sampling area.

For the amplification of **fungal ITS region** in the first PCR mixture the following ingredients were combined: 12.5 µl of KAPA HiFi Hot Start Ready Mix (2×), 0.375 µl of each primer 20 µM ITS1catta/ITS4ngs (Tedersoo *et al.*, 2014; Tedersoo & Anslan, 2019; Nilsson *et al.*, 2019a), approximately 20 ng of genomic DNA, water to a final volume of 25 µl. The following thermal cycling scheme was adopted: initial denaturation at 95 °C for 3 min, 28 cycles of: 20 sec at 98 °C, 15 sec at 59 °C, and 25 sec at 72 °C, final extension at 72 °C for 3 min. The success of the PCRs was confirmed by gel electrophoresis (2% agarose gel in 1× TBE buffer at 120 V for 120 min). Primer pair ITS1catta/ITS4ngs were designed to completely eliminate the co-amplification of vascular plant ITS sequences; nevertheless, we noticed the amplification of a common band in all the samples (stronger in root endosphere samples and weaker in rhizosphere ones). Therefore, fungal-specific bands were purified by gel extraction using GeneJET Gel Extraction Kit (Thermo Scientific)

according to the manufacturer's instructions and elution of DNA in 50 µl buffer. Concentration of gel extracted purified DNA was determined by NanoDrop ND-1000 spectrophotometer and adjusted to 20 ng/µl before being used in a second PCR targeting the ITS2 region and combining the following ingredients in the PCR mixture: 12.5 µl of KAPA HiFi Hot Start Ready Mix (2×), 0.375 µl of each primer 20 µM ITS3mix/ITS4ngs (Tedersoo *et al.*, 2014) with the MiSeq adaptors, 1 µl of diluted purified DNA, water to a final volume of 25 µl. The following thermal cycling scheme was used: initial denaturation at 95 °C for 3 min, 25 cycles of: 20 sec at 98 °C, 15 sec at 59 °C, and 25 sec at 72 °C, final extension at 72 °C for 3 min. The resulting PCR products were purified with the same kit as before and eluted in 22 µl of molecular grade water.

For the amplification of **oomycete ITS region** the primer pair ITS1Oo/ITS4ngs (Riit *et al.*, 2016), and the same mixture as described above were used in the first PCR. The following thermal cycling scheme was adopted: initial denaturation at 95 °C for 3 min, 28 cycles of: 20 sec at 98 °C, 15 sec at 62 °C, and 25 sec at 72 °C, final extension at 72 °C for 3 min. Since no co-amplification of plant-DNA was observed after agarose gel electrophoresis, PCR products were directly diluted 1:30 before the second PCR targeting the ITS2 region. The second PCR mixture combined the following ingredients: 12.5 µl of KAPA HiFi Hot Start Ready Mix (2×), 0.375 µl of each primer 20 µM ITS30o/ITS4ngs (Riit et al., 2016) containing the MiSeq adaptors, 1 µl of 1:30 diluted DNA, water to a final volume of 25 µl. The following thermal cycling scheme was used: initial denaturation at 95 °C for 3 min, 35 cycles of: 20 sec at 98 °C, 12 sec at 62 °C, and 20 sec at 72 °C, final extension at 72 °C for 3 min. The resulting PCR products were purified with the same kit as before and eluted in 22 µl of molecular grade water.

Pooling of fungal and oomycete amplicons

The purified fungal and oomycete amplicons were pooled together with a 3/1 molarity ratio after quantification using the NanoDrop ND-1000 spectrophotometer. The molarity was estimated for each sample considering a mean amplicon length of 370 bp for fungi and 600 bp for oomycetes. 16 µl of purified fungal products were taken for all the samples and mixed with the corresponding volumes of purified oomycete amplicons. Final volumes ranged between 16-28 µl with a concentration of 30-104 ng/µl. Samples were successively sent to the Institute of Applied Genomics (IGA, Udine, Italy) to determine paired-end sequences with an Illumina MiSeq 2×300 bp platform. A total of 48 samples were sequenced, 6 for each combination of compartment x sampling area. The reads are currently under submission to the NCBI database.

Bioinformatics and statistical analysis

The demultiplexed forward and reverse FASTQ files of each dataset were separately imported as Casava 1.8 paired-end reads and assembled using DADA2 (Callahan et al., 2016) with a minimum overlap of 20 nucleotides; sequences with a score below Q20 were then discarded by quality filtering. Since oomycetes ITS2-region is renowned to be approximately 600bp, non-overlapping sequences were concatenated with a 5 bp unidentified nucleotide spacer ("-NNNNN-"). Chimeras were also removed from the datasets. The remaining, high-quality reads were then binned into exact sequence variants (ESVs), equivalent to operational taxonomic units (OTUs) with a similarity threshold of 100%. In the rest of this work, ESV and OTU will be used as synonyms.

Taxonomic classification of ESVs was carried out using a naïve Bayes classifier trained on UNITE 8.0 (Nilsson *et al.*, 2019b) for fungal ITS reads, and oomycetes database downloaded from NCBI database (Clark *et al.*, 2016) for oomycete ITS reads, respectively. Actinidia ITS sequences were retrieved in NCBI database (Clark *et al.*, 2016) with the query: "txid3624[Organism:exp] AND internal transcribed spacer" and were also included in the database; all sequences classified as

Actinidia were removed from analysis. The classification of Oomycetes was further refined using ITSx (Bengtsson-Palme *et al.*, 2013) on Oomycetes taxonomy. Only sequences confirmed by ITSx were considered as bona fide Oomycetes.

Rarefaction curves were constructed and plotted using the R package vegan (Dixon, 2003). Diversity indices were computed using the R package vegan. Alpha-diversity indices included richness (number of observed OTUs per sample) and diversity (Shannon index). Difference in alpha-diversity indices between compartments and between groups was assessed using Wilcoxon rank sum test, for Fungi and Oomycetes separately.

Beta-diversity was assessed and plotted with the meta-MDS function of the vegan package. Initially the clustering was checked for root endosphere and rhizosphere considering all the samples without discerning by health group. Secondly each compartment was analysed separately clustering the data by health groups.

Interactive graphical representation of the taxonomy composition of samples was obtained using Krona (Ondov *et al.*, 2011).

To further inspect the relationships between the kiwifruit health status with both fungal and oomycete communities, the microbial compositions of the four plant groups were compared for each taxa levels using the FitZig function of the metagenomeseq R package (Paulson *et al.*, 2013), using alpha = 0.05 on adjusted P-values as the cut-off value for statistical significance. FitZig assesses significance of differential abundance assuming a zero-inflated Gaussian null distribution for each taxa, and returns p-values adjusted for multiple testing. The comparison was carried on for those groups which were well clustered by the beta-diversity analysis, grouping those that were not clustered. Totally 5 models were tested comparing: i) the communities of root endosphere compartment against the one of rhizosphere independently from the health groups, ii) the communities of samples from site 1 (CC1) against those from site 2 (AA2+AD2+DD2) for root endosphere and rhizosphere separately, and

finally iii) the communities of plants that remained asymptomatic till 2018 (CC1+AA2) against those that were already diseased in 2017 or that became diseased in 2018 (AD2+DD2) for root endosphere and rhizosphere separately.

RESULTS

Quality metrics of sequencing

Totally 7137243 reads were recovered from the Illumina Miseq sequencing. Sequences were equally distributed among the samples with approximately 148693 of raw reads per sample. After paired-end alignments, quality filtering and deletion of chimeric around 60% of the sequences were removed. Under our experimental procedure, only a small fraction (9%) of ITS sequences were classified as plant DNA. After removing reads associated with plants, singletons amounted approximately at 46800 reads, of which on average 61% were classified as Fungi and 10% as Oomycetes ITS reads.

All the rarefaction curves reached a saturation plateau, suggesting that all the samples were sufficiently sized, making them suitable for further community analysis (Fig. S1). Nevertheless, the rhizosphere sample #38 (AA2-Rh) had considerably lower amount of reads and species compared to the other samples from the same compartment, therefore considered as out layer and removed from the analysis (Fig. S1). Just looking at the shape of the curves, it is clear that the ESV richness and Shannon diversity were consistently higher in the rhizosphere community rather than in that one of root endosphere.

Table 2. Average of quality metrics and percentage of classified reads

Group[1]	Number of reads					Percentage of classified ESV		
	Raw	Filtered	No Chimeric	Merged	Concatenated	Fungi	Oomycetes	NA[2]
All	148693	62340	46800	45341	1459	61.2	9.3	29.2
RE	144454	67231	51184	50267	917	74.3	4.6	20.6
CC1-RE	146928	66812	47858	47086	771	65.6	8.1	26.0
AA2-RE	147875	65343	50303	49381	922	54.8	10.7	34.2
AD2-RE	150265	72868	57077	56172	905	49.9	13.9	35.8
DD2-RE	132749	63900	49499	48429	1069	66.1	17.4	16.4
Rh	152931	57449	42416	40415	2001	64.2	22.9	12.8
CC1-Rh	185041	73120	53402	50527	2875	69.7	11.7	18.6
AA2-Rh	176093	67204	50393	47903	2490	66.7	17.6	15.6
AD2-Rh	132994	44549	33317	31901	1417	63.8	17.5	18.4
DD2-Rh	117595	44922	32551	31329	1222	63.6	13.4	22.8

[1] *All* – overall average; *RE* – root endosphere; *Rh* – rhizosphere; *CC1 –sample form the control site; AA2, AD2 and DD2* samples from plants in the diseased site that were respectively asymptomatic until 2018, became symptomatic in 2018 and that were already symptomatic in 2017.
[2] unclassified

Alpha-diversity

Statistical differences in ESVs alpha-diversity were inferred from the richness and Shannon indices.

Our estimates of the alpha-diversity within both compartments showed that ESVs richness and Shannon diversity were highly dependent on the compartment and on the kingdom. A higher diversity was observed for Fungi compared to Oomycetes and in the rhizosphere compared to the root endosphere (Fig. 2).

The analysis of alpha-diversity by health groups revealed a bigger difference in the Oomycetes community rather than in the Fungi one (Fig. 3).

The diversity estimated by Shannon index in the fungal community did not evidence significant differences among the plant groups in both compartments (Fig. 3a); whereas in the oomycete community from the root endosphere compartment, the highest diversity was observed in the symptomatic plants (groups AD2-RE and DD2-RE) (Fig. 3b). Shannon indices of the rhizosphere

compartment were the highest in the symptomatic plants (groups AD2-Rh and DD2-Rh) but also in asymptomatic plants from the control site (group CC1-Rh) (Fig. 3c and d).

Regarding the root endosphere compartment, the highest richness in both the fungal and oomycete communities was observed in plants from site 2 especially in the symptomatic ones (groups AD2-RE and DD2-RE); while the lowest in the fungal and oomycete communities was observed in asymptomatic plants from the control site (CC1-RE) (Fig. 3e and g). Regarding the rhizosphere compartment, the highest richness in the fungal community was observed in asymptomatic plants from site 2 (AA2-Rh); whereas the highest richness in the oomycete community was observed in asymptomatic plants from site 1 (AA1-Rh) (Fig. 3f and h). Most of the differences were significant at the Wilcoxon rank sum test.

Beta-diversity

The NMDS plots depicting both communities at the same time revealed that there was a clear distinction among the two plant compartments, since the rhizosphere community formed a very well separated cluster from the root endosphere community (Fig. 4a).

Within each compartment, with regards to the health groups (groups CC1, AA2, AD2 and DD2), there was a clear distinction of the microbiota community of the plants from the control site (site 1, CC1-RE and CC1-Rh), from the microbial communities of the plant groups from the infected site (site 2, Fig. 4b and c).

Regarding the root endosphere compartment of samples collected in site 2, a very tight cluster was formed by the DD2-RE samples (diseased since 2017) while the clusters of AA2-RE (asymptomatic up to 2018) and AD2-RE (diseased in 2018) samples were more disperse. Nevertheless, all the AA2-RE samples were outside the 95% confidence interval of the DD2-RE cluster, while most of the samples from the AD2-RE cluster were close to or inside the DD2-RE cluster.

Rhizosphere samples from the area of site 2 (AA2-Rh) that was asymptomatic in 2018, formed a small cluster; while rhizosphere samples of plants that were already diseased in 2017 (DD2-Rh) were more scattered. It is interesting to note that the samples of the area that became diseased in 2018 (AD2-Rh), were somehow in between the AA2-Rh and DD2-Rh clusters.

Taxonomy composition

Regarding the taxonomical composition, the ratio between oomycete and fungal community was approximately 1:3 as expected. Therefore, the results hereinafter will be discussed considering the relative abundance within each community.

Fungal community of root endosphere compartment (Fig. 5) was almost totally represented by Ascomycota 89%-95%, while Basidiomycota and Mucormycota were poorly represented (both between, 2-4%). Nectriaceae alone constituted more than 33-53% of the Fungi, almost totally constituted by two *Ilyonectria/Dactylonectria* species: *Ilyonectria anthuriicola* (27-33%) and *Ilyonectria macrodidyma* (4% in CC1-RE and 11-14% in area of site 2). Another species highly represented was *Clamidospora parvula* (subclass, Hypocreomycetidae - family unknown) constituting approximately 17-23% of the Fungi.

Regarding oomycete community, *Phytophthora sojae* was the most abundant Oomycetes found in site 2 (75-92%), but was completely absent in site 1. Indeed, Oomycetes in root endosphere of site 1 (CC1-RE) were poorly represented (on 5% of the total reads) mostly characterized by *Phytopythium vexans* (95%). *P. vexans* was found also in site 2 (6-8%), together with *Phytopythium citrinum* (10-13%) and *Phytopythium chamaehyphon (3%).*

Regarding the rhizosphere compartment (Fig. 6), the relative abundance of Ascomycota within the fungi community was even greater that in root endosphere (approximately 98%). Once again Nectriaceae family was the most abundant (16-22%) but no dominant species were found.

Plectosphaerellaceae was another important family mostly found in site 2 (5% in site 1 an 8-12% in site 2). The relative abundance of other families was equal or below to 5%.

Regarding oomycete community, *Phytophthora sojae* was once again the species most frequently found in site 2 (47-69%), and almost completely absent in site 1. *Phytopythium* species were found with higher relative abundance in comparison to the root endosphere compartment ranging from 9 up to 27 %, depending on the species and the sampling areas. Beside the absence of *Phytophthora sojae* it is interesting to note that oomycete community of rhizosphere in site 1 was mostly characterized by *Aplanopsis terrestris* (63%) that was only marginally represented in samples from site 2.

Key taxa analysis.

Based on the beta-diversity results the differential abundance analysis was carried out for the five models described in section 2.6.

Comparison between the two compartments (root endosphere and rhizosphere) revealed significant differences between the relative abundance of several species (Fig. 7a). Root endosphere compartment was mostly characterised by a higher relative abundance of some fungal species, in particular of: *Ilyonectria anthuriicola* (23.9% in RE and 2.6% in Rh), *Campylospora parvula* (15% in RE and 3% in Rh), *Ilyonectria macrodidyma* (9.8% in RE and 2.7% in Rh). Rhizosphere compartment was instead characterised by several species (around 2-4.5%) that were almost absent in the root endosphere (0-0.4%); among them with a relative abundance above 4%: one unidentified fungal species from the Nectriaceae family and one from the genus *Cladosporium*, and the oomycete species *Aplanopsis terrestris.*

The differences between the control site (Site 1) and the diseased one (Site 2) were analysed separately for root endosphere (Fig. 7b) and rhizosphere (Fig. 7c). The most characteristic taxa of the root endosphere in CC1 plants were two unidentified fungal species: one belonging to the order

Chaetothyriales (11.3% in site 1, and 3.2% in site 2) and the other one from Sordariales (6.35% in site 1, and 0.81% in site 2). It is interesting to note that a key taxon for the diseased site (site 2) was the oomycete species *Phytophthora sojae* (0 % in CC1-RE and 12.8% in RE of site 2 areas). Other two species of Fungi more abundant in the diseased site were *Ilyonectria macrodidyma* (4.1% in site 1 and 11.75% in site 2) and *Thielaviopsis basicola* (0.1% in site 1 and 5.8% in site 2) (Fig. 7b). Finally, also *Ilyonectria robusta* was found significantly higher in diseased site but with a very low relative abundance (0.1% in site 1, and 2.20% in site 2)

Rhizosphere of samples from site 1 was instead mostly characterised by two microorganisms: *Aplanopsis terrestris* (14.3% in site 1 and 0.5%) and an unidentified *Fusarium* species (6.08% in site 1 and 0.66% in site 2). Similarly, to what has been described for the root endosphere, also in the rhizosphere from plants of site 2 *Phytophthora sojae* was the microorganism mostly represented (0.69% in CC1-Rh and 9.76% in Rh of site 2 areas) (Fig. 7c).

Regarding the differences between areas within site 2 they were minimal (<4%), although significant, when comparing AA (plant always asymptomatic up to 2018) vs AD+DD (respectively plants that became diseased in 2018 or that were already symptomatic in 2017). The most characteristic species belonged to the genus *Phytopythium* for both root endosphere (Fig. 7d) and rhizosphere (Fig. 7d) compartments, more represented in the symptomatic plants.

It should be noted that although *Phytophthora sojae* was the most abundant specie of the Oomycetes retrieved in diseased site (site 2), it wasn't differently abundant in the health groups belonging to this site.

DISCUSSION

To the best of our knowledge, this work represents the first study on the description of the root endosphere and rhizosphere biodiversity in kiwifruit agro-ecosystems in relation to Kiwifruit Decline.

Both fungal and oomycete communities have been described in this work, however one of the first things that catches the eye from the analysis of the microbiota is the total lack of basidiomycetes.

This is mostly linked to the excision procedure performed during the preparation of the library for the Fungi ITS sequences, that physically excluded some Basidiomycota before the nested amplification. Indeed we observed that the length of Basidiomycota ITS-region (Yang *et al.*, 2018) is slightly lower or approximately the same in length as the ITS-region of *Actinidia deliciosa* (720 bp c.a). Nevertheless, this choice was forced by the lack of Fungi-specific primer able to exclude *Actinidia deliciosa* ITS-region during library preparation. On the other hand, the primers ITS1Oo and ITS3Oo correctly amplified several oomycete species without co-amplification of plant DNA.

The alpha-diversity values were significantly lower in root endosphere compartment rather than in the rhizosphere one, confirming what observed in similar studies (Edwards *et al.*, 2015). Also the lower richness of the oomycete community in comparison to the fungal one has been previously reported in Gómez *et al.*, (2019).

It is not strange, either, that root endosphere and rhizosphere microbiota differ greatly and cluster in two well distinct groups (Edwards *et al.*, 2015). Results of NMDS analysis by health group, suggested that there were clear differences between the control site 1 (CC1, considered "healthy" because no KD symptoms were observed during surveys) and site 2 (unhealthy, AA2, AD2 and DD2) in both root endosphere and rhizosphere. Moreover, the microbiota associated to the asymptomatic plants of site 2 (AA) was more similar to the one of symptomatic plants within the same site rather than to the microbiota characterising the asymptomatic ("healthy") plants of the control site 1 (CC). From these results two equally valid hypotheses arise: i) the pathogen(s) involved in the disease was/were already widespread within the diseased orchards and became pathogenic when and where certain environmental conditions (f.i., waterlogging) occurred; ii) at the sampling date, the spread of the disease at site 2 had also reached the last asymptomatic area in the north-eastern corner of the orchard.

The absence of a method to assesses the disease during sampling, is indeed a limiting factor for community studies, since the only way to assess the disease is observing the dieback symptoms one year after the sampling or uproot the whole plant to check for the presence of rotting and "rat-tail" symptoms. Nevertheless, if technologies able to correctly predict the physiological status of the plants was implemented, a better positioning of the sampling could be obtained. In this direction the study proposed by Savian et al. (under submission 2, in Chapter 4) can indeed be a first step towards the improvement of field sampling activities.

Our results confirmed the involvement of Oomycetes in Kiwifruit Decline syndrome since they were usually found more abundant in the diseased site (site 2 AA2, AD2, DD2) compared to the control site (site 1, CC1). The same was observed in symptomatic areas (AD2 and DD2) when compared to the asymptomatic plants (AA2) within the diseased site (site 2). However, rather than a community of pathogenic oomycetes it seems that one major candidate prevails above all the others. Indeed, the most represented oomycete species was *Phytophthora sojae*, found with high abundance in all the samples from site 2, while it was completely absent or barely present in root endosphere and rhizosphere of site 1, respectively. *P. sojae* was previously found by Tosi et al (Tosi *et al.*, 2015) in plants affected by Kiwifruit Decline, although it had a very low occurrence and it pathogenicity was not tested. To the best of our knowledge, the only work attesting the pathogenicity of *P. sojae* is a study of Baudry et al. (Baudry *et al.*, 1991), which associated *Phytophthora megasperma* var. *sojae* to a kiwifruit decline occurred in France in 1988. Unfortunately, comparison with KD is difficult for the absence of a detailed description of the disease symptoms, nevertheless also the declines observed in France were linked to poorly drained soils and/or waterlogged conditions.

Among other oomycete species found in this study, there were some that have already been associated with KD, but their relative abundance was considerably lower than *Phytophthora sojae*. For instance, *Phytopythium vexans* has been demonstrated associated with KD by Prencipe et al. (submitted for

publication, Chapter 3) and previously reported in kiwifruit orchards affected by a root and root collar rot in Tukey (Polat *et al.*, 2017). In our study *P. vexans* has been found more abundant in infected areas (AD2+DD2), but at the same time it was also found within plants of the control site (site 1), suggesting that it could be already present also in "healthy" orchards. The other *Phytopythium* species were *Phytopythium citrinum* and *Phytopythium chamaehyphon*. The former has never been found on kiwifruit roots, while the latter has been isolated from several symptomatic plants by Savian et al. (submitted for publication, Chapter 1).

Among Fungi, the most important family was the Nectriaceae mainly constituted by two *Ilyonectria* species *I. anthuriicola* and *I. macrodidyma.* Several *Ilyonectria* species have been previously reported as pathogenic for kiwifruit by Erper et al. (Erper *et al.*, 2011, 2013). The species of the genera *Dactylonectria*, *Ilyonectria*, *Cylindrocarpon* and *Cylindrocladiella* are generally considered as pathogens and/or saprobes of various hosts and substrates in temperate, sub-tropical and tropical regions worldwide (Erper *et al.*, 2013). In our study, beside *I. robusta*, all the other *Ilyonectria* species have not been previously associated with root rot in kiwifruit. Nevertheless, *Ilyonectria macrodidyma* was found more abundant in the diseased orchard (site 2), suggesting its possible involvement in the disease.

Finally, it is interesting to note that the soil of site 1 was mostly characterised by *Aplanopsis terrestris,* a poorly studied oomycete species that has not yet been associated with any disease. The few studies we managed to find regarding this species suggest that *Aplanopsis* spp. are usually more common in dried soil, when compared to *Pythium* species distribution (Len & Dick, 1986).

CONCLUSIONS

This study is the first one characterising both Fungi and Oomycetes communities associated with Kiwifruit Decline. Our findings together with the many reports of pathogenic fungi/oomicetes associated with decline–like diseases suggested that more than one pathogen might be involved in the disease. *Phytophthora sojae* and *Ilyonectria macrodidyma* could be new potential pathogens whose pathogenicity should be tested. Furthermore, the almost complete absence of Oomycetes in the healthy site (CC1) is consistent with the hypothesis that some major taxa of this class are involved in the disease. Nevertheless, also *Ilyonectria* should not be excluded, since it was previously reported as pathogenic for kiwifruit. On the other hand, a preliminary analysis for the presence of these taxa could be used as an indicator of predisposition to KD.

Better protocols to selectively amplify fungal community are needed when processing Actinidia plant compartments, such as rhizosphere and root endosphere. Finally, improvements of scouting and sampling activities are highly desirable to promptly distinguish healthy plants from apparently healthy ones and to improve the quality of the material for downstream etiological analysis.

REFERENCES

Abdelfattah A, Malacrinò A, Wisniewski M, Cacciola SO, Schena L. **2018**. Metabarcoding: A powerful tool to investigate microbial communities and shape future plant protection strategies. *Biological Control* **120**: 1–10.

Akilli S, Serçe ÇiU, Zekaİ Katircioğlu Y, Karakaya A, Maden S. **2011**. Involvement of *Phytophthora citrophthora* in kiwifruit decline in Turkey. *Journal of Phytopathology* **159**: 579–581.

Baudry A, Morzieres JP, Ellis R. **1991**. Effect of *Phytophthor*a spp. on kiwifruit in France. *New Zealand Journal of Crop and Horticultural Science* **19**: 395–398.

Bengtsson-Palme J, Ryberg M, Hartmann M, Branco S, Wang Z, Godhe A, De Wit P, Sánchez-García M, Ebersberger I, de Sousa F, *et al.* 2013. Improved software detection and extraction of ITS1 and ITS2 from ribosomal ITS sequences of fungi and other eukaryotes for analysis of environmental sequencing data (M Bunce, Ed.). *Methods in Ecology and Evolution*: n/a-n/a.

Çiftçi O, Serçe ÇU, Türkölmez Ş, Derviş S. **2016**. First Report of *Phytophthora palmivora* causing crown and root rot of kiwifruit (*Actinidia deliciosa*) in Turkey. *Plant Disease* **100**: 210.

Clark K, Karsch-Mizrachi I, Lipman DJ, Ostell J, Sayers EW. **2016**. GenBank. *Nucleic Acids Research* **44**: D67–D72.

Conn KE, Gubler WD, Mircetich SM, Hasey JK. **1991**. Pathogenicity and relative virulence of nine *Phytophthora* spp. from kiwifruit. *Phytopathology* **81**: 974–979.

Edwards J, Johnson C, Santos-Medellín C, Lurie E, Podishetty NK, Bhatnagar S, Eisen JA, Sundaresan V. **2015**. Structure, variation, and assembly of the root-associated microbiomes of rice. *Proceedings of the National Academy of Sciences of the United States of America* **112**: E911-920.

Erper I, Agustí-Brisach C, Tunali B, Armengol J. **2013**. Characterization of root rot disease of kiwifruit in the Black Sea region of Turkey. *European Journal of Plant Pathology* **136**: 291–300.

Erper İ, Tunali B, Carlos A-B, Armengol J. **2011**. First Report of *Cylindrocarpon liriodendri* on Kiwifruit in Turkey. *Plant Disease* **95**: 76–76.

FAOSTAT. **2016**. Food and Agriculture Organization of the United Nations, Rome, Italy.

Gómez FJR, Navarro-Cerrillo RM, Pérez-de-Luque A, Oβwald W, Vannini A, Morales-Rodríguez C. **2019**. Assessment of functional and structural changes of soil fungal and oomycete communities in holm oak declined dehesas through metabarcoding analysis. *Scientific Reports* **9**: 1–16.

Huang Y, Qi P. **1998**. Studies on the cause of root rot of kiwifruit in Guangdong Province. *Journal of South China Agricultural University* **19**: 19–22.

Kurbetli İ, Ozan S. **2013**. Occurrence of *Phytophthora* Root and Stem Rot of Kiwifruit in Turkey. *Journal of Phytopathology* **161**: 887–889.

Latorre BA, Pak HA. **2003**. Diseases of kiwifruit. In: Ploetz RC, ed. Diseases of tropical fruit crops. Wallingford: CABI, 291–306.

Len L-HC, Dick MW. **1986**. Comparative estimates of minimum propagule densities of *Aplanopsis* and *Pythium* in soil. *Transactions of the British Mycological Society* **87**: 309–311.

Martini M, Musetti R, Grisan S, Polizzotto R, Borselli S, Pavan F, Osler R. **2009**. DNA-dependent detection of the grapevine fungal endophytes *Aureobasidium pullulans* and *Epicoccum nigrum*. *Plant Disease* **93**: 993–998.

Nilsson RH, Anslan S, Bahram M, Wurzbacher C, Baldrian P, Tedersoo L. **2019a**. Mycobiome diversity: high-throughput sequencing and identification of fungi. *Nature Reviews Microbiology* **17**: 95–109.

Nilsson RH, Larsson K-H, Taylor AFS, Bengtsson-Palme J, Jeppesen TS, Schigel D, Kennedy P, Picard K, Glöckner FO, Tedersoo L, *et al.* 2019b. The UNITE database for molecular identification of fungi: handling dark taxa and parallel taxonomic classifications. *Nucleic Acids Research* **47**: D259–D264.

Ondov BD, Bergman NH, Phillippy AM. **2011**. Interactive metagenomic visualization in a Web browser. *BMC Bioinformatics* **12**: 385.

Paulson JN, Stine OC, Bravo HC, Pop M. **2013**. Differential abundance analysis for microbial marker-gene surveys. *Nature Methods* **10**: 1200–1202.

Polat Z, Awan QN, Hussain M, Akgül DS. **2017**. First Report of *Phytopytium vexans* Causing Root and Collar Rot of Kiwifruit in Turkey. *Plant Disease* **101**: 1058.

Reid JB, Tate KG, Brown NS. **1992**. Effects of flooding and alluvium deposition on kiwifruit (*Actinidia deliciosa*). *New Zealand Journal of Crop and Horticultural Science* **20**: 283–288.

Riit T, Tedersoo L, Drenkhan R, Runno-Paurson E, Kokko H, Anslan S. **2016**. Oomycete-specific ITS primers for identification and metabarcoding. *MycoKeys* **14**: 17.

Sapp M, Lewis E, Moss S, Barrett B, Kirk S, Elphinstone JG, Denman S. **2016**. Metabarcoding of Bacteria Associated with the Acute Oak Decline Syndrome in England. *Forests* **7**: 95.

Simmons T, Caddell DF, Deng S, Coleman-Derr D. **2018**. Exploring the Root Microbiome: Extracting Bacterial Community Data from the Soil, Rhizosphere, and Root Endosphere. *Journal of Visualized Experiments: JoVE*.

Sorrenti G, Tacconi G, Tosi L, Vittone G, Nari L, Savian F, Saro S, Ermacora P, Graziani S, Toselli M. **2019**. Avanza la "moria del kiwi": evoluzione e primi riscontri della ricerca. *Frutticoltura* **2**: 34–42.

Sorrenti G, Toselli M, Reggidori G, Spinelli F, Tosi L, Giacopini A, Tacconi G. **2016**. Implicazioni della gestione idrica nella "Moria del kiwi" del veronese. *Frutticoltura* **3**: 1–7.

Tedersoo L, Anslan S. **2019**. Towards PacBio-based pan-eukaryote metabarcoding using full-length ITS sequences. *Environmental Microbiology Reports* **11**: 659–668.

Tedersoo L, Bahram M, Põlme S, Kõljalg U, Yorou NS, Wijesundera R, Ruiz LV, Vasco-Palacios AM, Thu PQ, Suija A, *et al.* 2014. Global diversity and geography of soil fungi. *Science* **346**: 1256688.

Tosi L, Tacconi G, Giacopini A. **2015**. La moria del kiwi, situazione e prospettive. *L'Informatore Agrario* **44**: 67–70.

Wang KX, Xie YL, Yuan GQ, Li QQ, Lin W. **2015**. First Report of Root and Collar Rot Caused by *Phytopythium helicoides* on Kiwifruit (*Actinidia chinensis*). *Plant Disease* **99**: 725.

Yang R-H, Su J-H, Shang J-J, Wu Y-Y, Li Y, Bao D-P, Yao Y-J. **2018**. Evaluation of the ribosomal DNA internal transcribed spacer (ITS), specifically ITS1 and ITS2, for the analysis of fungal diversity by deep sequencing. *PLOS ONE* **13**: e0206428.

FIGURE CAPTIONS

Fig 1. Spatial distribution of KD-affected orchards nearby San Giorgio della Richinvelda (Friuli-Venezia Giulia – NE Italy). In a), positioning of sampling sites: in green and red, asymptomatic (Site1) and diseased (Site 2) orchards respectively, used in this study, in orange positions of other infected orchards. In b) and c), satellite images in July-2015 and June-2017 highlighting the health condition of Site 1 and Site 2, respectively. Dotted line delimited the four sampling areas: CC1 represents the asymptomatic area in Site 1; while AA2, AD2 and DD2 represent the sampling areas in Site 2 in which plants remained asymptomatic up to 2018, became diseased in 2018, and were already diseased in 2017, respectively.

Fig. 2. Statistical analysis of alpha-diversity by compartment. Box plots illustrating the alpha-diversity indices of the fungal and oomycete communities from the root endosphere (green) and the rhizosphere (orange) of all selected kiwifruit plants: diversity estimated with Shannon index (a) and richness (b) based on ESVs. Different letters indicate significant differences across plant groups at the Wilcoxon rank sum test.

Fig. 3. Statistical analysis of alpha-diversity by health status. Box plots illustrating the alpha-diversity indices for fungal (a, b, e, f) and oomycete (c, d, g, h) communities: richness (a-d) based on ESVs and diversity estimated by Shannon (e-h). In green, microbiota of the root endosphere (a, c, e, g), in orange microbiota of the rhizosphere (b, d, f, h) of kiwifruit plants differing for health status: CC (asymptomatic plants from site 1), AA (asymptomatic plants from site 2), AD (plants showing symptoms since 2018 from site 2) and DD (plants showing symptoms since 2017 from site 2). Different letters indicate significant differences across plant groups at the Wilcoxon rank sum test.

Fig. 4. Non-metric multidimensional scaling (NMDS) analysis of kiwifruit microbiota diversity by compartment and plant health group. In a), the diversity of fungal and oomycete communities was assessed for all the samples of the two compartments: root endosphere (dark green) and rhizosphere (orange). In b) and c), the beta-diversity of root endosphere and rhizosphere was assessed separately and plants were distinguished by the health status: in red asymptomatic plants from the control site 1 (CC1); in purple, light blue, and light green samples of site 2 from plants that remained asymptomatic up to 2018 (AA2), that became diseased in 2018 (AD2), and that were already diseased in 2017 (DD2), respectively. Ellipsoids indicate, the normal probability of the point distribution at 95% confidence level.

Fig 5. Taxonomic composition of the root endosphere compartment of fungal and oomycete communities by health groups. In a) CC1-RE, control site (site 1) with asymptomatic plants; in b), AA2-RE area in site 2 with asymptomatic plants up to 2018; in c) AD2-RE area of site 2 with plants that became diseased in 2018, in d) DD2-RE area in site 2 with plants that were already diseased since 2017. Graphs were made using Krona (Ondov et al., 2011). In red Fungi, in green Oomycetes, in blue Plant (not Actinidia).

Fig 6. Taxonomic composition of the rhizosphere compartment of fungal and oomycete communities by health groups. In a) CC1-Rh, control site (site 1) with asymptomatic plants; in b), AA2-Rh area in site 2 with asymptomatic plants up to 2018; in c) AD2-Rh area of site 2 with plants that became diseased in 2018, in d) DD2-Rh area in site 2 with plants that were already diseased since 2017. Graphs were made using Krona (Ondov et al., 2011). In red Fungi, in green Oomycetes, in blue Plant (not Actinidia).

Fig. 7. Differently abundant taxa for the tested models. Only differences that were statistically significant p-value<0.05 were considered. In a), key taxa distinguishing root endosphere from rhizosphere. In b) and c), differently abundant taxa in the control site 1 (CC1) against the diseased site 2 (all the others, AA2+AD2+DD2). In d) and e), taxa distinguishing the areas within site 2: always asymptomatic up to 2018 (AA2) against those that in 2018 were diseased (AD2+DD2).

SUPPLEMENTARY MATERIAL

Table S1. Primer sequences.

Table S2. Quality metrics for each sample.

Fig. S1. Rarefaction curves. Rarefaction curves for the microbial communities of both compartments, root endosphere (in blu) and rhizosphere (in red), of all kiwifruit plants. In these graphs, the number of reads is plotted against the rarefied number of observed fungal and oomycete species/ESVs.

Fig 1. Spatial distribution of KD-affected orchards nearby San Giorgio della Richinvelda (Friuli-Venezia Giulia – NE Italy).

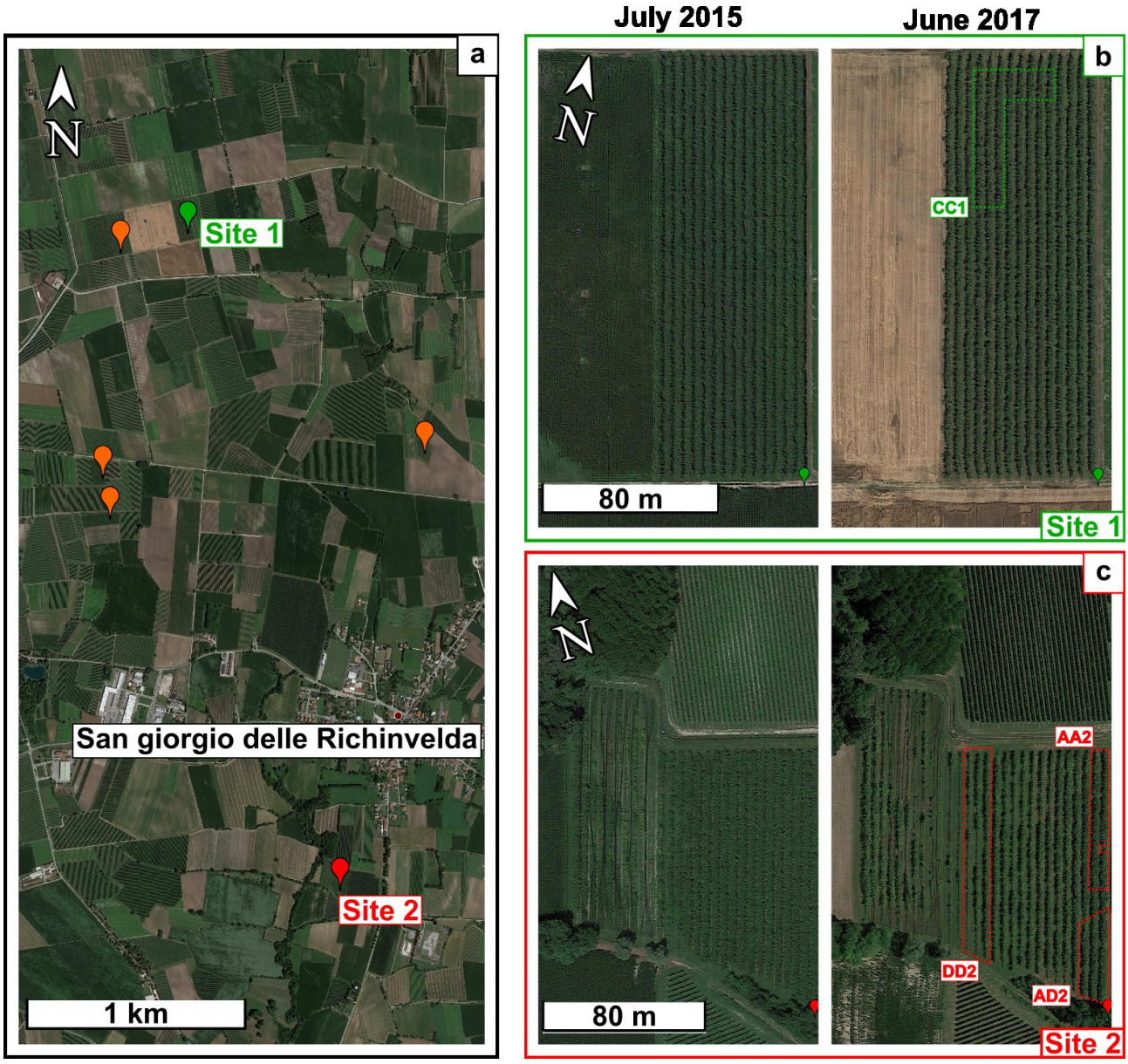

Fig. 2. Statistical analysis of alpha-diversity by compartment.

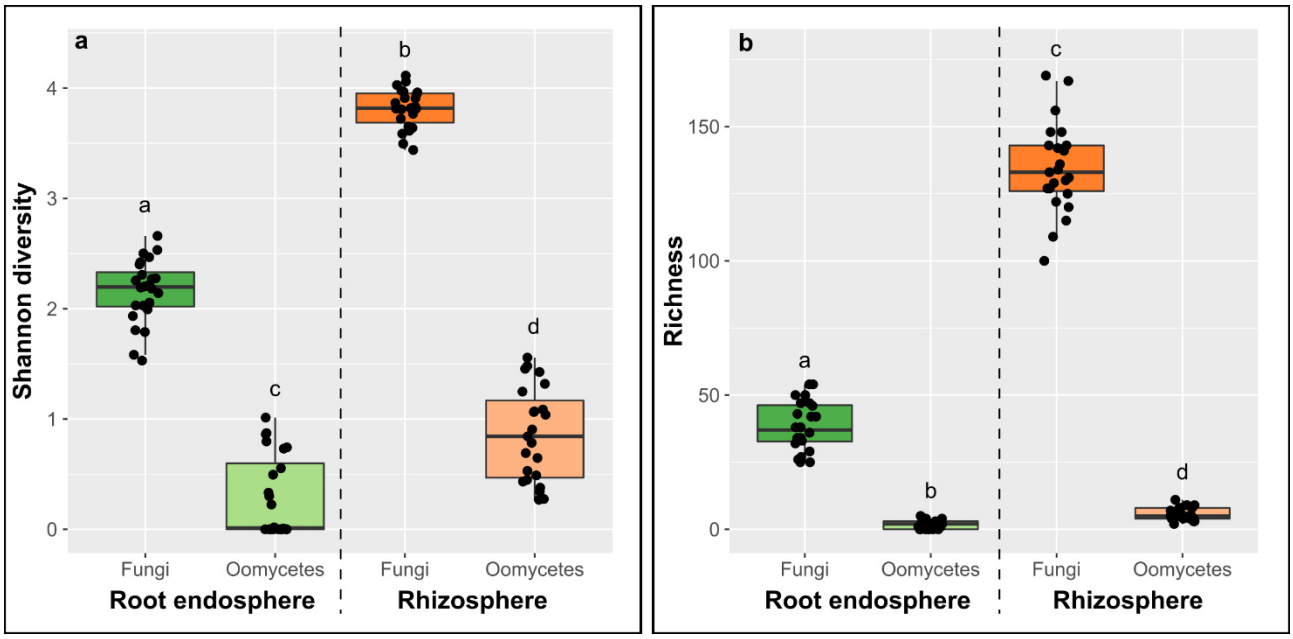

Fig. 3. Statistical analysis of alpha-diversity by health status.

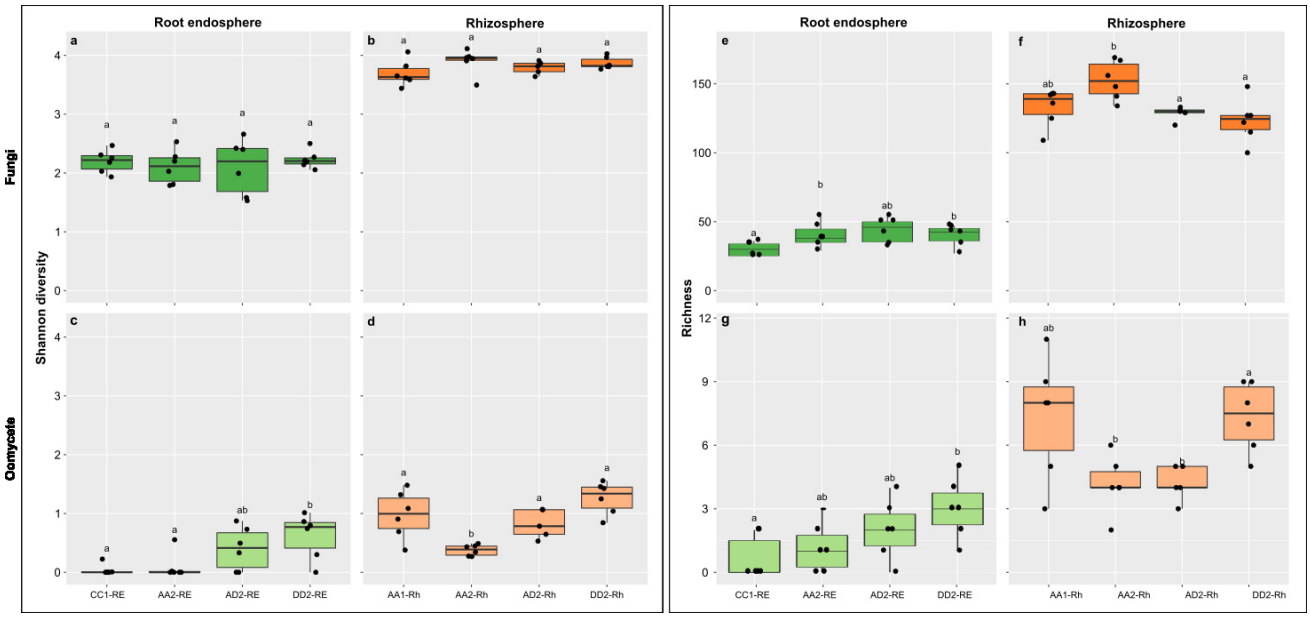

Fig. 4. Non-metric multidimensional scaling (NMDS) analysis of kiwifruit microbiota diversity by compartment and plant health group.

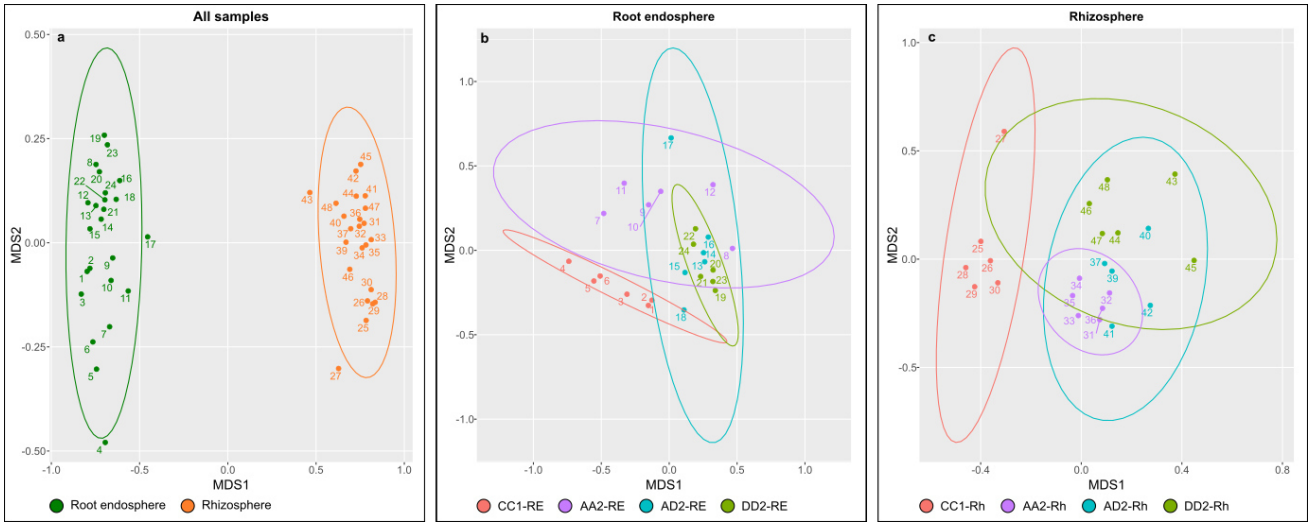

Fig 5. Taxonomic composition of the root endosphere compartment of fungal and oomycete communities by health groups.

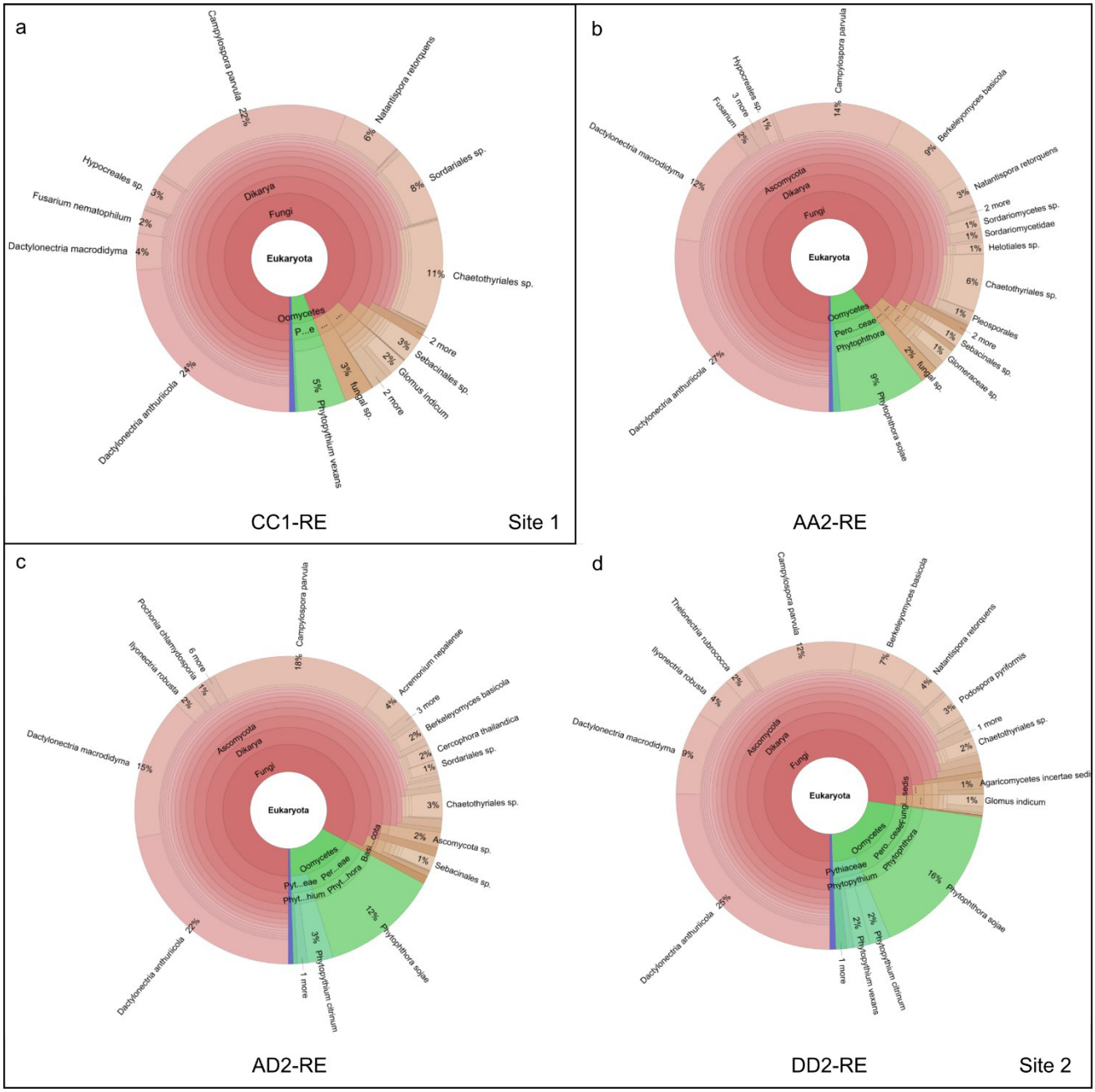

Fig 6. Taxonomic composition of the rhizosphere compartment of fungal and oomycete communities by health groups.

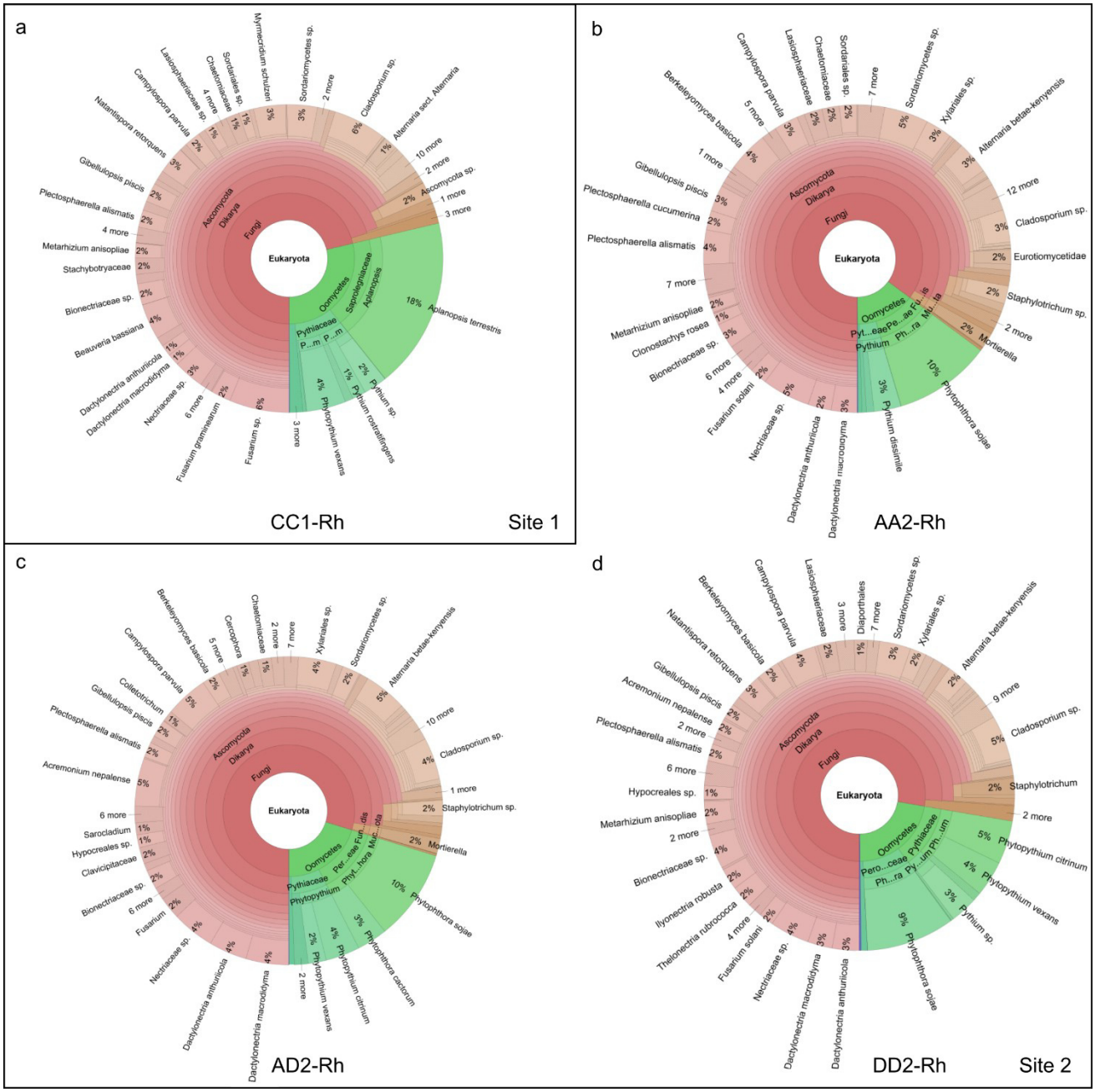

Fig. 7. Differently abundant taxa for the tested models

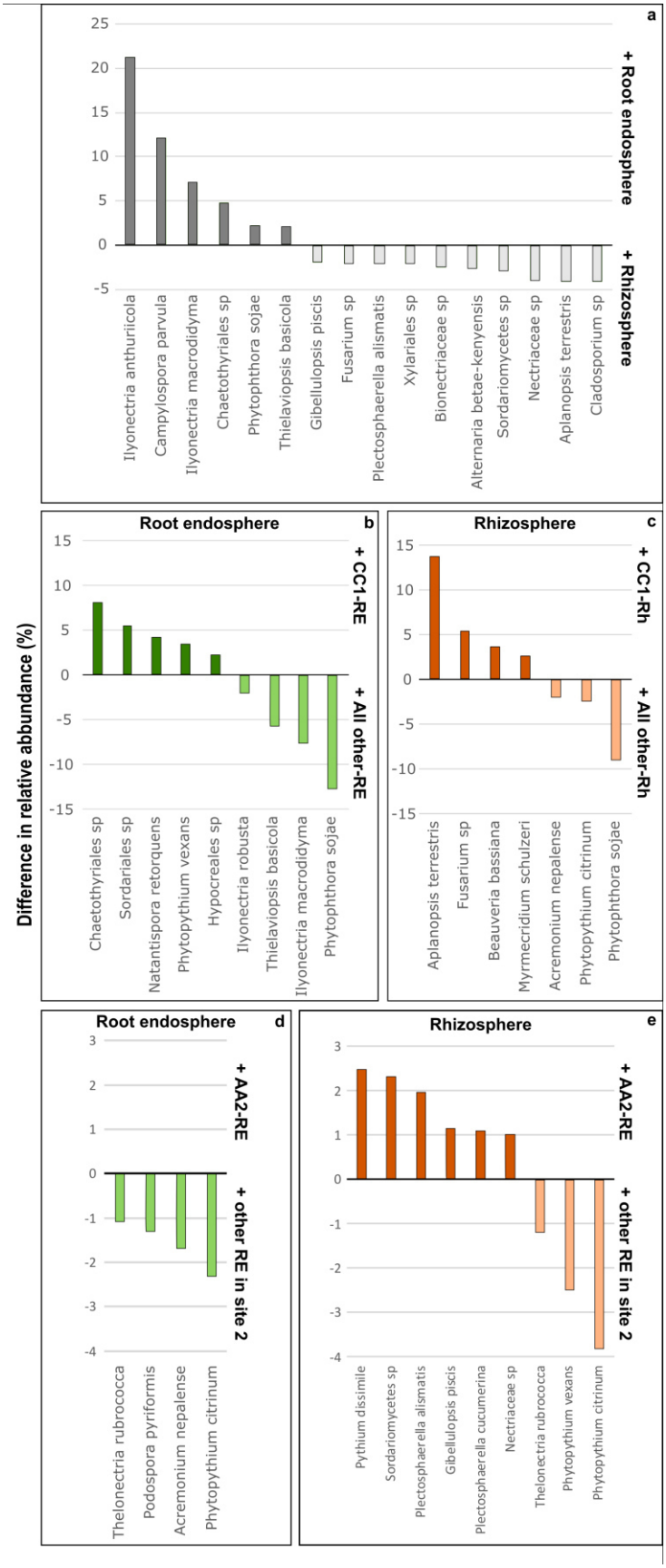

Table S1. Primer sequences.

Primer	Target and PCR round	Sequences	Reference
ITS1catta	Fungi (1st round)	ACCWGCGGARGGATCATTA	Tedersoo & Anslan, 2019
ITS3mix	Fungi (2nd round)	CANCGATGAAGAACGYRG	Tedersoo et al. 2014
ITS1Oo	Oomycetes (1st round)	GGAAGGATCATTACCACAC	(Riit et al., 2016),
ITS3Oo	Oomycetes (2nd round)	AGTATGYYTGTATCAGTGTC	(Riit et al., 2016),
ITS4ngs	All	TTCCTSCGCTTATTGATATGC	Tedersoo et al. 2014

Table S2. Quality metrics for each sample.

Sample ID	Area	Compartment	group	Number of reads				Number of ESV		
				N° raw reads	Filtered	Merged	Concatenated	Fungi	Oomycetes	NA
1	CC1	Root endophyte	CC1- RE	131591	70187	47397	1168	175	0	100
2	CC1	Root endophyte	CC1- RE	147415	85677	56396	1253	300	0	112
3	CC1	Root endophyte	CC1- RE	163029	76719	52608	646	206	0	104
4	CC1	Root endophyte	CC1- RE	173900	58362	44256	379	168	9	37
5	CC1	Root endophyte	CC1- RE	107904	40186	28467	513	151	17	57
6	CC1	Root endophyte	CC1- RE	157729	69740	53394	668	156	0	61
7	AA2	Root endophyte	AA2- RE	169265	85112	59470	1293	264	0	84
8	AA2	Root endophyte	AA2- RE	106329	50146	36898	657	127	5	74
9	AA2	Root endophyte	AA2- RE	162890	70216	55509	969	256	0	82
10	AA2	Root endophyte	AA2- RE	131137	62775	49173	833	174	32	56
11	AA2	Root endophyte	AA2- RE	188568	75091	58070	734	239	6	82
12	AA2	Root endophyte	AA2- RE	129062	48720	37164	1045	160	5	69
13	AD2	Root endophyte	AD2- RE	136639	70994	55173	866	145	43	114
14	AD2	Root endophyte	AD2- RE	136125	66798	50702	1138	151	48	81
15	AD2	Root endophyte	AD2- RE	109614	57561	46246	691	126	27	84
16	AD2	Root endophyte	AD2- RE	196227	88655	67472	1016	194	11	128
17	AD2	Root endophyte	AD2- RE	157463	62769	48012	867	189	5	48
18	AD2	Root endophyte	AD2- RE	165521	90432	69424	853	228	0	136
19	DD2	Root endophyte	DD2- RE	135411	62017	47553	1230	180	81	121
20	DD2	Root endophyte	DD2- RE	138746	66267	51181	1233	146	53	115
21	DD2	Root endophyte	DD2- RE	155408	77108	58875	1344	222	5	114
22	DD2	Root endophyte	DD2- RE	113620	50407	37130	865	145	36	82
23	DD2	Root endophyte	DD2- RE	131245	63984	49481	986	193	13	107
24	DD2	Root endophyte	DD2- RE	122063	63618	46356	757	162	28	111
25	CC1	Rhizosphere	CC1- Rh	207909	97644	75538	4508	446	28	169
26	CC1	Rhizosphere	CC1- Rh	154853	51381	35883	1593	422	22	171
27	CC1	Rhizosphere	CC1- Rh	171938	57427	40127	1697	333	71	230
28	CC1	Rhizosphere	CC1- Rh	204610	73668	49523	1845	449	79	177
29	CC1	Rhizosphere	CC1- Rh	178311	77571	50415	3420	445	59	154
30	CC1	Rhizosphere	CC1- Rh	192626	81031	51675	4185	478	87	180
31	AA2	Rhizosphere	AA2- Rh	140979	52761	37141	2362	433	11	180
32	AA2	Rhizosphere	AA2- Rh	150533	55046	39412	2827	431	20	141
33	AA2	Rhizosphere	AA2- Rh	206828	75361	54954	2188	520	46	218
34	AA2	Rhizosphere	AA2- Rh	203339	91481	67247	1974	540	15	215
35	AA2	Rhizosphere	AA2- Rh	190441	67435	46061	3891	569	10	201
36	AA2	Rhizosphere	AA2- Rh	164439	61137	42604	1695	418	20	165
37	AD2	Rhizosphere	AD2- Rh	153533	60711	43164	1131	393	75	213
38	AD2	Rhizosphere	AD2- Rh	92045	12950	9350	451	121	23	39
39	AD2	Rhizosphere	AD2- Rh	146691	56027	42023	2050	401	39	129
40	AD2	Rhizosphere	AD2- Rh	122799	41541	32732	1542	338	20	139
41	AD2	Rhizosphere	AD2- Rh	176271	60077	37218	1469	407	33	172
42	AD2	Rhizosphere	AD2- Rh	106625	35988	26917	1857	332	31	115
43	DD2	Rhizosphere	DD2- Rh	96313	37304	26386	1150	294	86	150
44	DD2	Rhizosphere	DD2- Rh	143336	54738	36657	1576	419	149	198
45	DD2	Rhizosphere	DD2- Rh	90959	32252	23041	1562	313	27	167
46	DD2	Rhizosphere	DD2- Rh	134714	51161	37522	773	405	61	164
47	DD2	Rhizosphere	DD2- Rh	128665	48588	33698	900	369	80	175
48	DD2	Rhizosphere	DD2- Rh	111585	45486	30668	1372	329	78	131

Fig. S1. Rarefaction curves.

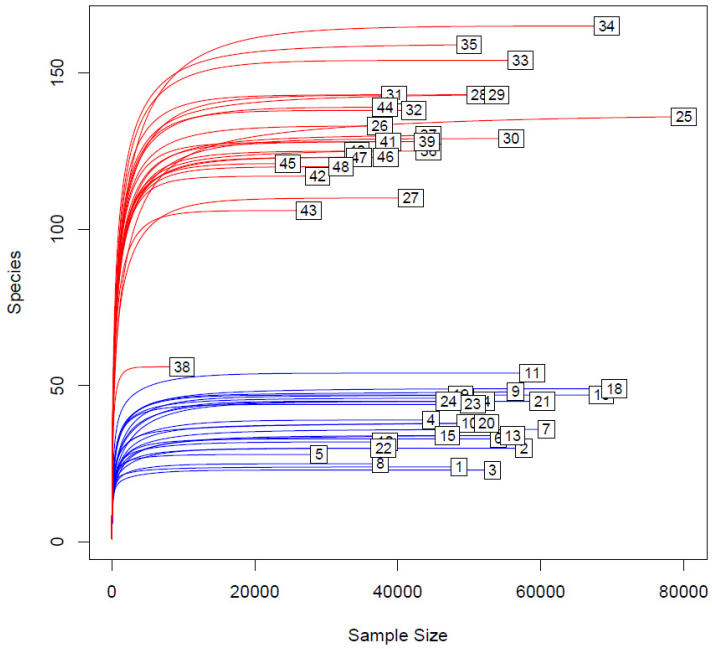

6 Final dissertation

The present thesis represents a mile stone work in etiological and epidemiological studies over Kiwifruit Decline, constituting a starting point for future studies regarding this disease. It is also an example of interdisciplinary study, in which new technologies are used together with canonical approaches, to develop new strategies for studying unknown diseases.

The etiological study in controlled condition (Chapter 2) showed how expertise from different disciplinary sectors can be merged to efficiently set up protocols to properly address etiological questions. One of the biggest breakthrough was indeed the proof of the necessary interaction between waterlogging and soil-borne pathogen(s) to incite the disease. Before our work, the involvement of waterlogging in KD was indeed inferred only from field surveys (Tosi *et al.*, 2015), literature (Smith *et al.*, 1989, 1990; Reid & Petrie, 1991; Reid *et al.*, 1992; Sorrenti *et al.*, 2016), and from experimental trails which, however, were focused to study the plant response in non-flooding conditions rather than to confirm its actual role on the disease onset (Sorrenti *et al.*, 2019). On the other hand, pathological studies basically had failed to satisfy the first Koch's postulate since no common pathogen was found in diseased plants (Tosi *et al.*, 2015).

Another hypothesis that arose from the results described in Chapter 2 was the involvement of one or more pathogens, probably Oomycetes, in Kiwifruit Decline. Indeed, the isolation results from Chapter 2 showed at least two major candidates: *Phytopythium vexans* and *Phytopythium chamaehyphon*. Nevertheless, these two species were found with a relative low occurrence (56% and 61% for *P. vexans* and *P. chamaehyphon*), in spite of the uniform conditions in which plants were grown: the same soil, the same temperature, and the same water management. Successively, the results from Chapter 3, clearly demonstrated the pathogenicity for *P. vexans* while for *Phytopythium chamaehyphon* the studies are still undergoing.

Results derived from the metabarcoding study in Chapter 5, have strengthen the idea that more than one pathogen might be involved in the disease, since significant differences in terms of oomycete relative abundance were found between a control site (considered "healthy") and a diseased one in both the root endosphere and rhizosphere compartments. These differences were mostly attributable to *Phytophthora sojae* that has never been isolated in our studies and rarely found in those of Tosi et al. (2015). Although reported as pathogenic in France (Baudry *et al.*, 1991), *P. sojae* isolation and pathogenicity tests must be performed to clearly demonstrate its involvement in KD. Our results together with the many reports of decline-like diseases associated with oomycetes (Latham & Dozier, 1989; Conn *et al.*, 1991; Latorre *et al.*, 1991; Stewart & McCarrison, 1992; Akilli *et al.*, 2011; Kurbetli & Ozan, 2013; Çiftçi *et al.*, 2016; Polat *et al.*, 2017), are consistent with a patho-system manly characterized by this class of microorganisms. Indeed, Oomycetes features, in particular the need of free water for the dispersion and movement of zoospores (Niklaus, 2010), are perfectly in agreement with the spreading pattern of KD observed in the field: initial spreading centre located in down slope areas, oil spot geometry of the diseased areas, and higher disease incidence of KD in poorly drained soils.

Nevertheless, also *Ilyonectria*/*Dactylonectria* species should not be overlooked, since they have been previously reported as pathogenic in an etiological context similar to KD (Erper *et al.*, 2011, 2013), and they have been abundantly found inside kiwifruit roots during the metabarcoding study of Chapter 5.

The metabarcoding experiment in Chapter 5 also highlighted the presence of a rather simple community within kiwifruit roots characterized by tree/four major taxa. It was interesting to note that *Phytopythium vexans* was found not only in a diseased site but also in a site were symptoms of KD were completely absent: "no rat-tail" symptoms even in the deeper layer, no rooting of the fine roots, high root density and healthy canopies. This allows some speculations on the KD aetiology: i) firstly

it suggests that potential pathogens can live inside the roots of kiwifruit plants without causing damage; ii) secondly, it suggests that specific environmental conditions (waterlogging) must occur to incite the disease. It is not yet known whether these conditions directly increase the aggressiveness of the pathogens or if they simply weaken the defences of the plants which consequently become more susceptible to attack by the pathogens.

One of the main challenges in kiwifruit decline regards the identification of diseased plants before the appearance of wilting. Indeed, sampling of the plants when symptoms are already manifested in the canopy might lead to inconsistent results, since the feeding roots are already extremely compromised to be informative for etiological studies. Secondly, due to its astonishing spreading speed, kiwifruit decline can easily compromise, in only one season, wide areas of the orchard. Epidemiological studies are therefore greatly limited at the moment because tracking the disease evolution is almost impossible when only canopy is observed, and extensive surveys for the observation of symptoms at root level seems highly unfeasible. The study reported in Chapter 4, managed to find alternative strategies to study the disease evolution relying on remote sensing technologies. Multispectral data were found to be a reliable tool to distinguish asymptomatic from symptomatic plants, while thermal data were able to correctly predict future KD outbreaks.

The capability of multispectral data to discern between asymptomatic and symptomatic plants was expected, since, especially near infrared wavelength (NIR 700-1100nm) has been proved to be a reliable estimator of plant biophysical traits, such as vigour or biomass production (Thenkabail *et al.*, 2000; Boelman *et al.*, 2003; Xue & Su, 2017; Quirós Vargas *et al.*, 2019). The real breakthrough of this study is the capability to predict the evolution of the disease based on temperature data. Indeed temperature has been reported as a highly informative parameter, especially when trying to predict the stressor effect that modify directly or indirectly the leaf stomatal conductance and the transpiration rates (Jones & Schofield, 2008; Maes & Steppe, 2012; Calderón *et al.*, 2013; Mangus *et al.*, 2016;

Ortiz-Bustos *et al.*, 2017; Zarco-Tejada *et al.*, 2018). The integration of these technologies could lead to great improvement of field scouting activities focusing the attention on homogenous areas characterized by plants shearing the same physiological status.

FUTURE PROSPECTIVE

With this thesis we made some steps forward in the comprehension of etiological aspects connected with Kiwifruit Decline, however, further studies are needed to specifically address how plant and pathogen interact and to understand which is the exact role played by waterlogging in the disease. Moreover, the full extent of potential pathogenic Oomycetes involved in the disease should be further addressed. Metabarcoding studies can provide a reliable tool to screen the oomycete communities within diseased sites, but pathogenicity tests on all the oomycete isolates obtained from diseased plants should be performed independently from the isolation occurrence. Furthermore, for those species resulting pathogenic, molecular specific assays should be developed in order to increase rapidity, sensitivity and specificity of the diagnostic procedure for KD. Probably the best solution could be the development of a multiplex assay which allows to check simultaneously for the presence of more than one pathogen.

Epidemiological studies should rely on robust climate analysis to highlight differences occurred after the disease outbreak. It is highly probable that climatic shifts might be behind the disease outbreaks, however from our study in Chapter 2, major shifting on the rainfall distribution seemed to be marginally related to disease outbreak. In the future the characterization of pathogenic microorganisms could provide significant information to correctly set the climate analysis.

Concerning remote sensing technologies further studies are needed to better characterise the spectrum of plants affected by KD. This would allow to develop more reliable tools for the inspection of the disease in the field. Moreover, it should be interesting to test the feasibility of using high-resolution

multispectral satellite images to identify diseased sites at territorial scale. In this way, the awareness of the disease spreading will be highly improved.

Nevertheless, the multifactorial nature of Kiwifruit Decline is difficult to address if a topic-specific approach is used. The several aspects involved in the diseased should be studied all together in order to fully uncover KD aetiology and epidemiology, possibly with one ad hoc coordinated multidisciplinary project.

Finally, even if this PhD thesis did not directly address the development of control strategies, the use of resistant rootstocks seems to be the most promising and reliable countermeasure under evaluation.

In this regard, the tools and knowledge deriving from this thesis will certainly prove useful during the screening process.

III. Acknowledgments

On the verge of this important attainment, I would like to express my deepest gratitude to all those who made this work possible.

First of all, I would like to thank my Supervisor Prof. Marta Martini and my Co-Supervisor Dr. Paolo Ermacora for their commitment, technical advice and guidance during all the stages of this thesis. I could not forget their support, encouragement and assistance in the difficult moments encountered during this work.

I would like to express my gratitude to all the other members of the Plant Pathology research group of the University of Udine for the great opportunity they gave me to carry out this research: Prof. Giuseppe Firrao, Prof. Rita Musetti, Prof. Nazia Loi, Stefano Borselli and Alberto Loschi.

I really want to thank very much all the members of the Remote sensing group of the Institute of Sugar Beet Research (IfZ), for their support and assistance during my period in Gottingen where I learned so much and felt so much welcomed. First of all, Professor Anne-Katrin Mahlein and Dr. Stefan Paulus for their valuable interest on my research and Abel, Roxana, and all the staff from IfZ.

Many thanks also to Dr. Fabio Marroni, his support in the last steps of the thesis has been fundamental for the completion of the metabarcoding analysis.

Last but not least, thank you very much to all my colleagues and friends in Udine for their friendship and the wonderful time spent together inside and outside the university, this experience would have been less bright without the presence of all these people around me.